Title

The morphology and fluid dynamics of chemical scent detection in stingrays and their relatives (Elasmobranchii: Batoidea)

Permalink

https://escholarship.org/uc/item/4qn7v6v5

Author

Rutledge, Kelsi Marie

Publication Date

2023

UNIVERSITY OF CALIFORNIA

Los Angeles

The morphology and fluid dynamics of chemical scent detection

in stingrays and their relatives (Elasmobranchii: Batoidea)

A dissertation submitted in partial satisfaction of the

requirements for the degree Doctor of Philosophy

in Biology

by

Kelsi Marie Rutledge

2023

ABSTRACT OF THE DISSERTATION

The morphology and fluid dynamics of chemical scent detection

in stingrays and their relatives (Elasmobranchii: Batoidea)

by

Kelsi Marie Rutledge

Doctor of Philosophy in Biology

University of California, Los Angeles, 2023

Professor Malcolm S. Gordon, Chair

Batoid fishes (rays, skates, sawfishes, and guitarfishes) are macrosmatic which means they rely heavily on their sense of smell for survival and reproduction. Olfactory cues provide important information for navigation and tracking, recognition of prey/predators/conspecifics, and reproductive signaling. For batoid fishes to receive an olfactory signal for sensory processing, an odorant molecule must traverse the external fluid environment, funnel into the nose, and bind with an odorant receptor. Therefore, sensory processing times will depend on odor capture and nasal irrigation efficiency. However, batoid fishes are dorsoventrally compressed with their nostrils on the ventral surface of their body. Their nostrils, called the nares, are disconnected from the pharynx and mouth, and physically separate olfaction from respiration. Therefore, there is not a direct pump-like mechanism to irrigate their nares. The ventral position and pump-less design of the batoid nare presents several challenges for odor

capture and irrigation, which may have led to the expansive nasal diversity we see in this group. This dissertation explores the comparative functional morphology and fluid dynamics of the olfactory apparatus and its functions in these fishes. The first chapter of this dissertation categorizes the diversity of nare morphology across Batoidea into discrete morphotypes within a comparative, phylogenetic, and functional framework. The second chapter examines how the internal anatomy of different morphotypes influences nasal irrigation efficiency. The final chapter examines how the external anatomy of different morphotypes influences odor capture potential.

The batoid nares consist of two paired, blind chambers on the medioventral surface of the fish, near the mouth and gills. There are two major anatomical components: an incurrent nostril where water is thought to enter and an excurrent nostril where water is thought to leave. There is considerable morphological diversity in the shape, size, and placement of the incurrent and excurrent nostrils. Batoid fishes possess one or more nasal flaps situated around their incurrent nostrils. Most batoid fishes also have a nasal curtain that loosely covers the excurrent channel and forms the excurrent nostril. The nasal curtain is also variable in its morphology. Housed inside the incurrent nostril is the olfactory rosette, which is composed of a longitudinal array of numerous parallel plates of tissue called lamellae. These lamellae are coated in sensory and non-sensory epithelium. To elicit an olfactory response, an odorant molecule must pass into the nose and make contact with the sensory epithelium.

Therefore, batoid fishes rely on water flow to direct odorants into their olfactory chamber for sensory processing. Water needs to be actively drawn into the olfactory chamber due to slow diffusion times and the impeding boundary layer surrounding a swimming fish. There are several hypothesized nasal irrigation mechanisms for batoid fishes. First, the beating of cilia of non-

sensory cells (kinociliated cells) likely assists in internal circulation of water through the chamber by generating velocity gradients. However, these cells are unlikely to draw water into the incurrent nostril. Without an internal pump, batoid fishes must rely on harnessing external flows. These flows include the relative forward motion of a swimming fish (i.e., the motion "pump"), indirect respiratory flow (i.e., buccopharyngeal pump), pitot- and venturi-like mechanisms, and/or viscous entrainment. Actively swimming fishes may rely on the motion pump. However, the ventral placement of the batoid nares is not aligned with the freestream flow direction, which limits the motion pump. Stationary or slow swimming batoids may draw from the indirect respiratory current generated by the buccopharyngeal pump. The close proximity of the excurrent nostril with the mouth suggests that mouth suction may help to facilitate flow through the olfactory chamber. The morphology and relative position of the incurrent and excurrent nostrils may also assist in nasal irrigation by generating a secondary flow through pressures differences (pitot/venturi) or a shearing force (viscous entrainment). Additional morphological features, like the nasal flaps or nasal curtain may also have some sort of hydrodynamic function.

To understand how this unique nasal morphology influences olfaction, I first explored the functional morphology of the nares across Batoidea. In the first chapter, I develop a morphometric model to quantify the diversity in incurrent nostril shapes, sizes, and positions on the head in an ecological, phylogenetic, and functional framework. Specifically, swimming mode, lifestyle (benthic vs. pelagic), habitat, and diet were examined for correlations with nasal morphotype. Morphometric measurements were taken on all 4 orders present in Batoidea to broadly encompass nasal diversity (Rhinopristiformes 4/5 families; Rajiformes 2/4 families; Torpediniformes 4/4 families; Myliobatiformes 8/11 families). External nasal diversity was

categorized into 3 major morphological groups with several subtypes, termed: flush [subtypes: circle, comma, intermediate], open, and protruding nasal morphotypes.

There were several phylogenetically independent and statistically different morphological traits within these nasal morphotypes. Specifically, the position and angle of the nostril on the head, the width of the incurrent nostril, and the spacing of the incurrent nostrils largely distinguished these groups. These significant measurements correlated best with the swimming mode of the animal. Oscillatory swimmers (e.g., eagle rays, bat rays, manta rays) and body-caudal-fin (BCF) swimmers (e.g., guitarfishes, sawfishes) have narrower heads with larger nostrils that are positioned closer to the edge of their disc. However, while BCF and oscillatory swimmers had statistically similar traits, they occupied distinct regions of the morphospace. This is likely because BCF swimmers could be discriminated from oscillatory swimmers due to differences in the nasal curtain (or anterior nasal flap). Generally, oscillatory and BCF swimmers are some of the largest, fastest swimming batoids that operate at higher Reynolds numbers compared to their congeners.

However, correlations with morphology and ecology were not straightforward. There was no significant difference in the nasal morphology of fast-swimming, pelagic rays vs. slow-swimming, benthic rays, suggesting that morphology is not driven strictly by Reynolds number. Swimming mode may have been most influential for predicting nasal morphology because the motion in which the animal swims will directly affect how water and odorants are directed into its nose. For example, BCF swimmers move their heads in wide lateral sweeping motions (i.e., yawing) which may help entrain and flush their horizontally expanded, open nostrils. Oscillatory swimmers that swim with a vertical up and down motion (i.e., pitching) have vertically oriented, flush nostrils. Undulatory swimmers have more variable swimming movements that include

pitching, yawing, and quick turns, and they have a diversity of nostril types. Overall, the open nare morphotype is seen in exclusively BCF swimmers, the protruding nare morphotype is seen exclusively in "true" punters (see Ch.1 for definition), and the flush morphotype was seen across a diversity of swimming modes.

In the second chapter, we aimed to understand how these discrete nasal morphotypes may influence nasal irrigation by visualizing flow into and through the differing olfactory chambers. We CT-scanned representative species of each major morphotype and one subtype (open, flush, protruding, and comma subtype) and 3D printed clear models of the head of each morphotype. Clear models were mounted in a water tunnel and neutrally buoyant dye was injected one cm from the leading edge of all models and filmed with a high-speed camera. To understand how relevant ecological and behavioral parameters may influence nasal irrigation, we tested models at varying Reynolds number (Re = 100, 500), angles of attack (head pitch 0°, 8°), and with and without mouth induced respiratory suction.

To compare morphotypes across parameters, we recorded the time it took for dye to reach important components of the olfactory system. We hypothesized that increasing Reynolds number, head pitch, and mouth suction would result in faster nasal irrigation times. However, we found that these parameters influenced nasal irrigation differently across morphotypes. Some morphotypes displayed quicker nasal irrigation at higher Reynolds numbers (open, flush), while other morphotypes (protruding, comma) were not significantly influenced by Reynolds number. These morphotypes (protruding, comma) displayed internal recirculating flow near their olfactory lamellae. This recirculating fluid could help increase the chances an odorant comes in contact with the sensory epithelium by increasing the time near the lamellae. Respiratory suction and head pitch were crucial for nasal irrigation in the morphotypes without this internal

recirculation (open, flush). Because the open and flush morphotypes required certain behavioral modifications to irrigate their nares, these morphotypes were classified as "specific smellers." Morphotypes that could efficiently irrigate their nares independent of respiration, head pitch, and Reynolds number were classified as "dynamic smellers." The open morphotype, a specific smeller, is seen in BCF swimmers that swim at relatively fast speeds. Therefore, this morphotype may necessitate a higher Reynolds number flow and the yawing motion of its swimming mode to efficiently irrigate its nares. The flush morphotype, also a specific smeller, is seen across Batoidea, from oscillatory eagle rays to undulatory stingrays. This morphotype required a slight head pitch and benefitted from indirect respiratory flow. Fast swimming, oscillatory swimmers likely irrigate their flush nostrils with the assistance of the head pitching motion seen during this swimming mode. Slower swimming rays with undulatory or intermediate swimming modes may rely more on the respiratory current to irrigate their flush nostrils. The dynamic smellers are seen in a variety of swimming modes, further highlighting their versatile nasal morphology. Finally, the ability to change flow patterns through the nasal chamber with changes in behavior (head orientation, respiratory mode, swimming speed) suggests batoids could play an active role in their own chemoreception. This challenges the longstanding theory that fishes passively sense their chemical environment and have no active control of their chemoreception.

In the third chapter, we aimed to understand how the external anatomy of the nares influences odor capture by visualizing flow around the entrance of the incurrent nostrils. We tested three nasal morphotypes seen in batoid fishes with distinct flap-like protrusions situated around the nares (open, protruding, comma nasal morphotypes). Models of the nasal morphotypes were 3D printed and mounted in a water tunnel and the incoming flow was visualized using particle image velocimetry methods (PIV). Models were tested at varying

Reynolds numbers (Re = 500, 1000, 2000, 3000, 6000), angles of attack ($0°$, $8°$), and with and without respiratory induced mouth suction. We hypothesized that morphotypes with a longer sagittal nostril protrusion will have a greater nostril reach and odor capture potential. Nostril reach was measured as the expanse (width) of the time averaged streamlines that enter the incurrent nostril. Odor capture potential was measured by calculating a 2D closed loop flux integral around the incurrent nostril and comparing it to the available upstream flux.

This was the first time PIV was used to visualize olfactory flow around the nare of a fish and there were several surprising results. First, olfactory flow around the nares of these morphotypes was much more complex and expansive than previously thought. Second, nostril protrusion length was inversely proportional to nostril reach. The comma morphotype, which had the smallest nostril protrusion, had the largest nostril reach and odor capture potential, with a nostril reach over three times the width of its incurrent nostril. Third, flow into two of the three morphotypes enters the incurrent nostril from multiple directions. This is the first recorded instance of multidirectional olfactory flow into the nostril of a fish. In all morphotypes, the flap-like structures appear to play an important role in protruding out of the boundary layer and locally disturbing the flow to create recirculation around the nares. In two of these morphotypes (open, comma) these recirculation regions funnel water into the incurrent nostril from behind and to the side of the nostril, greatly expanding the reach and odor capture potential of the nares. Fourth, the open morphotype had a large portion of water entering the "excurrent" nostril, suggesting that flow patterns are more complex than simply an incurrent and excurrent nostril. Finally, head pitch, respiration, and Reynolds number were found to impact odor capture differently across morphotypes.

The flap-like external nasal features seen in the open, protruding, and comma

morphotypes appear to be an adaptation to increase nostril reach and odor capture potential. However, there appears to be a trade-off in nasal flap length and nostril reach. The long nasal protrusion seen in the protruding morphotype extends out of the boundary layer even at the slowest swimming speeds for this species. But, the nasal protrusion is sufficiently long to prevent flow from entering from behind the incurrent nostril, greatly decreasing the nostril reach. The nares of this morphotype are also situated the farthest from the leading edge of their disc. This morphotype is also exclusively seen in batoids that "punt," a very slow form of underwater locomotion. For these reasons, the boundary layer at the nostrils is likely to be relatively thicker for this morphotype and it may sacrifice nostril reach to aid in odor capture in a challenging environment. Conversely, the open and comma morphotypes had shorter nostril protrusions that allowed for recirculating flow to enter the nares from multiple directions.

In summary, there are several ways batoids can irrigate their nostrils and these irrigation strategies likely represent many-to-one mapping. Specifically, batoid nasal irrigation and odor capture strategies likely differ across and within the same nasal morphotype and likely even vary situationally with the ecology and behavior of the animal. Batoid fishes with the flush morphotype that are oscillatory swimmers likely rely on the motion pump and their already positive body angle during swimming. Batoid fishes with the flush morphotype that are undulatory, intermediate, or BCF swimmers may need to behaviorally mediate their olfaction by changing their mode of respiration or head angle. Batoid fishes with nostril protrusions (open, protruding, comma) may rely less on behavioral modifications. However, the length of the nasal protrusion is important for nostril reach. Morphotypes with shorter nostril protrusions induce multidirectional flow into the incurrent nostril which could increase the likelihood that an odorant is captured. The open nare morphotype, a fast BCF swimmer, has the least pipe-like

geometry and the only morphotype that lacks a nasal curtain. This morphotype has multiple nasal flaps that help disturb and redirect the flow into its nares, but it also relies on behavioral modifications to irrigate its nares at low Reynolds number flows. Finally, the comma morphotype performed the best out of all nasal morphotypes in terms of nasal irrigation speeds, nostril reach, and odor capture potential. This dynamic smeller uses both its anterior nasal flap and nasal curtain to channel a large expanse of water into its incurrent nostrils without behavioral modifications.

The comma nasal morphotype could be a possible candidate for bioinspired design. Specifically, this morphotype does not depend on an internal pump to bring water to their olfactory lamellae and is effective at irrigating its nares at low and high Reynolds numbers (Re =100, 500, 1000, 2000) and with changing orientation into a plume. The internal geometry of this morphotype recirculates fluid around the sensory structures and the external geometry passively captures water over 3 times the width of its own nostril. Therefore, this geometry could be a potential candidate geometry for chemical detection systems onboard underwater vehicles that are often limited by the power demand of the pump. By changing the geometry of the inlet, there is potential to passively increase the amount of water sampled.

This dissertation provides new insights into the unexpected complexity of fish olfaction and highlights the multifactorial nature of successful odor capture and nasal irrigation in these dorsoventrally flattened fishes and may be relevant odor-harnessing geometries for future underwater chemical detection systems.

The dissertation of Kelsi Marie Rutledge is approved.

John O. Dabiri

Misty W.M. Paig-Tran

Jeffrey D. Eldredge

Blaire Van Valkenburgh

Malcolm S. Gordon, Committee Chair

University of California, Los Angeles

2023

Dedication

To Derek Kirkbride, whose unconditional support and constant and unwavering belief

in me made all the difference.

TABLE OF CONTENTS

LIST OF FIGURES

Chapter 2

flush nares are classified here as "specific smellers," which necessitate specific behavioral conditions (Reynolds number/swimming speed, head pitch, respiratory flow) for effective chemoreception. The protruding and intermediate nare are classified as "dynamic smellers," which perform similarly at a variety of behavioral conditions. The protruding nare allowed for quick odor capture and circulation at both head pitch angles and was minimally influenced by the respiratory pump. The comma nare morphotype, with intermediate features, allowed for fast odor capture and circulation at both Reynolds numbers and was also minimally influenced by the respiratory pump. The flush morphotype was not able to capture dye at a pitch of 0° and performed slower in odor capturing metrics at a pitch of 8°. The open morphotype had some of the quickest capture and circulation times at Re= 500 but was by far the slowest morphotype at Re=100, taking minutes for dye to diffuse from the chamber……………………………………………………………………90

Chapter 3

ACKNOWLEDGMENTS

I would first and foremost like to thank my doctoral thesis committee and advisors, Malcolm Gordon, the late Don Buth, John Dabiri, Jeff Eldredge, Misty Paig-Tran, and Blaire Van Valkenburgh. This thesis would not be possible without their research guidance and support. I feel honored to have been mentored by these amazing scientists and look forward to continue learning from the them. I would specifically like to wholeheartedly thank my advisors Malcolm Gordon and Don Buth for consistently supporting me throughout my graduate career and always being available to provide me with guidance both in science and life. I am forever grateful for the scientific and career trajectory both Malcolm and Don led me down. I would also like to deeply thank John Dabiri for his overwhelming support over the past year and half. Thank you for providing me with research facilities, office space, continual guidance, and adopting me as an unofficial member of the Dabiri Lab. I look forward to becoming an official member of the Dabiri Lab as a Postdoctoral Scholar.

I would also like to thank Thomas Lankford (UNCW) whose passionate introductory ichthyology class first sparked my interest in fishes. And I would like to thank Troy Alphin (UNCW) who mentored me through my first independent research study and taught me the value of field work. I would also like to thank Adam Summers (UW), Alice Gibb (NAU), Matt Kolmann (UofL), Cassandra Donatelli (CU), and Sarah Hoffman for cultivating my love for fish biomechanics through the Friday Harbor Laboratories Fish Biomechanics course. A huge thanks to Matt Kolmann for being a wonderful mentor and batoid-loving friend during this experience.

I would also like to thank the many museum staff and curators that allowed me to visit their collections and provided specimen access and loans. Thank you to Bill Ludt and Todd Clardy at the NHMLA, Andrew Williston and Megan Source at MCZ, Ben Frable at SIO, and

PREFACE

Chapter 1 of this dissertation is a version of: Rutledge, K.M. 2022. Sniffing out stingray noses: the functional morphology of Batoid olfaction. *Journal of Integrative and Organismal Biology.* Obac043. https://doi.org/10.1093/iob/obac043.

Chapter 2 of this dissertation is a version of: Rutledge, K.M., Murphy, C.T., Eldredge, J., Gordon, M.S. 2023. The fluid dynamics of chemical scent detection in stingrays and their relatives. *In Revision at the Journal of Experimental Biology.* C.T. Murphy provided the experimental facilities, advised in experimental design, and provided general supervision. J. Eldredge provided supervision with computational fluid dynamic analysis. M.S. Gordon provided general supervision.

VITA

Previous Degrees Awarded

2016   B.Sc. in Marine Biology, UNC-Wilmington

2016   B.Sc. Environmental Science, UNC-Wilmington

2018   M.Sc. in Biology, UCLA

Select Awards

2023   Uncommon Bruin: UCLA Campus Wide Winner

2022   UC Grad Slam Thesis Competition Winner

2021   Schechtman Award in Recognition of Outstanding Service as a Teaching Associate

2020   Life Science Excellence Award Winner for Research Paper

2020   Lasiewski Award in Recognition of Outstanding Research in Organismal Biology

2019   UCLA Faculty Women's Club Scholarship and Departmental Nominee

Select Grants and Fellowships

2021   Office of Naval Research (ONR) Naval Research Enterprise Fellowship

2020   Department of Defense (DOD) National Science and Engineering Fellowship

2019   Sigma Xi Grant in Aid of Research

2019   Grant in Aid of Research (GIAR) Society for Integrative and Comparative Biology

Select Publications

2023   **Rutledge, K.M.**, Murphy, C.T., Eldredge, J., Gordon, M.S. 2023. The fluid dynamics of chemical scent detection in stingrays and their relatives. *In Revision at the Journal of Experimental Biology.*

2022   **Rutledge, K.M**. 2022. Sniffing out stingray noses: the functional morphology of Batoid olfaction. *Journal of Integrative and Organismal Biology.* Obac043. https://doi.org/10.1093/iob/obac043

2020	Gordon, M.S., Lauritzen, D.V., Wiktorowicz, A.M., **Rutledge, K.M.** Aracaniform Swimming: a swimming mode used by deep-water boxfishes (Teleostei: Tetraodontiformes: Aracanidae). Physiological and Biochemical Zoology Special Issue: Biomechanics, 93(3): 235-242. https://doi.org/10.1086/708163
2019	**Rutledge, K.M.** A new guitarfish of the genus Pseudobatos (Batoidea: Rhinobatidae) with key to the guitarfishes of the Gulf of California. Ichthyology and Herpetology, 107 (3): 451-463. https://doi.org/10.1643/CI-18-166
2019	**Rutledge, K.M.,** Summers, A. P., Kolmann, M.A. 2019. Killing them softly: ontogeny of jaw mechanics and stiffness in mollusk-feeding freshwater stingrays. Journal of Morphology, 280: 796-808. https://doi.org/10.1002/jmor.20984

Select Presentations

2023	Society for Integrative and Comparative Biology, Austin, Texas
2022	Seminar at Whitney Marine Biological Laboratory, St. Augustine, FL
2022	APS Division of Fluid Dynamics Conference, Indianapolis, IN
2022	UCLA Sloan Fellowship Film and Science Symposium, UCLA
2022	NDSEG Fellowship Awardee National Conference, Boston, MA
2022	Association for the Sciences of Limnology and Oceanography, Virtual
2022	UC Campus Wide Grad Slam Thesis Competition, San Francisco, CA
2022	UCLA Grad Slam Thesis Competition, Los Angeles, CA
2022	Association for Sciences of Limnology and Ocean Sciences, Virtual
2022	Society for Comparative and Integrative Biology, Phoenix, AZ
2021	UCLA Annual Biology Research Symposium, Virtual

Select Media Coverage

NPR Science Friday

Forbes x2

Spectrum 1 News

Chapter 1

The functional morphology of stingray

(Elasmobranchii: Batoidea) olfaction

Kelsi M. Rutledge[1]

[1]Department of Ecology and Evolutionary Biology, University of California Los Angeles, California, 90095-7246, U.S.A.

ABSTRACT

Batoid fishes (rays, skates, sawfishes and guitarfishes) are macrosmatic, meaning they rely on their sense of smell as one of the primary senses for survival and reproduction. Olfaction is important for long-distance tracking and navigation, predator and prey recognition, and conspecific signaling. However, the mechanisms by which batoids harness odorants is unknown. Without a direct pump-like system, it is hypothesized that batoids irrigate their nostrils via one or a combination of the following: the motion pump, buccopharyngeal pump, pressure (ex. pitot-like mechanism), or a shearing force (ex. viscous entrainment). These mechanisms rely on the size, shape, and position of the nostrils with respect to the head and to each other. Batoids are united as a group by their dorsoventrally compressed body plans, with nostrils on the ventral side of their body. This position presents several challenges for odor capture and likely limits the effectivity of the motion pump. Batoid fishes display an expansive nasal morphology, with inlet nostrils ranging from thin, vertical slits to wide, horizontal ovals to protruding, tube-like funnels, and more. In this paper, a morphometric model is developed to quantify the vast diversity in batoid nose shapes, sizes, and positions on the head in an ecological and functional framework. Specifically, swimming mode, lifestyle, habitat, and diet are examined for correlations with observed nasal morphotypes. Morphometric measurements were taken on all 4 orders present in

Batoidea to broadly encompass batoid nasal diversity (Rhinopristiformes 4/5 families; Rajiformes 2/4 families; Torpediniformes 4/4 families; Myliobatiformes 8/11 families). All batoid external nasal diversity was found to be categorized into 5 major morphological groups and were termed: flush nare [circle, comma, intermediate], open nare, and protruding nare. Several morphometric traits remained significant when accounting for shared ancestry, including the position and angle of the nostril on the head, the width of the inlet hole, and the spacing of the nostrils from each other. These measurements were found to be closely correlated and statistically significant with the swimming mode of the animal. This study provides the first crucial step in understanding batoid olfaction, by understanding the diversity of the morphology of the system. Because odor capture is a strictly hydrodynamic process, it may be that factors relating more directly to the fluid dynamics (i.e. swimming mode, velocity, Reynolds number) may be more important in shaping the evolution of the diversity of batoid noses than other ecological factors like habitat and diet.

INTRODUCTION

A successful chemical detection system must have both accurate and precise internal sensors and a reliable odor harnessing and directing system. For a fish to detect an odorant, a chemical signal must traverse the external fluid environment, funnel into the nose, and bind with an odorant receptor. The odorant receptor must identify the specific odorant and send a signal to the brain with information on the nature of the chemical signal. Thus, a fish's olfactory system can be generally broken into two major components: 1) the external interaction with the environment and 2) the internal flow and sensory mechanics. While there have been numerous studies looking at the internal sensory architecture of a fish's nose (with an impressive sub-

nanomolar detection capability; Meredith and Kaijura, 2010), there is far less research on the external morphology and odor harnessing mechanisms.

Batoid fishes (rays, skates, sawfishes and guitarfishes) present a unique system to study the morphology and fluid dynamics of olfaction for several reasons. First, batoid fishes have an expansive diversity in external nasal morphology of any other group of fishes, including differences in nostril shapes, sizes, relative positions, and external protruding features. Second, they are dorsoventrally compressed, with their nostrils positioned ventrally and medial on the underside of their body near their mouth and gills. Third, batoid fishes are macrosmatic, meaning they rely on their sense of smell as one of their primary senses for survival and reproduction (Collins et al., 2015). This includes long-distance tracking and navigation, predator and prey recognition, and conspecific signaling (Hart and Collin, 2015; Gardiner, 2012; Gardiner et al., 2014). Fourth, the niche space of batoids is expansive, with diversification into many environments and life histories. Finally, they lack an apparent pump-like mechanism to irrigate their nostrils. Their nostrils are disconnected from the pharynx and mouth, and they lack olfactory accessory sacs, the water-pumping nasal chambers seen in many teleost fishes. Without a direct pump-like mechanism and this ventral positioning, how are odorants efficiently captured? With this morphological nasal diversity in mind, are there unifying properties across species? How do these design parameters change with diversification into different habitats and lifestyles?

To answer these functional questions, the morphology of the system must first be examined. The typical arrangement of the olfactory organ of batoids is found as a blind chamber partially divided by an anterior, inlet nostril (termed the incurrent nostril) though which water enters and a posterior, outlet channel (excurrent nostril) through which water leaves (Tester,

1963; Theisen et al., 1986; Zeiske et al., 1987; Abel et al., 2010; Compagno, 1999). The incurrent nostrils (also called the nares) range from thin, vertical slits to wide, horizontal ovals to protruding tube-like funnels, and more. Batoids also possess one or more dividing nasal flaps flanking the incurrent nostrils. Many batoids have one major nasal flap, called the nasal curtain, which is an elongated flap of tissue that extends from the medial side of the incurrent nostrils to the anterior edge of the mouth (Figure 1a). This curtain loosely covers the excurrent channel of the nose and forms the respective outlet hole. This curtain is also variable in shape, size, and length with respect to the mouth. In addition to the nasal curtain, some species possess additional flaps of tissue that flank or project from the incurrent nostril hole. In species that lack a nasal curtain (guitarfishes and sawfishes), these nasal flaps act as rudimentary divisions between the nasal chamber, designating the inlet from the outlet (Figure 1b). Housed inside the nostril is the olfactory rosette, which is composed of a longitudinal array of numerous (up to 300) flexible, parallel plates of tissue, called lamellae. The lamellae have numerous, microscopic folds called secondary folds that increase the surface area of the structure (Ferrando et al. 2017). The lamellae are coated in non-sensory and sensory epithelium (Takami et al. 1994; Meredith and Kajiura, 2010; Ferrando et al. 2017; Simonitis and Marshall, 2022). The sensory epithelium is coated in supporting cilia and houses the olfactory receptor neurons (Theisen et al. 1986; Zeiske et al., 1987; Schluessel et al., 2008). It is unknown whether the supporting cilia propels mucus or water, but evidence suggests they likely propel mucus (Cox, 2013). To receive olfactory information for sensory processing, odorants must enter the inlet nostril, pass through the incurrent channel and across the olfactory rosette where it then binds with an olfactory receptor neuron on the lamellae that sends a signal to the brain via the olfactory bulb (Yopak et al., 2015).

Therefore, the shape, size, and position of a fish's nostrils determine how odor is

4

captured and transported (Cox et al. 2008; Settles, 2005). Fishes will orient into an odor plume by comparing the bilateral odor concentration differences of their paired nostrils, turning towards the higher concentration, or the nostril that is stimulated first (Atema, 1971; Bardach, Todd, and Crickmer, 1967; Gardiner and Atema, 2010; Johnson and Teeter, 1985; Mathewson and Hodgson, 1972; Tester, 1963). Therefore, the spacing and position of the paired nostrils will directly impact its olfactory abilities. Additionally, because many fishes, including batoids, lack a direct pump-like system to irrigate their nostrils, they must rely on harnessing external flows to capture odorants. These include the relative forward motion of a swimming fish (motion-pump), indirect respiratory flow (buccopharyngeal pump), pitot- and venturi-like mechanisms, and viscous entrainment (Vogel, 1977). These hypothesized ventilation methods rely on nare morphology and position, with incurrent and excurrent nostrils positioned at right angles (pitot), different heights (venturi), or perpendicular to flow (viscous entrainment) allowing for the generation of a secondary flow through pressure differences or a shearing force (Cox, 2008). Most bony fishes have small, circular nostrils located on the most anterior, dorsal part of their head. At this anterodorsal position, a fish facing into a current will capture odorants by funneling them into the forward-facing incurrent nostrils through the motion-pump (Vogel, 1977; Garwood et al., 2019, 2020). This position, almost on the apex of the snout, also minimizes the odor-impeding effects of the boundary layer (the stationary layer of fluid surrounding a swimming fish) (Cox, 2008). However, the nostrils of batoid fishes, on the underside of their body, are positioned in a thicker region of the boundary layer and not in the direct path of water flow, likely limiting the effectivity of the motion pump. This may have influenced the expansive external nasal morphology observed in batoids. This unique positioning and disparate morphology will impact the way batoids sense and harness odorants.

The hypothesized odor-harnessing mechanisms in batoids may also depend on environmental and species-specific factors. Possible relevant ecological influences include swimming mode, position in the water column (benthic vs. pelagic), habitat, and diet. Batoids exhibit a variety of swimming modes, including oscillatory, undulatory, and body caudal fin swimming. Many benthic species also display a form of locomotion called "punting," where the animal is in close association with the ground. Each of these swimming modes will influence the pitch, yaw, and swimming speed of the animal. It is likely that for these reasons, swimming mode will directly influence how odorants are tracked and ultimately harnessed into the nose. The position in the water column will also likely influence odor capture, with pelagic species known to rely on the motion-pump as they swim at fast speeds (Cox, 2008). With fewer sensory cues in the open ocean, pelagic species may also rely more on olfaction than other ecologies. In fact, pelagic batoids were found to possess significantly more olfactory lamellae and larger sensory epithelial surface area than benthic species (Schluessel et al., 2008). Benthic species are generally slower swimmers and odor capture is likely affected by the proximity to the substrate and the associated ground effects. While it has not been explored in batoids, benthic sharks were found to have more complex nasal morphologies, with multiple flap-like structures that may aid in odor uptake. The nostrils of benthic sharks are also positioned closer to their mouth, suggesting the indirect respiratory current may aid in nasal irrigation (Timm and Fish, 2012). Similar to batoids, shark nostrils are also considered ventrally positioned, but unlike batoids their incurrent nostrils are anterior and forward-facing in the transverse plane of their body, allowing for a more optimal configuration for harnessing odorants via the motion pump.

Habitat may have also influenced the evolution of batoid nasal morphology (Hara, 1993; Kajiura, 2001; Schluessel et al., 2008; Timm and Fish, 2012). Batoids living in the deep sea or

murky waters were found to have larger olfactory bulbs, a region of the brain that is used as a reliable proxy for olfactory capability (Lisney et al., 2007; Yopak 2015; Theiss et al., 2009; Camilieri-Asch et al., 2020). Reef-associated species were found to possess the smallest olfactory bulbs, possibly suggesting reliance on other senses such as vision or electroreception (Hart et al., 2006; Collin 2012; Kempster et al., 2012; Lisney et al., 2012; Yopak et al., 2015). Additionally, batoids that rely heavily on olfactory cues for spatial navigation, such as long-distance migration or active prey tracking and localization, may have a more acute olfactory system (Jacobs, 2012). This has been unexplored in batoids, but the highly migratory Port Jackson shark was found to have an especially large sensory surface area, olfactory rosette mass, and deep secondary folding on the lamellae, suggesting an increased olfactory ability (Timm and Fish, 2012). While certain ecologies appear to have increased olfactory abilities, it is unknown if these ecologies have also evolved specific odor harnessing morphological adaptations.

While ecological trends in internal nasal morphology (lamellae count, surface area) and brain size (olfactory bulb volume) have been explored in batoids, the external morphology has received far less attention. Specifically, there are no studies that have quantified the external nasal morphology of batoids in relation to their ecology. This study broadly classifies external batoid nasal diversity in a quantitative, ecological, and phylogenetic framework. Specifically, a morphometric model is created for quantifying the observed diversity in batoid morphology into discrete morphotypes. Relevant ecological parameters (swimming mode, lifestyle, habitat, diet) are examined for correlations with observed nasal morphotypes. I hypothesized that the diversity seen in batoid nasal morphology is more than just the result of shared ancestry, with convergence on certain morphotypes that may act as functional adaptations for odor capture. This study lays the foundation for better understanding the evolution and function of a unique olfactory system

that likely relies heavily on its morphology to capture and direct odorants.

METHODS

A. Morphometric Model

A morphometric model was created with 18 measurements to broadly encompass nose shape, size, angle, and position on the head across batoids. Measurements included and were designated as: prenarial distance minimum (PDM), prenarial distance maximum (PDX), tip of nose width (TDW), head width at narial opening (HWN), narial oral distance minimum (NOM), narial oral distance maximum (NOX), distance from nostril to disc margin minimum (NDMM), distance from nostril to disc margin maximum (NDMX), head nostril angle (HNA), anterior nasal flap to mouth distance (ANFM), nostril length (NOW), anterior aperture width/nare opening (AAW), exposed nostril length (NSTRL), distance across anterior nasal apertures (INM), internarial distance minimum(INW), anterior nasal flap base length (ANF), anterior nasal flap length (ANL), anterior nasal flap distal width (ANW), proximal angle of nare (PAN), and head narial angle (HNA). Exact measurement specifications are diagrammed in Figure 1 on two opposing nasal morphotypes. Acronyms mostly follow terminology in Last et. al 2016b, however, some are newly created here and some acronyms were changed for clarity (ex. ANW is anterior nasal flap width here, but anterior nasal flap length in Last et al., 2016b). Nasal curtain (anterior nasal flap) terminology also follows Last et al., 2016b, including: square (the anterior and posterior width of the nasal curtain are approximately the same), skirt-shaped (the anterior width is narrower than the posterior width, forming a "skirt" or triangular shape), incomplete (the posterior edge of the nasal curtain is incompletely joined, forming two lobes that make a "W" shape), and reduced (the nasal curtain is reduced to a small flap that does not cover the nasal channel or outlet).

B. Measurements and replicates

Eighteen different morphometric measurements relating to nose morphology were taken on over 144 adult individuals (Fig. 1). These data span all 4 orders present in Batoidea, 17 families and 28 genera, to broadly encompass batoid nasal diversity (Rhinopristiformes 4/5 families; Rajiformes 2/4 families; Torpediniformes 4/4 families; Myliobatiformes 8/11 families) (Table 1; Supplementary Table 1). The purpose of taxon selection was to sample broadly across the phylogeny to capture as much variation in nose morphology as possible. There were no significant differences in external nose morphology between species in the same genus therefore sampling was focused on maximizing genera. In instances where replicates of the same species were rare in visited collections (ex. *Mobula*) other species within the same genus were considered replicates for that genus. There was also no morphological sexual dimorphism in external nasal morphology, which agrees with the same conclusion of previous studies on internal nasal morphology (Schluessel et al., 2010). Preliminary analysis for determining the appropriate sample size found that there was no difference in standard error between 3, 6, and 11 replicate individuals in the genus *Pseudobatos* and *Myliobatis*. Replicates ranged from 2-11 individuals per species, with an average of 5 individuals. However, there were 2 species (*Pteroplatytrygon violacea* and *Rhina ancylostoma)* where the minimum sample size of 3 was not possible due to rarity in visited collections.

C. Choosing the representative specimen

One replicate specimen was chosen to be the representative species for each genus. The goal of this method was to minimize distortion of these data that can come with averaging replicates. Instead of analyzing data from a hypothetical species that was the result of averaged measurements, I analyzed data from the actual measurements from the most representative

specimen (Burns, 2019). To choose which replicate would be the representative, I used PCA plots to find the replicate point that was nearest to the centroid of a cloud of all replicate points. The replicate point plotted in space that had the shortest distance to the centroid was chosen as the representative species to be used for further analyses. PCA plots of the replicates were generated for each species in R using ggbiplot with packages devtools and ggbiplot.

Pteroplatytrygon and *Rhina* with only 2 replicates could not be used for this method, therefore for these individuals I chose the specimen that was larger in overall body size (disc width) to be the representative.

D. Size correction

To correct for differences in body size, a linear model was created where each measure was log scaled and regressed against a metric for body size. The statistical analyses were then performed on the size corrected residuals of the regression. Disc width or length is commonly used in interspecific studies to correct for body size in batoids. However, because of the great variance in disc shapes across species (ranging from round to triangular) and because of the comparatively very small measurements relating to the nose morphology, this did not seem appropriate. Head length would also not be appropriate due to the drastic differences in head shapes across batoids (i.e., the long snout of a small guitarfish has a larger head length than a much larger manta ray). Therefore, a new body size metric was created to minimize the effects of the broad differences in body shape across this group. This metric was measured from the last gill slit to the most anterior portion of the nostril, termed "gill to nare" length (GL), which accounts for differences in body size while not conflating measurements due to differing head shapes (Figure 1).

E. Phylogenetic ANOVAs and Mapping

To determine if morphological differences were more than just the result of a shared lineage, I accounted for covariance due to shared ancestry by performing a phylogenetic principal component analysis and phyloANOVA. The phylogeny used was obtained from the open-source database "Vertlife.org" under the "shark subsets" where I was able to manually add each species. The database generated 100 phylogenies using a fully resolved 10-fossil set of 10K phylogenies from Stein et al. (2018). While the relationships were very similar across the 100 phylogenies, I chose the phylogeny that most closely resembled Aschliman et al. (2012), one of the most extensive batoid phylogenies to date. This phylogeny was then used to create a phylogram for ancestral state reconstruction and a phylomorphospace to visualize how nose and snout diversity evolved across Batoidea.

F. Life history

To determine if ecology and other life history traits correlated with nose shape, size, and structure, I compiled data of possible relevant life history literature across the genera sampled here. Traits that may be relevant to olfaction and thus nose morphology included: lifestyle, habitat, swimming mode, and diet. Other metrics that I thought may be relevant to olfaction, including whether the species was migratory, would bury in the substrate, or segregate by sex, were not well-documented enough and ultimately too subjective to include with reasonable sample sizes. Therefore, the ecological metrics chosen here are well-established in the literature.

Lifestyle was categorized as benthic, demersal, bathydemersal, benthopelagic, and pelagic, following the categories and designations outlined in Last el. al, (2016a). It should be noted that all categories have overlap of different degrees. Lifestyle categories represent a sliding scale of water depth where species are categorized by where they spend the majority of their time.

Habitat data were obtained via Fishbase (Froese and Pauly, 2022) and Allen and Robertson

(1994), Arkhipkin et al. (2008), Compagno (1999), Eschmeyer et al. (1983), Last et al. (2016), and Micheal (1993). Habitat data were classified into 4 categories: soft/sandy bottom, rocky/reef bottom, open ocean, and deep sea. For habitat, many rays have some portion of their habitat with a soft/sandy substrate. Species here were categorized into the soft/sandy bottom category if they are exclusively found in this substrate type. Species were categorized into the rocky/reef bottom category if they are also found on rocky/reef substrate as noted by Fishbase. Only three species of batoids in this analysis were considered truly open ocean: the manta ray (*Mobula hypostoma*), the pelagic stingray (*Pteroplatytrygon violacea*), and the spotted eagle ray (*Aetobatus narinari*).

Swimming mode definitions followed traditional classification (Breder, 1926; Webb, 1998) with some recent modification including: body caudal fin (BCF), oscillatory, undulatory, intermediate, and a benthic locomotion "punting." Designations into swimming mode categories follow Breder (1926), Koester and Spirito (2003), Macesic and Kajiura (2010), Rosenberger (2001), Rosenberger and Westneat (1999), Schaefer and Summers (2005), Webb (1994), and Wilga and Lauder (2004). Swimming mode also has varying degrees of overlap, as most batoid locomotion presents on a continuum between undulation and oscillation (Rosenberger, 2001). Batoids were classified as undulatory (>1 wave) or oscillatory (<1/2 wave) based on the number of waves present along their pectoral fin. Batoids between these categories were classified as intermediate. Batoids that distinctly use axial-based locomotion via their caudal fin/tail were classified as body-caudal-fin (BCF) swimmers. Batoids that are also capable of true "punting," a type of benthic locomotion associated with the pelvic fins, were classified as punters (Koester and Spirito, 2003; Macesic and Kajiura, 2010). While punting is not a true swimming mode, it is a method of slow propulsion that could be relevant to odor capture. "True punting" was defined in Macesic and Kajiura, 2010 as batoids that engage only their pelvic fins during benthic

locomotion (and not their disc or caudal fin). In this study, batoids were only classified as punters if they displayed this true punting locomotion, and not "augmented punting" seen in many benthic batoid species.

Diet follows the extensive batoid diet database outlined in Rutledge et al., (2019) that designates diet by biomechanical processing differences, included here were: soft prey (worms, fish), molluscivory (hard bivalves), and crustivory (shelled crustaceans). If diet data were not available for the exact species in question, the diet was inferred based on the diet of its closest intrageneric relative.

G. Statistical analyses

To test if nasal morphology varied with differing life histories in batoids, a one factor analysis of variance (ANOVA; $\alpha = 0.05$) was performed for each life history metric. An ANOVA was performed on each of the 18 measurement variables (PDM, PDX, etc..) for each life history metric (lifestyle: 5 levels, habitat: 4 levels, swimming mode: 5 levels, and diet: 3 levels.) For significant measurements, a post hoc Tukey honest significant differences test was run. ANOVAs were run separately on the size corrected data and again on phylogenetically corrected data (PhyloANOVAs) to understand how shared ancestry influenced the results.

Principle component analyses (PCA) and linear discrimination analyses (LDA) were also completed to visualize nasal morphotypes and correlations with life history. These analyses were performed on all 16 phylogenetically and size corrected continuous measurement traits listed in the morphometric model (therefore excluding two measurements that were count data: (PAN) proximal angle of nare and (HNA) head narial angle).

While useful, dimensionality reductions can exclude important traits for delimitation by focusing only on the axes that explain the most variation (Uyeda et al., 2015; Cadena et al.,

2018). Therefore, a normal mixture model (NMM) analysis, that uses automatic variable selection with no *a priori*i information about delimitating groups, was performed. NMMs assume no information about group designation and instead identifies the number of groups (i.e., morphotypes) and assigns individuals to groups based on the number of distinct normal distributions in the phenotypic data.

All analyses were performed in R studio (R Core Team, 2019) with packages: ggplot2, ape, phytools, geiger, plyr, ggpubr, ggbiplot, devtools, factoextra, MASS, picante, geomorph, tidyverse, magrittr, ggally, clustvarsel, raster, rasterVIS, RColorBrewer.

RESULTS

A. Life History ANOVAs

11 of the 18 morphometric measurements were found to be significantly different between the life history metrics tested (swimming mode, diet, habitat, and lifestyle). These include: HWN, NDMX, ANFM, NSTRL, INM, ANF, AAW, ANW, PAN, HNA, NDMM (see methods for terminology). Of these metrics, 5 of the 11 remained significant with life history: HWN, NDMX, AAW, INM, and PAN (Table 2). These traits include the position and angle of the nostril on the head, the width of the inlet hole, and the spacing of the nostrils from each other. All 5 of these measurements were found to be significant between swimming mode, while 1 (NDMX) was also found to be significant in the lifestyle category. After phylogenetic correction, there were no significant differences in these measurement traits in the habitat or diet categories.

1A. Swimming Mode

With 5 swimming mode levels and 10 significant morphometric measurements, there were 25 significant pairs (See Table 3 for pairs and p-values). The nasal measurements associated with BCF swimmers were significantly different from all other swimming modes

(oscillatory, undulatory, and true punters). Specifically, metrics relating to the size and shape of the inlet hole (AAW, NSTRL), the anterior nasal flap (ANFM), the placement (angle and distance from disc edge) of the nostril on the head (PAN, HNA, INM, NDMX) were all significant metrics that distinguished BCF swimmers from the other swimming modes. However, after correcting for shared ancestry, half of these variables remained significant: HWN, NDMX, AAW, INM, and PAN.

Oscillatory, undulatory, and punting swimmers were found to have nostrils positioned closer to the edge of their head (NDMX) compared to BCF and intermediate swimmers. However, only oscillatory and intermediate swimming modes were significantly different from each other before and after phylogenetic correction. Specifically, oscillatory swimmers had a shorter distance from their nostril to disc margin (NDMX) compared to all other swimmers but were significantly different between intermediate swimmers only ($t= 3.37, p=0.03$). Oscillatory swimmers also had shorter head widths at their nostrils (HWN) compared to intermediate swimmers ($t=2.97, p=0.02$).

BCF swimmers were found to have the greatest distance from their anterior nasal flap (the nasal curtain that covers the excurrent outlet in most rays) to their mouth (ANFM) than undulatory, oscillatory, and intermediate swimmers. The width of the anterior nasal flap (ANF) was also much smaller in BCF swimmers, with oscillatory and intermediate swimmers having the widest anterior nasal flap. Oscillatory and intermediate swimmers were found to have the shortest distance from this flap to their mouth (ANFM). The exposed nostril length (NSTRL) was also much larger in BCF swimmers compared to all others, with oscillatory and intermediate swimmers having the smallest nostril length. However, these traits did not remain significantly different with phylogenetic correction.

BCF swimmers were found to have their nostrils spaced farther apart (INM) than other swimmers, while undulatory swimmers had their nostrils positioned the closest together. This was significantly different in BCF vs. undulatory swimmers ($t=3.75, p=0.04$) after phylogenetic correction. Anterior aperture width, the diameter of the inlet hole (AAW), was found to be significantly different after phylogenetic correction in punters vs. BCF swimmers ($t=4.50, p=0.03$) and undulatory vs. BCF swimmers ($t=5.09, p=0.03$) with both punters and undulatory swimmers having smaller inlet hole diameters than BCF swimmers. Interestingly, oscillatory swimmers were not found to be significantly different from BCF swimmers in this metric.

The angle of the nostril with respect to the head/gill position (HNA) was greater in BCF swimmers compared to all other swimmers (126° vs. 114°), however this metric was not significant after phylogenetic correction. But, the proximal angle of the nare (PAN) was found to be significantly different from all swimming modes after phylogenetic correction when compared to BCF swimmers: undulatory vs. BCF ($t= -6.06, p= 0.01$), punters vs. BCF ($t= -5.32, p=0.01$), intermediate vs. BCF ($t= -5.32, p=0.016$), and oscillatory vs. BCF ($t=-5.32, p=0.035$). Intermediate, oscillatory, and punters had nostrils positioned between ~102°-105°, while undulatory swimmers had nostrils positioned at ~114° and BCF swimmers' nostrils were positioned at ~37°.

3A. Lifestyle

With 5 lifestyle levels and 1 significant morphometric measurement, there were 2 significant pairs (Table 3; Supplementary Table 1). The position of the nostril on the head (NDMX) was significantly different when comparing demersal batoids to both benthopelagic and pelagic batoids. This remained significant after phylogenetic correction with benthopelagic ($t= -3.69, p=0.03$) and pelagic batoids ($t=-2.29, p=0.03$) with nostrils positioned closer to the

edge of their disc and head compared to demersal batoids.

4A. Habitat and Diet

There was no significant difference in any nasal measurements between the 4 habitat levels tested (soft/sandy, rocky/reef, open ocean, and deep sea). Rocky/reef animals and open ocean animals were close to significance for the NDMX metric (*p=0.08*); however, this was not near significance after phylogenetic correction.

With 3 diet levels and 2 significant morphometric measurements, there were 3 significant pairs (Table 3). These traits related to head size and nostril position on the head (HWN, NDMM). Molluscivore batoids like eagle rays and bowmouth guitarfish that eat hard-shelled prey were found to have narrower head widths at their nostrils compared to the other feeding modes. Molluscivores were also found to have nostrils that were positioned closer to the edge of their head than batoids that consume soft prey. However, these traits did not remain significant with phylogenetic correction. The metric NDMM was close to significance between soft prey eaters and molluscivores after phylogenetic correction (Table 3; *t=-2.68, p=0.06*).

B. Phylogenetic Analysis

The phylogram and phylomorphospace highlighted some evolutionary trends. In the phylogram, the ancestral values can be seen in green, while areas of divergence are in blue, red, and yellow. Most of the Rhinopristiformes (excluding *Trygonorhinna*), or guitarfishes, are clustered in blue, while *Psammobatis* (sand skate), *Mobula* (manta ray) are in red, and *Benthobatis* (blind ray) and *Rhinoptera* (cownose ray) are in yellow, suggesting possible evolutionary convergence or parallelism of these corresponding nasal features. The phylomorphospace also showed distinct grouping in space, with long branches across the phylogeny, specifically with the open nare morphotype on the far right and the flush nare on the

far left (Figure 3).

C. Dimensionality Reductions

Swimming mode was found to be the most relevant ecological metric to correlate with nose morphology and an in-depth description of the swimming mode dimensionality reductions are described below. The other ecological metrics (habitat, lifestyle, and diet) were not as informative once phylogenetically corrected (Figures 5-7). However, there were some interesting observations. Benthic and demersal batoids generally occupied larger regions of the morphospace, suggesting more nose diversity in very ground-associated ecologies (Figure 5). While deep sea and bathydemersal species occupied the narrowest region of morphospace. The LDA for lifestyle found that benthic species occupy the largest region of morphospace (Figure 5). Demersal species occupied a smaller but overlapping region in the benthic morphospace. Pelagic and bathydemersal batoids occupied another distinct but partially overlapping region of the morphospace, with benthopelagic species occupying the opposite end of the morphospace (Figure 6). All four habitat types were in complete overlap, with soft sandy habitat and rocky reef occupying the largest morphospace, and open ocean and deep sea occupying smaller regions (Figure 6). The LDA for habitat was not able to discriminate between soft sandy and rocky reef habitat types, but open ocean and deep-sea habitats were in distinct regions in the morphospace, suggesting these nose morphologies are less diverse or possibly more specialized. Batoids that eat soft prey occupied the largest region of morphospace and overlapped with crustacivores (Figure 7). While the LDA for diet revealed that molluscivores can be mostly discriminated in the morphospace, but still had partial overlap with crustacivores (Figure 7). All PCA, PhyloPCA, and LDA loadings for habitat, lifestyle, and diet ecologies can be found in the supplementary.

1C. Swimming Mode Principle Component Analysis

The first two PCs accounted for 65.2% of the total variance (Figure 4). PC1 primarily loaded with traits relating to the position of the nostril in relation to the mouth (NOM, NOX), the distance from the nostril to the most anterior region of the snout (PDM, PDX), the spacing of the nostrils (INM), the size of the inlet hole (AAW) and total exposed nostril length (NSTRL). These traits all loaded negatively. PC2 primarily loaded with traits relating to the anterior nasal flap, also known as the nasal curtain (ANF, ANW, ANL), as well as the distance from this flap to the mouth (ANFM), and the spacing between the outlet nasal chambers (INW). ANF, ANW, and ANL all loaded negatively while ANFM and INW loaded positively. See Table 4 for a complete list of PC1-4 loadings, accounting for 87.9% of the total variance. In the morphospace, we can see BCF swimmers loaded in the top left, while oscillatory swimmers loaded in the bottom left, with almost no overlap. Undulatory, intermediate, and punting batoids all loaded in the middle. Intermediate swimmers did not overlap with undulatory or punting batoids but were in the oscillatory space with some overlap in BCF swimmers. Undulatory and punters had a fair amount of overlap, but both extended farther into opposite regions of the morphospace.

2C. Swimming Mode Phylogenetic Principle Component Analysis

The phylogenetic PCA resulted in grouping patterns quite similar to the standard PCA, but with more overlap (Figure 4, Table 4). PC1 and PC2 loaded with the same traits as described in the standard PCA. The first two PCs accounted for 61.5% of the total variance. The first four PCs accounted for 82.8% of the total variance. The major difference between the two PCAs is that now the undulatory swimmers' noses fully overlap with the oscillatory swimmers' noses. Punters are now distributed evenly between BCF and oscillatory swimmers in the morphospace, while the noses of intermediate swimmers lie mostly in the oscillatory space.

3C. Swimming Mode Linear Discriminant Analysis

The linear discriminant analysis found that the traits that best distinguish nasal morphology by swimming were relating to the distance from the nostril to the most anterior region of the snout (PDX, PDM), the spacing of the incurrent and excurrent nostrils from each other (INM, INW), the distance from the incurrent nostril to the mouth (NOX), and the distance from the nostril to the edge of the head/disc (NDMX). The first two LDs accounted for 80% of the total variance. See Table 4 for a complete list of LDA 1-4 loadings.

C. Normal Mixture Models

The first three principal components were the most useful for group discrimination (number of morphotypes) in the Normal Mixture Models (NMMs). The mixture model that specified 5 morphological groups received the strongest support (Figure 8a). The gaussian finite mixture model identified a Bayesian Information Criterion (BIC) for each of the 16 possible models. The model with the highest BIC score was spherical, unequal volume (VII) with a BIC score of -347.4 (*log-likelihood: -2.03, n=28, ICL=-377.26*). The clustering table found that of the 5 identified morphological groups, there were 10, 7, 5, 4 and 2 individuals in each group (Figure 8b). I hypothesized that there would be 7, 6, 5, 5, and 5 individuals in each group (see the following section on morphotype classification and limitations in discussion section). The second-best model was the diagonal, varying volume, equal shape (VEI) with BIC score of -352.6. The model identified only 2 morphological groups. However, the best model (VII) had a difference of 6 points in BIC score between the second-best model (VEI). BIC scores with differences of six or greater are regarded as strong evidence against lower support models (Kass and Raftery 1995). Therefore, there is strong support for the VII model which parsed out 5 groups or distinct morphotypes from these data.

D. Morphotype Classification

Based on visual examination, statistical significance of measurement traits, and the results of the normal mixture models, appear 5 morphological groups, or morphotypes, found in batoid nasal diversity. Here I suggest a morphological classification system that can be used when describing batoid nasal morphology with ecological and likely hydrodynamic implications (see discussion section). Batoid nasal diversity can be classified into 3 major morphotypes that can be further subdivided into 5 total morphological groups.

The first and most common nasal morphotype is termed the "flush" morphotype, where the incurrent nostril (AAW) is flush on the head of the animal, with no external protrusions. This morphotype can be further subdivided into categories based on the shape of the inlet hole: circle, comma, or intermediate (slit) shaped. This is the most diverse morphotype and can be accompanied with a nasal curtain of square, skirt, or incomplete type (see methods for descriptions). The circle shape can be seen in some myliobatids, dasyatids, narcinids, and gymnurids (Table 1). To be classified as a circle morphotype, the incurrent nostril width should be approximately as wide as it is long. The representative species for the flush circle morphotype is *Narcine entemedor* with a square nasal curtain (Figure 9).

The next subdivision of the flush morphotype, is the comma shape, which describes an inlet opening that resembles a comma or curved kidney bean. The comma shape can be seen in many different species of dasyatids and urotrygonids. To be classified as a comma morphotype, the incurrent nostril opening should be longer than it is wide and narrowest in the medioposterior region of the inlet with a distinct, identifiable constriction. The representative species for the comma shape is *Urobatis maculatus* with a skirt shaped nasal curtain (Figure 10).

The last subdivision of the flush morphotype is the intermediate shape, which describes an oval inlet shape or narrow, slit like opening. The intermediate shape can be seen in some

rhinopterids, dasyatids, and potamotrygonids. To be classified as an intermediate morphotype, the incurrent nostril should be longer than it is wide, with approximately the same width along the length of the inlet, without the distinct constriction seen in the comma morphotype. This can look like the angled oval inlet shape seen in *Rhinoptera* and *Aetobatus*, or long and skinny like in *Potamotrygon*. The representative species for the intermediate shape is *Rhinoptera bonasus* with a skirt shaped nasal curtain (Figure 9).

The next morphotype is the easily identifiable "open" nare morphotype, that was named due to its absence of a closed nasal chamber and excurrent channel. In the open morphotype, the incurrent and excurrent regions of the nostril are not distinct, and only partially divided by the anterior nasal flap (ANF). The nasal lamellae, which are thin sheets of sensory tissue that line the internal nasal chamber in batoids, are easily visible and fully exposed to the environment. The open nare morphotype is exclusively seen in Rhinopristiformes, the guitarfishes and sawfishes. However, not all guitarfishes have this morphotype, as *Trygonorhinna* has a nasal curtain that separates the inlet from the outlet. This morphotype is accompanied with either a reduced or square nasal curtain. The representative species for the open nare morphotype is *Rhina ancylostoma* with a reduced nasal curtain (Figure 9).

The last morphotype is termed the "protruding morphotype" that describes a protruding structure that partially or fully encloses the incurrent nostril. This morphotype can be easily identified by looking at the batoid from the side, laterally, to determine if the nostril protrudes downwards from the body. The protruding morphotype can be seen in torpedids, narkids, and Rajiformes. The protruding morphotype can be either cylindrical, conical, or cupped. Cylindrical nostrils are seen in some torpedo rays, where the inlet hole is fully enclosed in a fleshy, protruding tube. Conical or cupped nostrils are seen in skates, where the inlet hole is flanked

with a protruding flap that can be cone or paddle shaped that extends only partially around the circumference of the inlet opening. This morphotype is accompanied with either an incomplete or square nasal curtain. The representative species for the protruding morphotype is *Beringraja rhina* with an incomplete nasal curtain (Figure 9).

DISCUSSION

This study is the first to quantitatively describe and broadly classify batoid nasal diversity within an ecological and phylogenetic framework. While batoids have impressive olfactory abilities (Meredith et al. 2012) and an expansive nasal morphology, there has been little research into the morphology and biomechanics of their olfactory system, specifically the external odor-harnessing morphology. The morphometric measurements that best distinguish batoid nasal morphology were traits related to the position and angle of the nostrils on the head (NDMX, NDMM, PAN, HNA), the diameter of the inlet and total exposed nostril (AAW, NSTRL), the spacing of the nostrils from each other (INM), the size and shape of the nasal curtain (ANF, ANW), and the distance from the nasal curtain to the mouth (ANFM). This study specifically identified 5 major morphotypes seen in Batoidea and found that swimming mode was the ecological metric that correlated best with batoid external nasal diversity, in terms of statistical significance and distinct groupings in the phylomorphospace.

Swimming mode (BCF, undulatory, oscillatory, intermediate, and punting) correlated best with nasal morphology, resulting in 5 significant morphometric measurements with phylogenetic correction: HWN, NDMX, AAW, INM, and PAN. Oscillatory swimmers (like the eagle rays, bat rays, manta rays) and BCF swimmers (guitarfishes, sawfishes) had narrower heads with nostrils positioned closer to the edge of their disc. BCF swimmers generally had larger incurrent nostril diameters (AAW) when compared to both undulatory and punting

23

batoids, like many Dasyatid stingrays. Oscillatory swimmers were also distinct from intermediate swimmers, with their nostrils positioned closer to the edge of their disc. BCF swimmers also had their nostrils positioned farther apart on their head and positioned at a smaller angle on the head when compared to all other swimmers. These results were slightly unexpected, as generally BCF and oscillatory swimmers had statistically similar traits but were still in distinct regions of the morphospace. This is likely because BCF swimmers could be discriminated from oscillatory swimmers due to differences in the nasal curtain (or anterior nasal flap), but in terms of the inlet hole shape, size, and position, were similar to each other. This could be because compared to the other swimmers, oscillatory and BCF swimmers may operate at higher Reynolds numbers (Re= $uL/v,$ where u is the fluid velocity, L is the characteristic linear dimension, and v is the kinematic viscosity). Many oscillatory and BCF swimmers are some of the largest batoids, with larger inlet hole diameters (even with size correction) and swim at fasters speeds than many of their counterparts. However, swimming mode does not correlate directly with velocity, and if it did, oscillatory swimmers would likely be statistically significant from all other swimming modes, which it was not. The motion in which the animal swims, and thus directs odors into its nose, may also influence odor capture. For example, BCF swimmers move their heads in a wide lateral sweeping motion (i.e. yawing), which may help entrain and flush their more horizontally expanded nostrils. Oscillatory swimmers, that swim with a more vertical up and down motion (i.e. pitching), have more vertically oriented nostrils, that are oval or comma shaped. Undulatory swimmers are generally more dynamic swimmers, capable of quick movements and turns, and displayed a diversity of flush nostril types. Overall, of the proposed morphotypes, BCF swimmers were found to possess the open nare morphotype, punters had the protruding nare morphotype, and oscillatory, undulatory, and intermediate swimmers had the flush morphotype.

Within the flush morphotype, oscillatory and undulatory swimmers generally had comma or intermediate shaped inlets, and intermediate swimmers had circle or intermediate inlet shapes.

Habitat (soft/sandy, rocky/reef, deep sea, open ocean) was not a relevant metric for discriminating external nasal morphology in batoids. This was surprising because elasmobranchs that live in the open ocean and deep-sea have been shown to have the largest olfactory bulbs, a reliable proxy for olfactory sensitivity, indicating that a heightened sense of smell may be important for these ecologies (Yopak et al., 2015, 2019). Additionally, reef associated species were found to have the smallest olfactory bulbs but enlarged optic tecta (a region of the brain associated with visual cues). While there was no statistical difference in the measurement traits of habitat groups in this study, both deep sea and open ocean batoids did show discrimination in the linear discriminant analysis (LDA), both in distinct regions of the morphospace from the overlapping rocky reef and soft sandy habitats. Both deep sea and open ocean species represented much smaller regions of the morphospace, suggesting less diversity in external nasal features. However, there was also fewer representative species in both of these categories. The deep sea and open ocean species in this study generally had more circular inlet holes, with the circle or protruding nare morphotypes, and most commonly, the incomplete nasal curtain. Whether this circular inlet shape confers any sort of odor-harnessing advantage over other inlet shapes (comma, slit shaped) is unknown. Open ocean batoids, that generally swim at faster speeds, may not require a more specialized odor capturing morphology. Many deep-sea species, like skates, are generally slow moving and their protruding nare morphotype may help to capture odor in these slow flow environments.

The five lifestyle categories (benthic, demersal, bathydemersal, benthopelagic, and pelagic) following Last et al. (2016b) resulted in only one statically significant morphometric

measurement: NDMX, the distance from the medial edge of the incurrent nostril to the disc. Specifically, demersal rays were found to have their nostrils positioned more medially on their head, farther away from the edge of their disc when compared to both benthopelagic and pelagic rays. Benthopelagic and pelagic batoids included the pelagic stingray, eagle rays, bat rays, cownose rays, and manta rays. Previous research looking at the lamellae count of benthopelagic elasmobranchs found that on average they have 93 lamellae, as opposed to an average of 56 in benthic species (Meng and Yin, 1981). However, as previously noted, lamellae count alone is not a reliable proxy for olfactory sensitivity. The myliobatid rays in this open ocean group (manta ray, eagle ray, bat ray, and cownose ray) also have some of the largest brains of all elasmobranchs, with an enlarged telencephalon (Northcutt, 1978), which, like the olfactory bulb, also processes olfactory information. The spotted eagle ray is also known to have a very large sensory surface area relative to other elasmobranchs, and an allometric relationship with lamellae count and internarial distance (INM), suggesting olfaction may be very important to this species throughout its life (Schluessel et al., 2010). These more open ocean, migratory batoids generally have their nostrils positioned closer to the edge of their disc and head. From a sensory perspective, it is likely more advantageous to have nostrils positioned more anterolaterally on the body, where it could be easier to receive a chemical cue. Contrary to the typical stingray body plan, many myliobatids also have more prominent, protruding heads and snouts, which is likely why the head widths at the nare (HWN) did not remain significant with phylogenetic correction. Regardless, a more sharply pointed head with nostrils positioned closer to the edge, may help quicken the time it takes for an odorant to reach the nostril (if already oriented into a plume). Overall, benthopelagic and pelagic rays were commonly observed with the intermediate or comma nare morphotype. These nostrils were generally oval in shape and the incurrent nostril

was angled to a higher degree on the head. Demersal rays were generally more variable in morphology, with all 5 nare morphotypes observed in this group. The phyloPCA did show separation between demersal and benthopelagic rays, and the LDA was able to discriminate between benthopelagic, pelagic, and bathydemersal species.

Diet (molluscivory, crustacivory, soft prey) based on biomechanical processing differences, was found to be not very informative for discriminating nasal morphologies. It seemed possible that certain prey items (fish vs. bivalves) would require a greater degree of fine scale odor tracking that may influence the evolution of a more robust nasal morphology. Previous research looking at elasmobranch olfactory bulb mass found that crustacean eating elasmobranchs had lower bulb mass than mollusk and echinoderm eating elasmobranchs (Schluessel et al., 2010). However, the external morphology of batoids that eat different prey items did not reflect this. Without accounting for phylogeny, molluscivore batoids (eagle rays, bat rays, and bowmouth guitarfish) had nostrils positioned significantly closer to the edge of their head than batoids that consume soft prey. However, with phylogenetic correction, this pattern did not hold and there was much overlap in the morphospace between diet types. Interestingly, the LDA was able to distinguish molluscivores from the other two overlapping prey types, but this could be more related to the narrow head widths seen in myliobatids than other nasal features.

Based on the morphometric measurements of this study alone, the NMMs identified 5 major morphotypes seen in batoids. This model was able to identify the open nare morphotype easily. It was also able to identify a separate group inside the comma morphotype. However, all other groups had some discrepancy with hypothesized and realized groups. This is likely because these data did not include all relevant features including important angle measurements, as well

as other defining traits such as nasal protrusion length and the complex shapes of the inlet hole. These data had to be omitted for this type of analysis. Specifically, measurements had to be applicable across all batoids and was therefore limited to features present in all batoids and known homologous features (like the anterior nasal flap and nasal curtain). Therefore, presence/absence traits like the additional nasal flaps of guitarfish and butterfly rays, and the conical projection of many skates and electric rays, could not be incorporated into this model. If these unique features could be better captured quantitatively, this may help explain additional variance between morphotypes. The measurements in this study aimed to be as discrete as possible to minimize subjectivity. The width and length of the incurrent nostril was measured, but this alone could not capture the variation in complex nostril inlet shapes. Angle data also could not be included in the NMMs analyses because it was count data, but it did show statistical significance across groups, suggesting this is an important character for discrimination. It may be beneficial for future studies to incorporate geometric morphometric analyses of nostril inlet shapes, however picking repeatable points around the incurrent nostril may be challenging.

The proposed 5 major morphotypes all have functional implications for odor capture. Batoid olfaction is a hydrodynamic process, that relies upon odor to be directed into the nose. Without a direct pump inside the nasal cavity, the morphology of the system is likely crucial for successful odor capture. Additionally, an odorant molecule will have the challenge of overcoming the boundary layer surrounding a swimming fish: the thin layer of stationary fluid (*velocity = 0*) that encapsulates its body. This layer acts a barrier to odor transport. While the mechanisms for which odor is harnessed into the batoid nose has not been explored, it is hypothesized that batoid olfaction relies upon one or a combination of the following mechanisms: RAM ventilation, the buccopharyngeal pump, pressure differences, or some other

form of unknown mechanical agitation (movement of jaw bones) (Settles, 2005; Cox, 2008).

RAM ventilation is more likely to be observed in faster swimming animals with nostrils

positioned directly in the path of water flow. The buccopharyngeal pump refers to the water that

is drawn into the mouth of the animal during mouth-associated respiration (vs. spiracle only

respiration). Because the outlet nostril channel of some batoids is positioned directly above the

mouth underneath the nasal curtain, this could help to direct water flow through the nasal

chamber as water is sucked into the mouth. The farther the nostrils are positioned from the

mouth, the less likely the buccopharyngeal pump plays a meaningful role in nasal irrigation.

Pressure differences between the outlet and inlet could also generate flow through the nose. If the

incurrent and excurrent nostrils are positioned at right angles from each other, or at different

heights, this could help stimulate flow into and through the nasal chamber. Specific odor

harnessing mechanisms are more likely in some morphotypes than others.

The open nare morphotype, seen exclusively in guitarfishes and sawfishes, was easily

identified and discriminated in all statistical tests. Batoids with the open nare morphotype are

benthic or demersal and all BCF swimmers. This morphotype is fully exposed to the

environment with visible lamellae, the absence of a nasal curtain, and a less distinct path for odor

to follow for through the nasal chamber. The open nare morphotype was generally positioned

close to the edge of the head and relatively far from the mouth. Because the open nare

morphotype is not fully enclosed like the other morphotypes, it would be more difficult to

generate a pressure difference between the inlet and outlet. Additionally, the buccopharyngeal

pump may be less influential in odor capture in this morphotype.

The flush morphotype, the most common morphotype seen across a diversity of batoids,

ranging from fast swimming, oscillatory eagle rays to slower swimming, undulatory round rays,

was harder to statistically discriminate. While this morphotype has a diversity of inlet shapes, the flush morphotype may have the least specialized external morphology for odor capture. If a batoid is swimming parallel in the water column with flush nostrils on the underside of its head, odorants will have to make a sharp turn of up to 90° to enter the nasal chamber for sensory processing. This, coupled with the odor-impeding boundary layer, may make odor capture more difficult for the flush morphotype. However, this is not to say batoids with this nose type have reduced olfactory abilities. In fact, we know that eagle rays have some of the most sensitive noses (Schluessel et al., 2010). However, eagle rays are more pelagic, swim at faster speeds, and have their nostrils positioned more anteriorly on their head, which may make odor capture easier. Additionally, it is also possible that more specialized external morphologies did not provide a selective advantage for some species.

The protruding nare morphotype is seen across the batoid phylogeny and may represent convergence on an odor harnessing morphotype. The protruding nare morphotype may be an adaptation to overcome the challenge of the boundary layer, by projecting the incurrent nostril out of the boundary layer to make odor harnessing easier. The protruding nare morphotype is seen in batoids that are generally slower swimmers that associate closely with the ground, often in the deep sea, and display a "true" punting behavior (skates and electrics rays).

This study provides the first crucial step in better understanding batoid olfaction, by understanding the diversity of the morphology of the system. My analyses reveal that batoid nasal morphology is not just the result of shared ancestry and appear to be convergence on specific morphotypes. Specifically, the swimming mode of the animal, was found to be most significant ecological factor. Because odor capture is a strictly hydrodynamic process, it may be that factors relating more directly to the fluid dynamics (i.e. swimming mode, velocity, Reynolds

number) may be more important in shaping the evolution of the diversity of batoid noses than other ecological factors like habitat and diet. Future studies should explore the fluid dynamics of odor capture of each morphotype, to determine if there are functional differences in the odor-harnessing mechanisms of these nose shapes.

Figure 1. The morphometric measurements used in this study to describe batoid nose morphology. Measurements are outlined on two disparate morphotypes, as shown on a generic a) urotrygonid stingray and b) rhinobatid guitarfish. The central drawings show the ventral view of the head and oronasal region. The flanking drawings are of the nose and mouth (oronasal region) isolated from the head. The incurrent channel is designated by the anterior aperture width (AAW). The nasal curtain in stingrays and anterior nasal flap in guitarfish (ANF), a homologous structure, is colored in light blue. The excurrent channel in stingrays is underneath the lifted nasal curtain, shown on the right-hand side drawing. The excurrent channel in guitarfishes is to the left of the anterior nasal flap.
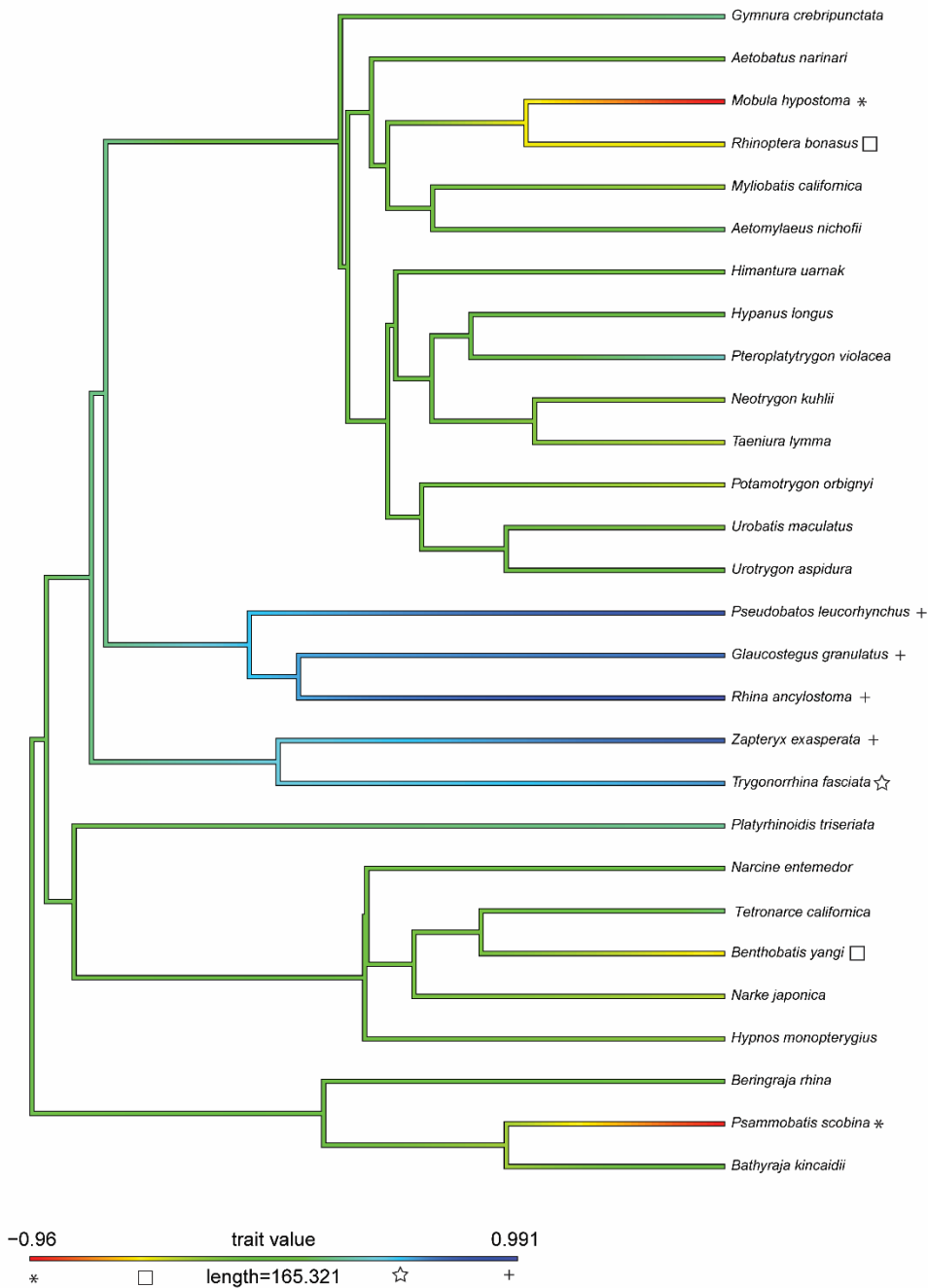
Figure 2. Phylogram showing the evolutionary relationships (based on Aschliman et al. 2012) of all 28 species in this study. The trait value heat map shows intermediate trait values in green (that are reconstructed to be ancestral) and evolutionary divergence in red or blue. Here, most guitarfishes are highlighted in dark blue (+) except for one (☆), a skate and manta ray in red (*), and cownose ray and blind electric ray in yellow (□), suggesting divergent nasal features in these groups. Symbols added for colorblind assistance.
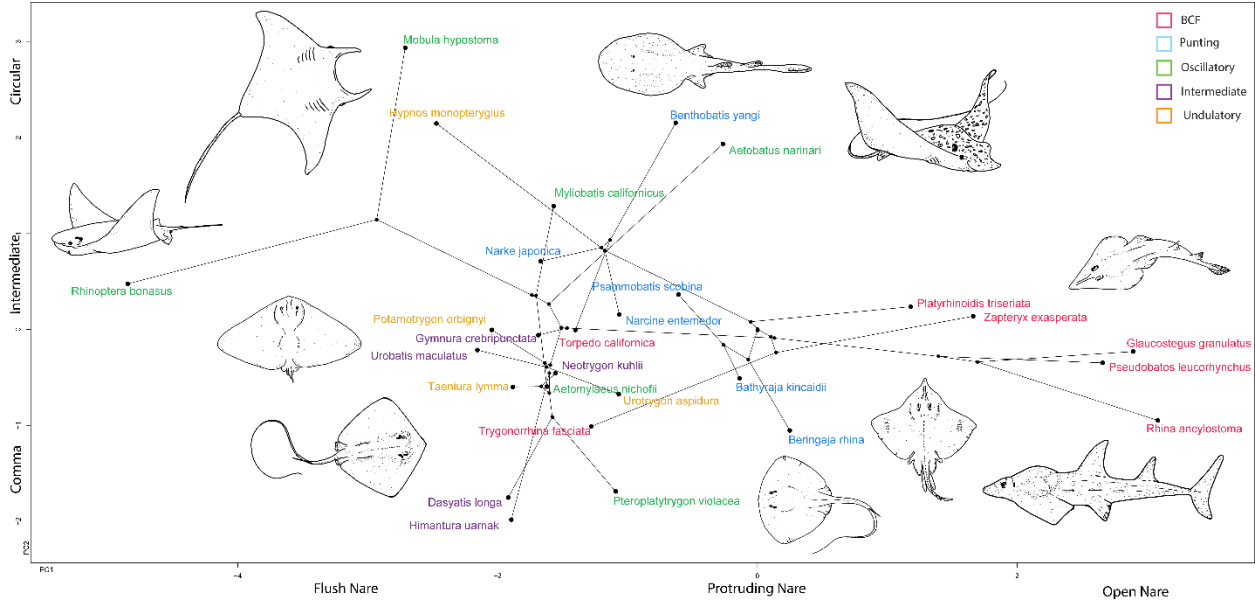
Figure 3. Phylomorphospace (relationships based on Aschliman et al. 2012) showing the results of the PhyloPCA morphometric measurements on nasal morphology colored coded by swimming type. Morphotypes overlaid on axes and representative batoids illustrated in the morphospace. Long branches extending across the phylomorphospace indicate convergent evolution.
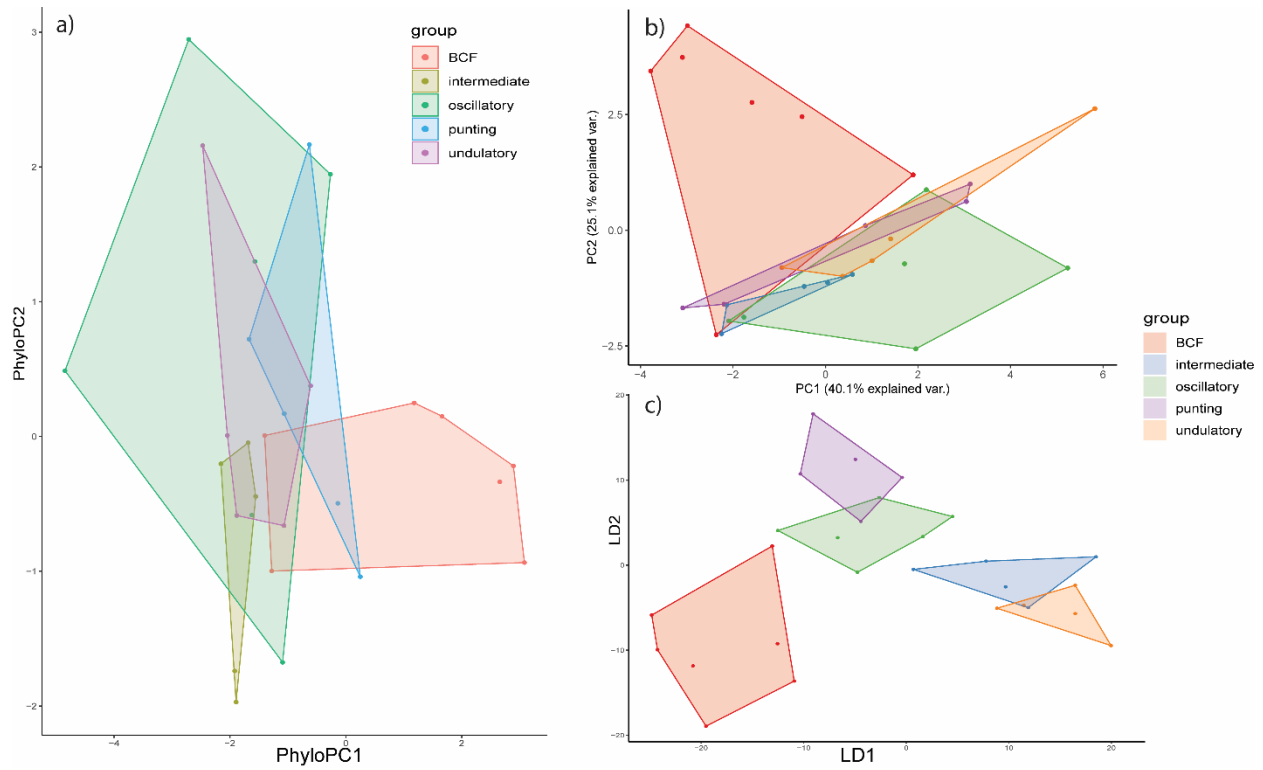
Figure 4. Results of nasal morphology grouped by swimming mode for a) phylogenetically corrected principal component analysis b) standard principal component analysis and c) linear discriminant analysis. Axis loadings are listed in Table 4.
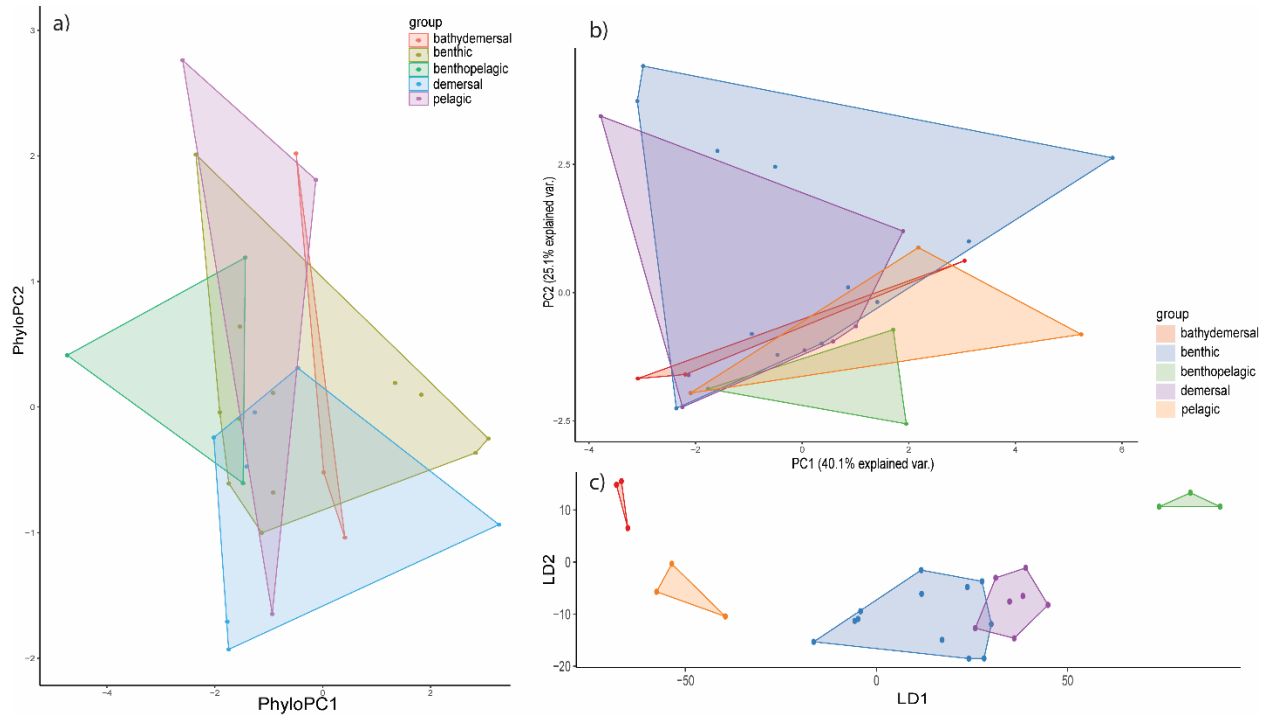
Figure 5. Results of nasal morphology grouped by lifestyle for a) phylogenetically corrected principal component analysis b) standard principal component analysis and c) linear discriminant analysis. Axis loadings are listed in supplementary.
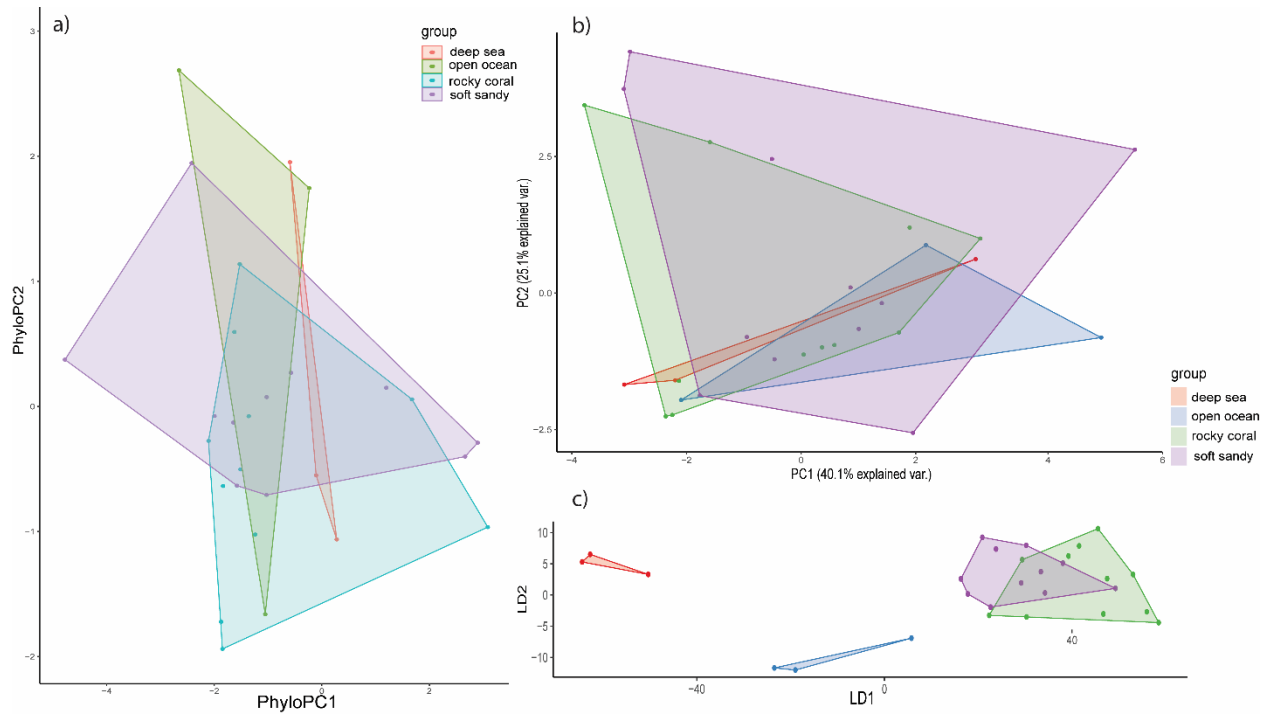
Figure 6. Results of nasal morphology grouped by habitat for a) phylogenetically corrected principal component analysis b) standard principal component analysis and c) linear discriminant analysis. Axis loadings are listed in supplementary.
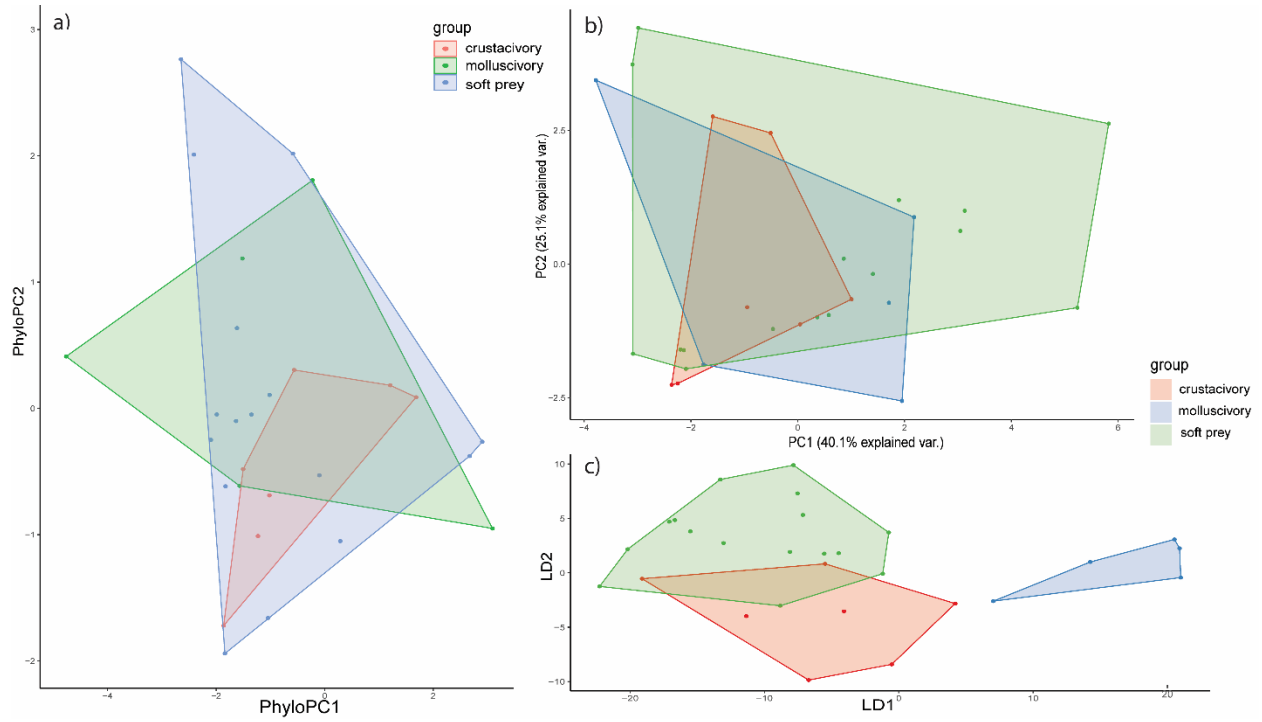
Figure 7. Results of nasal morphology grouped by diet for a) phylogenetically corrected principal component analysis b) standard principal component analysis and c) linear discriminant analysis. Axis loadings are listed in supplementary.
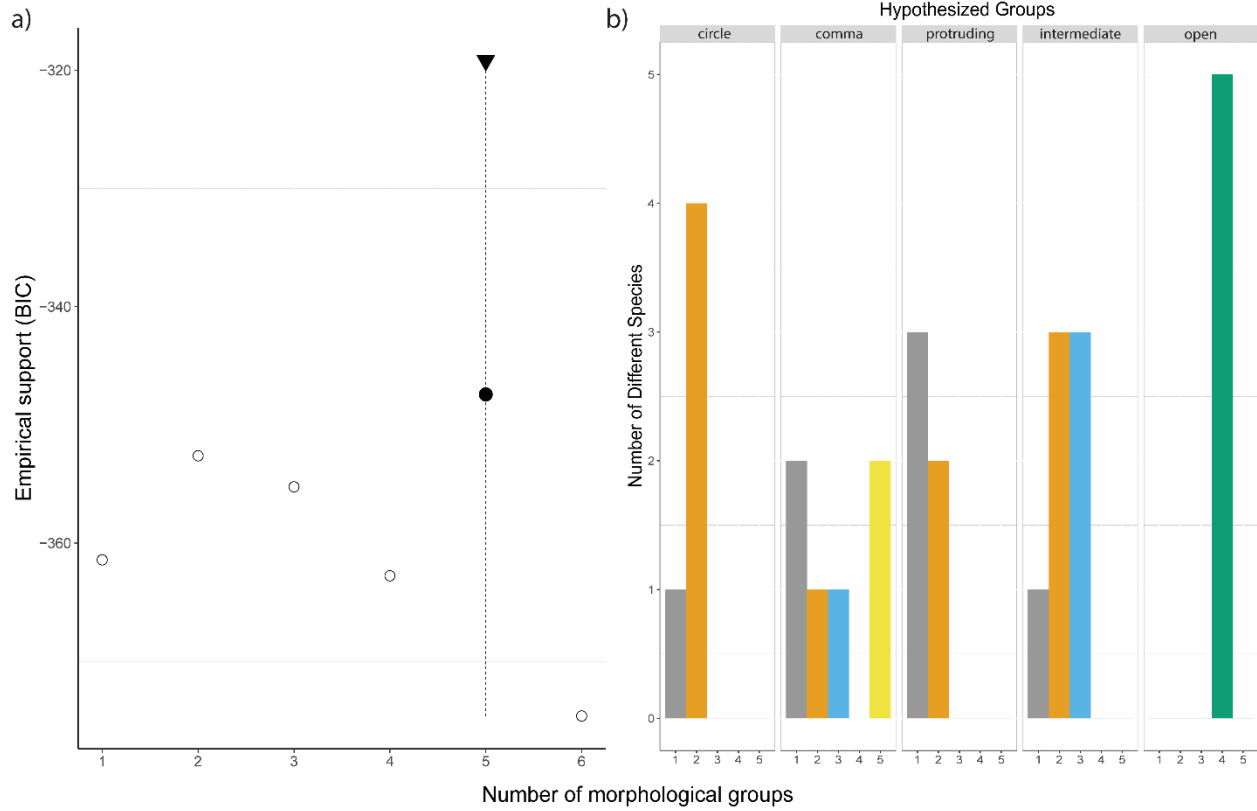
Figure 8. Results from the Normal Mixture Model analysis that assumes no *a priori* information about groups. A) graph showing the BIC score and corresponding model (VII) with the highest empirical support identified 5 distinct morphotypes in these data. B) histogram comparing the assignment of individuals to groups between the best Mclust models and the hypothesized morphotypes (open, flush [circle, comma, intermediate], and protruding).

39
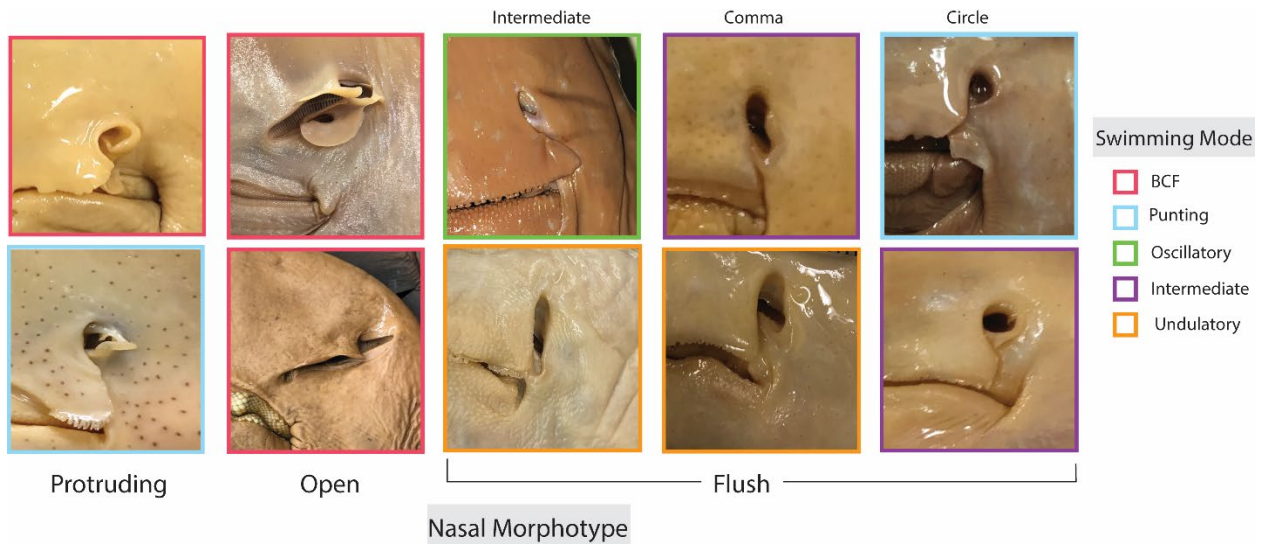
Figure 9. The major nasal morphotypes identified in this study: protruding, open, and flush. Flush has 3 subcategories including intermediate, comma shaped, and circular. From top left going down each row: *Tetronarce california, Beringraja rhina, Pseudobatos leucorhynchus, Rhina ancylostoma, Rhinoptera bonasus, Potamotrygon orbignyi, Urobatis maculatus, Urotrygon aspidura, Narcine entemedor, Gymnura micura*. Color coded based on swimming mode.

Table 1. Representative species in this study across all four orders in Batoidea and 17 families classified by nasal curtain and the newly described here "nare type."

Order	Family	Species	Nasal Curtain	Nare Type	Replicates
Rajiformes	Arhynchobatidae	*Bathyraja kincaidii*	incomplete	protruding	6
Rajiformes	Arhynchobatidae	*Psammobatis scobina*	incomplete	protruding	4
Rajiformes	Rajidae	*Beringaja rhina*	incomplete	protruding	5
Myliobatiformes	Aetobatidae	*Aetobatus narinari*	incomplete	comma	6
Myliobatiformes	Dasyatidae	*Taeniura lymma*	skirt shaped	intermediate	4
Myliobatiformes	Dasyatidae	*Neotrygon kuhlii*	skirt shaped	intermediate	4
Myliobatiformes	Dasyatidae	*Pteroplatytrygon violacea*	skirt shaped	comma	2
Myliobatiformes	Dasyatidae	*Hypanus longus*	square	comma	7
Myliobatiformes	Dasyatidae	*Himantura uarnak*	skirt shaped	comma	4
Myliobatiformes	Gymnuridae	*Gymnura crebripunctata*	skirt shaped	circle	10
Myliobatiformes	Hypnidae	*Hypnos monopterygius*	incomplete	circle	3
Myliobatiformes	Mobulidae	*Mobula hypostoma*	square	circle	2
Myliobatiformes	Myliobatidae	*Aetomylaeus nichofii*	square	intermediate	4
Myliobatiformes	Myliobatidae	*Myliobatis californica*	square	intermediate	11
Myliobatiformes	Rhinopteridae	*Rhinoptera bonasus*	skirt shaped	intermediate	5
Myliobatiformes	Urotrygonidae	*Urotrygon aspidura*	skirt shaped	comma	4
Myliobatiformes	Urotrygonidae	*Urobatis maculatus*	skirt shaped	comma	7
Myliobatiformes	Potamotrygonidae	*Potamotrygon orbignyi*	square	intermediate	6
Rhinopristiformes	Rhinidae	*Rhina ancylostoma*	reduced	open	2
Rhinopristiformes	Rhinobatidae	*Trygonorrhina fasciata*	reduced	intermediate	3
Rhinopristiformes	Rhinobatidae	*Zapteryx exasperata*	reduced	open	6
Rhinopristiformes	Rhinobatidae	*Glaucostegus granulatus*	reduced	open	4
Rhinopristiformes	Rhinobatidae	*Pseudobatos leucorhynchus*	reduced	open	11
Rhinopristiformes	Trygonorrhinidae	*Platyrhinoidis triseriata*	reduced	open	5
Torpediniformes	Torpedinidae	*Tetronarce californica*	square	protruding	5
Torpediniformes	Narcinidae	*Benthobatis yangi*	square	circle	5
Torpediniformes	Narcinidae	*Narcine entemedor*	square	circle	5
Torpediniformes	Narkidae	*Narke japonica*	square	protruding	3

Table 2. Significant nasal measurements with their corresponding life history variables. Bolded measurements remained significant with phylogenetic correction. Acronyms are as follows: head width at narial opening (HWN), distance from nostril to disc margin maximum (NDMX), anterior nasal flap to mouth distance (ANFM), anterior aperture width/nare opening (AAW), exposed nostril length (NSTRL), distance across anterior nasal apertures (INM), anterior nasal flap base length (ANF), anterior nasal flap distal width (ANW), proximal angle of nare (PAN), head nostril angle (HNA), distance from nostril to disc margin minimum (NDMM).

Life History Variable	Significant Measurement
swimming, diet	**HWN**
swimming, lifestyle	**NDMX**
swimming	ANFM
swimming	**AAW**
swimming	NSTRL
swimming	**INM**
swimming	ANF
swimming	ANW
swimming	**PAN**
swimming	HNA
diet	NDMM

Table 3. Significant pairs of ecological traits for ANOVAs and PhyloANOVAs. Ecological traits are classified by swimming mode, lifestyle, and diet. There were no significant values for habitat. If measurement values remained significant after phylogenetic correction, they are bolded here. Residual mean pair 1 refers to the size corrected mean of the first listed ecological trait for that measurement in the pairwise comparison. Residual mean pair 2 refers to the second trait in the listed pair. The metrics PAN and HNA were angle measurements and therefore not size corrected.

Ecological Trait	Significant Pair	Measurement	p-value	phylo p-value	Residual Pair 1	means Pair 2
Swimming Mode	**oscillatory-intermediate**	**HWN**	**0.048**	**0.020**	-0.318	0.267
	oscillatory-BCF	NDMX	0.031	0.680	-0.699	0.239
	oscillatory-intermediate	**NDMX**	**0.020**	**0.030**	-0.699	0.384
	intermediate-BCF	ANFM	0.006	0.230	-0.916	1.461
	oscillatory-BCF	ANFM	0.004	0.256	-0.906	1.461
	undulatory-BCF	ANFM	0.021	0.234	-0.577	1.461
	intermediate-BCF	AAW	0.016	0.315	-0.061	0.625
	oscillatory-BCF	AAW	0.001	0.136	-0.220	0.625
	punt-BCF	**AAW**	**0.004**	**0.030**	-0.169	0.625
	undulatory-BCF	**AAW**	**3.25E-04**	**0.030**	-0.381	0.625
	punt-BCF	NSTRL	0.049	0.320	-0.705	0.661
	undulatory-BCF	**INM**	**0.008**	**0.040**	-0.345	0.369
	intermediate-BCF	ANF	0.028	0.630	0.290	-0.480
	oscillatory-BCF	ANF	0.017	0.630	0.299	-0.480
	intermediate-BCF	ANW	0.002	0.120	0.618	-1.176
	oscillatory-BCF	ANW	0.001	0.126	0.610	-1.176
	punt-BCF	ANW	0.051	0.217	0.062	-1.176
	undulatory-BCF	ANW	0.020	0.160	0.234	-1.176
	intermediate-BCF	**PAN**	**1.87E-04**	**0.016**	105.4	37.3
	oscillatory-BCF	**PAN**	**1.87E-04**	**0.035**	102.0	37.3
	punt-BCF	**PAN**	**2.63E-04**	**0.010**	103.6	37.3
	undulatory-BCF	**PAN**	**3.22E-05**	**0.010**	114.8	37.3
	oscillatory-BCF	HNA	0.020	0.544	114.0	126.6
	punt-BCF	HNA	0.041	0.306	114.6	126.6
	undulatory-BCF	HNA	0.021	0.210	113.4	126.6
Lifestyle	**demersal-benthopelagic**	**NDMX**	**0.010**	**0.030**	0.520	-0.740
	demersal-pelagic	**NDMX**	**0.018**	**0.030**	0.520	-0.650
Diet	crustacivory-molluscivory	HWN	0.043	0.084	0.120	-0.360
	soft prey-molluscivory	HWN	0.044	0.084	0.060	-0.360
	soft prey-molluscivory	NDMM	0.033	0.063	0.150	-0.670

Table 4. Loadings for the three dimensionality reduction analyses performed based on swimming mode and benthic locomotion for nasal morphology.

	PhyloPC1	PhyloPC2	PhyloPC3	PhyloPC4		PC1	PC2	PC3	PC4		LD1	LD2	LD3	LD4
PDM	0.358415	-0.731064	-0.329224	-0.17423	**PDM**	-0.3662	0.04277	-0.015	-0.0929	**PDX**	-5.8775	5.38019	-0.097	-5.641
PDX	0.296977	-0.795711	-0.2877	-0.246346	**PDX**	-0.3661	-0.0138	0.00842	-0.1765	**NDMM**	-5.8267	4.20162	-0.1314	-2.6832
TDW	-0.354549	-0.012878	0.1915779	0.621617	**TDW**	0.1497	-0.0353	0.25069	0.73888	**NOX**	-4.2282	13.9905	5.34926	-5.0602
HWN	-0.069644	-0.814708	0.1138645	0.386129	**HWN**	-0.2169	-0.1271	0.454	0.0979	**NOM**	-2.781	-6.8678	-3.4465	5.55828
NOM	0.091308	-0.755899	-0.514956	-0.077232	**NOM**	-0.305	-0.2583	-0.0741	-0.0618	**INM**	-2.6928	-12.98	-3.8538	5.81279
NOX	0.332519	-0.697453	-0.309181	-0.325707	**NOX**	-0.3668	0.02301	-0.1609	0.05602	**AAW**	-2.4437	0.67281	-1.494	-3.2768
NDMM	-0.265482	-0.81828	0.250002	0.2819955	**NDMM**	-0.0987	-0.1793	0.54049	-0.1477	**ANF**	-1.5483	4.17596	1.03328	-1.164
NDMX	-0.017161	-0.89367	0.3302264	0.185599	**NDMX**	-0.2245	-0.0016	0.49494	-0.1011	**TDW**	-1.1788	0.50317	-0.4022	1.20264
ANFM	0.945218	0.099712	-0.154005	0.2371911	**ANFM**	-0.2017	0.32414	-0.0925	-0.0207	**ANFM**	-0.4606	0.68761	0.52935	0.47914
AAW	0.447764	-0.624716	0.0014959	0.0643149	**AAW**	-0.2937	0.2262	0.04218	0.29185	**NSTRL**	1.0319	-1.7538	-0.9231	-0.4729
NSTRL	0.37073	-0.591269	0.3409369	-0.260535	**NSTRL**	-0.2934	0.12316	0.03765	0.01334	**ANW**	1.65861	-2.6363	-0.6476	1.29334
INM	0.3993	-0.377495	-0.412658	0.0542433	**INM**	-0.3077	0.06441	-0.2209	0.38583	**INW**	1.70149	7.7058	2.10868	-10.95
INW	-0.085349	-0.310122	-0.829685	0.1893928	**INW**	-0.1808	-0.3627	-0.2163	0.28184	**ANL**	2.54744	-1.5242	-1.2392	2.45297
ANF	-0.366511	-0.259489	-0.815896	0.2267964	**ANF**	-0.0331	-0.4695	-0.0918	0.09302	**HWN**	3.26275	2.67096	2.30476	2.9632
ANL	-0.18226	-0.447088	-0.547436	-0.413395	**ANL**	-0.1494	-0.3699	-0.2113	-0.2033	**NDMX**	5.87935	-5.8719	1.35638	0.34538
ANW	-0.703215	-0.164903	-0.518738	0.2262684	**ANW**	0.10449	-0.4657	0.0431	0.04066	**PDM**	7.11214	-6.7245	-0.3669	7.25542

CHAPTER 1- SUPPLEMENTARY MATERIALS

Supplementary Table 1. Mueseum accession numbers.

Mueseum #	Family	Species
MCZ_coffin_M15_117	Myliobatidae	Aetobatus_narinari
MCZ_coffin_M15_397	Myliobatidae	
MCZ_36327	Myliobatidae	
MCZ_37003	Myliobatidae	
LACM_948	Myliobatidae	
FFNU_P_2001	Myliobatidae	
LACM_38317_8	Myliobatidae	Aetomylaeus_nichofii
LACM_38117_32	Myliobatidae	
LACM_38117_32	Myliobatidae	
MCZ_S_1393	Myliobatidae	
LACM_10438_5	Arhynchobatidae	Bathyraja_kincaidii
LACM_44364_7	Arhynchobatidae	
LACM_37056_2	Arhynchobatidae	
LACM_11757_4	Arhynchobatidae	
LACM_11757_4	Arhynchobatidae	
LACM_38368_1	Arhynchobatidae	
JFBN_49336	Narcinidae	Benthobatis_yangi
JFBN_49337	Narcinidae	
JFBN_49338	Narcinidae	
JFBN_49339	Narcinidae	
JFBN_49340	Narcinidae	
LACM_31982_11	Rajidae	Beringraja_binoculata
LACM_30633_3	Rajidae	
LACM_W59_116	Rajidae	
LACM_44347_3	Rajidae	Beringraja_rhina
LACM_36256_2	Rajidae	
LACM_38132_46	Glaucostegidae	Glaucostegus_granulatus
LACM_38132_46	Glaucostegidae	
MCZ_59272	Glaucostegidae	
MCZ_S_981	Glaucostegidae	
LACM_W49_126	Gymnuridae	Gymnura_crebripunctata
LACM_W49_126	Gymnuridae	
LACM_W49_126	Gymnuridae	
LACM_W49_126	Gymnuridae	
LACM_W49_126	Gymnuridae	
LACM_W49_126	Gymnuridae	

LACM_J540	Gymnuridae	
LACM_J540	Gymnuridae	
LACM_J540	Gymnuridae	
LACM_J540	Gymnuridae	
MCZ_S_675	Dasyatidae	Himantura_uarnak
MCZ_S_809	Dasyatidae	
LACM_38306_22	Dasyatidae	
LACM_38136_48	Dasyatidae	
LACM_1_108	Dasyatidae	Hypanus_longus
MCZ_40415	Dasyatidae	
MCZ_40416	Dasyatidae	
MCZ_40417	Dasyatidae	
LACM_38106_1	Dasyatidae	
LACM_31780_38	Dasyatidae	
LACM_31778_45	Dasyatidae	
MCZ_985	Dasyatidae	Hypnos_subnigrum
MCZ_984	Dasyatidae	
MCZ_38602	Dasyatidae	
MCZ_S_683	Mobulidae	Mobula_hypostoma
MCZ_S_1378	Mobulidae	
LACM_30206_1	Mobulidae	Mobula_japanica
LACM_W62_90	Myliobatidae	Myliobatis_californica
LACM_W62_90	Myliobatidae	
LACM_W62_90	Myliobatidae	
LACM_W62_90	Myliobatidae	
LACM_W62_90	Myliobatidae	
LACM_3_104	Myliobatidae	
MCZ_348	Myliobatidae	
MCZ_348	Myliobatidae	
MCZ_348	Myliobatidae	
MCZ_36559	Myliobatidae	
LACM_1_187	Myliobatidae	
LACM_32099_1	Narcinidae	Narcine_entemedor
LACM_W52_31	Narcinidae	
LACM_9444_6	Narcinidae	
LACM_4996	Nacrinidae	
LACM_4997	Narcinidae	
MCZ_S_1340	Narkidae	Narke_japonica
MCZ_S_1340	Narkidae	
MCZ_S_1340	Narkidae	
LACM_42482_1	Dasyatidae	Neotrygon_kuhlii

MCZ_S_810	Dasyatidae	
MCZ_S_227	Dasyatidae	
MCZ_50651	Dasyatidae	
LACM_6669_6	Trygonorrhinidae	Platyrhinoidis_triseriata
LACM_6669_6	Trygonorrhinidae	
LACM_6669_6	Trygonorrhinidae	
LACM_W70_7	Trygonorrhinidae	
LACM_2031	Trygonorrhinidae	
LACM_30370_1	Potamotrygonidae	Potamotrygon_humboldtii
LACM_30370_1	Potamotrygonidae	
MCZ_79174	Potamotrygonidae	
LACM_57139_1	Potamotrygonidae	
LACM_43187_1	Potamotrygonidae	
LACM_43187_1	Potamotrygonidae	
LACM_10455_1	Arhynchobatidae	Psammobatis_scobina
LACM_10455_2	Arhynchobatidae	
LACM_10455_3	Arhynchobatidae	
LACM_10455_4	Arhynchobatidae	
LACM_33805_73	Rhinobatidae	Pseudobatos_leucorhynchus
LACM_48221_10	Rhinobatidae	
LACM_48225_6	Rhinobatidae	
LACM_48242_2	Rhinobatidae	
LACM_48242_2	Rhinobatidae	
SIO_79_221	Dasyatidae	Pteroplatytrygon_violacea
LACM_39578_1	Dasyatidae	
LACM_CCS79_3_6	Rhinidae	Rhina_ancylostoma
LACM_38117_38	Rhinidae	
MCZ_S_374	Rhinopteridae	Rhinoptera_bonasus
MCZ_S_374	Rhinopteridae	
MCZ_coffin_24_2_37981	Rhinopteridae	
MCZ_coffin_24_2_37982	Rhinopteridae	
LACM_38129_82	Rhinopteridae	
MCZ_1251	Dasyatidae	Taeniura_lymma
MCZ_40480	Dasyatidae	
MCZ_40480	Dasyatidae	
LACM_37430_7	Dasyatidae	
LACM_57727_1	Torpedinidae	Tetronarce_californica
LACM_44846	Torpedinidae	
LACM_57727_1	Torpedinidae	
LACM_318914	Torpedinidae	
LACM_26485	Torpedinidae	

LACM_42623_3	Rhinobatidae	Trygonorrhina_fasciata
LACM_42623_8	Rhinobatidae	
MCZ_ S_982	Rhinobatidae	
LACM_31771_11	Urotrygonidae	Urobatis_maculatus
LACM_31771_11	Urotrygonidae	
LACM_31771_11	Urotrygonidae	
LACM_31771_11	Urotrygonidae	
LACM_31771_11	Urotrygonidae	
LACM_31759_32	Urotrygonidae	
LACM_31771_11	Urotrygonidae	
LACM_33805_90	Urotrygonidae	Urotrygon_aspidura
LACM_33805_91	Urotrygonidae	
LACM_33805_92	Urotrygonidae	
LACM_33805_93	Urotrygonidae	
LACM_8844_3	Rhinobatidae	Zapteryx_exasperata
LACM_38094_2	Rhinobatidae	
LACM_8824_21	Rhinobatidae	
LACM_8824_22	Rhinobatidae	
LACM_coffin	Rhinobatidae	
LACM_32086_23	Rhinobatidae	

Supplementary Table 2. Size corrected morphological data matrix for all species with ecological data. The last variables PAN and HNA are not size corrected since they are angle data.

lifestyle	swimming	habitat	diet	nasal_curt	nare_type	family	species	PDM	PDX	TDW	HWN	NOM	NOX	NDMM	NDMX	ANFM	AAW	NSTRL	INM	INW	ANF	ANL	ANW	PAN	HNA
bathydem	punt	deep	soft_prey	incomple	conical	Arthynchol	Bathyraja_kincaidii	0.32944	0.25002	-0.93117	0.19542	0.61806	0.33862	0.25822	2.14E-05	0.81608	0.06906	-0.72859	0.28855	0.40872	0.54659	0.61736	-0.08813	136	120
demersal	punt	soft_sand	crustaciv	incomple	conical	Arthynchol	Psammobatis_scobina	-0.34013	-0.27494	-1.04114	-0.24229	0.10853	-0.02025	0.13711	-3.67E-05	0.66352	-0.92579	-0.00054	-0.30812	-0.12497	-0.06853	0.44676	0.55251	115	114
bathydem	punt	deep	soft_prey	incomple	conical	Rajidae	Raja_rhina	0.8146	0.70221	-0.73997	0.21929	0.48827	0.33879	0.4499	2.72E-01	1.19382	0.02775	-0.18998	0.28155	0.48991	0.64641	0.6368	0.07393	90	123
benthic	undulatory	soft_sand	soft_prey	incomple	circle	Hypnidae	Hypnos_monopterygius	-0.89483	-1.05013	0.68483	-0.24086	-1.10706	-1.06993	-0.03509	-2.19E-01	-1.41335	-0.25872	-1.40816	-0.76831	-0.85895	-0.72513	-1.33112	-0.56705	90	106
benthic	punt	rocky_cor	soft_prey	square	conical	Narkidae	Narke_japonica	-0.81777	-0.57584	0.71922	-0.15285	-0.35779	-0.40107	0.23383	1.34E-01	-0.54995	-0.35793	-0.05119	-0.73713	-0.5984	-0.47831	-0.25078	-0.12315	112	115
bathydem	punt	deep	soft_prey	square	conical	Narcinidae	Benthobatis_yangi	-0.20631	-0.31671	0.37788	-0.40813	-0.25894	-0.46151	-0.72772	-8.66E-01	0.94692	-0.53592	-1.77555	-0.3615	-0.07731	-0.01344	-0.77073	0.19163	90	111
demersal	BCF	rocky_cor	soft_prey	square	conical	Torpedini	Torpedo_californica	-0.20067	-0.26993	0.46563	0.27416	-0.22555	-0.71948	1.23132	8.37E-01	-0.12655	0.1974	-1.02156	-0.56044	-0.59207	-0.37296	-1.09339	-0.14858	30	126
benthic	punt	soft_sand	soft_prey	square	circle	Narcinidae	Narcine_entemedor	0.11506	0.02443	0.60152	0.04275	-0.26271	-0.31204	0.43615	2.79E-01	0.27172	-0.04558	-0.78028	-0.15899	-0.04051	0.10451	-0.59359	0.25566	90	104
benthic	BCF	soft_sand	crustaciv	reduced	open	Trygonorrh	Platyrhinoidis_triseriata	-0.17436	-0.22028	0.54007	0.01782	-0.21426	0.14185	-0.16449	5.24E-02	1.46615	0.28659	0.72071	0.48449	-0.10923	-0.57625	-0.37798	-1.57656	30	128
benthic	BCF	rocky_cor	crustaciv	reduced	intermedia	Rhinobati	Trygonorrhina_fasciata	0.29896	0.18769	0.61033	0.18588	0.52944	0.46902	0.06638	8.70E-02	-0.08811	0.60482	0.12197	0.4804	0.60706	0.74624	0.57634	0.99454	90	129
benthic	BCF	rocky_cor	crustaciv	reduced	open	Rhinobati	Zapteryx_exasperata	0.17243	-0.04819	-0.0113	-0.03988	0.00232	0.36598	-0.51313	-1.58E-01	1.79217	0.75234	0.78817	0.53862	-0.04501	-0.79449	-0.36039	-1.23056	15	128
demersal	BCF	rocky_cor	crustaciv	reduced	open	Rhinidae	Rhina_ancylostoma	0.58669	0.32819	0.01634	0.27584	0.16382	0.78389	-0.33496	8.01E-01	2.88062	0.99068	1.56502	0.59352	-0.06012	-0.68737	-0.74262	-1.80513	30	135
benthic	BCF	soft_sand	crustaciv	reduced	open	Rhinobati	Glaucostegus_granulatus	0.89848	0.84998	-0.74927	-0.1706	-0.13201	0.57912	-0.54498	4.47E-02	2.20926	0.7015	1.0957	0.42964	-0.33521	-1.0959	-0.63137	-2.4196	31	115
benthic	BCF	soft_sand	crustaciv	reduced	open	Rhinobati	Rhinobatos_leucorhynchus	0.73367	0.68146	-0.81286	-0.12399	-0.19748	0.62585	-0.68661	9.36E-03	2.09084	0.84263	1.35381	0.61792	-0.35729	-0.57818	-0.30142	-2.04656	35	125
benthic	undulatory	soft_sand	crustaciv	skirt_shap	comma	Urotrygon	Urotrygon_aspidura	0.30481	0.29921	-1.12372	0.42537	0.0178	-0.18903	0.4691	3.49E-01	-0.21563	0.01911	-0.06943	-0.0709	0.00039	0.25399	0.14802	0.3873	140	113
demersal	intermedia	rocky_cor	crustaciv	skirt_shap	comma	Urotrygon	Urobatis_maculatus	-0.20396	-0.13902	0.10626	0.13454	-0.0746	-0.13626	0.15765	1.44E-01	-1.20527	-0.19582	0.16274	-0.07169	0.04554	0.21398	0.08258	0.46745	107	112
benthic	undulatory	soft_sand	crustaciv	skirt_shap	intermedia	Potamotry	Potamotrygon_orbignyi	-0.24568	-0.13874	0.88752	0.16945	-0.14686	-0.32772	0.15512	8.77E-02	-1.05452	-0.36903	0.36789	-0.34231	-0.16262	-0.1341	-0.21471	0.233	117	119
benthic	undulatory	rocky_cor	crustaciv	skirt_shap	intermedia	Potamotry	Taeniura_lymma	-0.26775	-0.04067	0.19848	0.14484	-0.00418	-0.10827	0.40425	3.50E-01	-0.8659	-0.37218	0.69637	-0.23628	-0.02433	-0.01502	0.40187	0.56653	112	115
benthic	intermedia	rocky_cor	crustaciv	skirt_shap	intermedia	Dasyatida	Neotrygon_kuhlii	-0.2031	0.00418	0.0768	-0.0286	0.08067	0.03325	0.20283	2.52E-01	-0.49039	-0.29738	0.48853	-0.11189	0.07327	0.1561	0.4617	0.61243	105	107
pelagic	oscillatory	ocea	soft_prey	skirt_shap	intermedia	Dasyatida	Pteroplatytrygon_violacea	0.19602	0.24248	1.7235	0.59128	0.45744	0.18874	1.1214	8.40E-01	0.41984	0.38052	0.29372	0.12326	0.30743	0.45095	0.39204	0.90002	130	122
demersal	intermedia	soft_sand	soft_prey	skirt_shap	comma	Dasyatida	Dasyatis_longa	0.35103	0.3983	0.44012	0.53616	0.33768	0.30369	0.73137	7.23E-01	-0.97452	0.04523	0.71647	0.20887	0.37609	0.56191	0.45773	0.70278	100	118
demersal	intermedia	rocky_cor	soft_prey	skirt_shap	comma	Dasyatida	Himantura_uarnak	0.44211	0.58797	-0.82669	0.5061	0.32007	0.20471	1.5959	8.70E-01	-1.23872	-0.13221	0.84655	-0.24137	0.01155	0.06348	0.5357	0.5773	125	117
pelagic	intermedia	ocea	mollusciv	square	intermedia	Myliobati	Aetomylaeus_nichofii	0.41777	0.46312	0.03158	-0.28451	0.5473	0.53164	-0.58549	-6.31E-01	-0.89197	0.20087	0.7609	0.17011	0.30502	0.44621	1.02495	0.95299	99	107
demersal	intermedia	rocky_cor	mollusciv	square	intermedia	Myliobati	Myliobatis_californicus	-0.60423	-0.46288	-0.41796	-0.66639	0.15831	0.04127	-1.08096	-1.04E+00	-0.60395	-0.30461	0.05075	-0.057	0.17959	0.2289	0.20388	0.67694	106	115
benthopelo	intermedia	soft_sand	mollusciv	skirt_shap	intermedia	Rhinopter	Rhinoptera_bonasus	-0.26542	-0.21199	0.55865	-0.22005	-0.06869	-0.08088	-0.17309	-5.63E-01	-3.76475	-0.47298	-1.0887	0.04074	0.26195	0.39389	0.48247	1.03076	131	124
pelagic	oscillatory	ocea	soft_prey	square	circle	Mobulida	Mobula_hypostoma	-1.00742	-0.96111	0.42054	-0.49985	-0.77735	-0.92288	-1.15876	-1.70E+00	-1.03873	-0.95993	-1.42544	-0.0306	0.21326	0.40153	-0.3187	0.80471	56	111
pelagic	oscillatory	ocea	mollusciv	incomple	intermedia	Aetobatid	Aetobatus_narinari	-0.2404	-0.27979	-0.64541	-0.91665	-0.09026	-0.22738	-1.17336	-1.10E+00	0.44342	-0.16317	-0.8684	-0.40755	-0.22392	-0.12721	0.60316	-0.7034	105	105
benthic	intermedia	soft_sand	soft_prey	skirt_shap	circle	Gymnurid	Gymnura_crebripunctata	0.07097	-0.02902	-0.60863	0.14123	0.08804	0.03027	-0.02612	-6.77E-02	-0.67205	0.2741	-0.62147	0.22637	0.33018	0.45217	-0.08453	0.72825	90	126

REFERENCES

1. Abel, R.L., Maclaine, J.S., Cotton,R., Xuan, V. B., Nickels, T.B., Clark, T.H.,Wang, Z., Cox, J.P.L. 2010. Functional morphology of the nasal region of a hammerhead shark. *Comparative Biochemistry and Physiology - Part* A, 155, 464-475.

2. Allen, G.R., Robertson, D.R. 1994. Fishes of the Tropical Eastern Pacific. University of Hawaii Press. p. 34.

3. Arkhipkin, A. I.; Baumgartner, N.; Brickle, P.; Laptikhovsky, V. V.; Pompert, J. H. W.; Shcherbich, Z. N. 2008. Biology of the skates Bathyraja brachyurops and B. griseocauda in waters around the Falkland Islands, Southwest Atlantic. *ICES Journal of Marine Science*. 65: 560–570.

4. Aschliman, N. C., Nishida, M., Miya, M., Inoue, J. G., Rosana, K. M., & Naylor, G. J. 2012. Body plan convergence in the evolution of skates and rays (Chondrichthyes: Batoidea). *Molecular Phylogenetics and Evolution*, 63(1), 28–42.

5. Atema J. 1971. Structures and functions of the sense of taste in the catfish (*Ictalurus natalis*). *Brain Behav. Evol*, 4: 273-294.

6. Bardach J.E., Todd, J.H., Crickmer R. 1967. Orientation by taste in fish of the genus Ictalurus. *Science,* 155: 1276-1278.

7. Breder, C. M. 1926. The locomotion of fishes. *Zoologica*, 50, 159–297.

8. Burns, M.D. and Sidlauskas, B.L., 2019. Ancient and contingent body shape diversification in a hyperdiverse continental fish radiation. *Evolution*, *73*(3), pp.569-587.

9. Camilieri-Asch V, Yopak KE, Rea A, Mitchell JD, Partridge JC, Collin SP. 2020. Convergence of Olfactory Inputs within the Central Nervous System of a Cartilaginous and a Bony Fish: An Anatomical Indicator of Olfactory Sensitivity. *Brain, Behavior and Evolution*. 95(3-4):139-161.

10. Collin S.P., Kempster, R.M., Yopak, K.E. 2015. How Elasmobranchs Sense Their Environment. *Fish Physiology*. 34: 19–99.

11. Collin, S. 2012. The neuroecology of cartilaginous fishes: sensory strategies for survival. *Brain, Behavior and Evolution*, 80:80–96.

12. Compagno, L.J.V., 1999. Systematics and body form. In: Hamlet, W.C. (Ed.), Sharks, Skates, and Rays: The Biology of Elasmobranch Fishes. Johns Hopkins University Press, Baltimore, 1–42.

13. Cox, J.P.L. 2008. Hydrodynamic aspects of fish olfaction. *Journal of the Royal Society Interface*, 5, 575-593.

14. *Cox JPL. 2013.* Ciliary function in the olfactory organs of sharks and rays. *Fish Fish 14:364–90.*

15. Eschmeyer, W.N., Herald, E.S. Hammann, H. 1983. A field guide to Pacific coast fishes of North America. Boston (MA, USA): Houghton Mifflin Company.

16. Ferrando, S., Gallus, L., Ghigliotti, L., Amaroli, A., Abbas, G., Vacchi, M. 2017. Clarification of the Terminology of the Olfactory Lamellae in Chondrichthyes. *Anatomical Record*, 300, 2039-2045.

17. Froese, R. and D. Pauly. Editors. 2022. FishBase. World Wide Web electronic publication. www.fishbase.org. (02/2022).

18. Gardiner, J.M., Hueter, R.M., Maruska, K.P., Sisneros, J.A., Casper, B.M., Mann, D.A., Demski, L.S. 2012. Ch. 12: Sensory physiology and behavior of elasmobranchs. In Biology of Sharks and their Relatives, 2nd Ed., edited by E.C. Carrier, J.A. Musick, M.R. Heithaus (CRC Press: Boca Raton, FL).

19. Gardiner, J. M., Atema, J., Hueter, R. E. and Motta, P. J. 2014. Multisensory integration and behavioral plasticity in sharks from different ecological niches. *PLoS One,* 9, e93036.

20. Garwood, R. J. Behnsen, J. Haysom, H.K., Hunt, J.N., Dalby, L.J. Quilter, S.K., Maclaine, J.S., Cox, J.P. 2019. Olfactory flow in the sturgeon is externally driven. *Comp. Biochem. Physiol. A*, 235 (2019), pp. 211-225

21. Garwood, R.J., Behnsen, J., Ramsey, A.T., Haysom, H.K., Dalby, L.J., Quilter, S.K., Maclaine, J.S., Wang, Z., Cox, J.P.L., 2020. The functional anatomy of the pike, *Esox lucius* (L.). *Comp. Biochem. Physiol. A* 244, 110688.

22. Hara, T.J. 1993. Role of olfaction in fish behavior. In: Pitcher, T.J. (Ed.), Behavior of Teleost Fishes, 2nd Edition. Chapman and Hall, London, pp. 171–199.

23. Hart, N.S., Collin, S.P. 2015. Shark senses and shark repellents. *Integrative Zoology*, 10(1), 38-64.

24. Hart, N.S., Lisney, T.J., Collin, S.P. 2006. Visual communication in elasmobranchs. In: Ladich F, Collin SP, Moller P, Kapoor BG, eds. Communication in Fishes. Science Publishers, Enfield, NH, pp. 337–92.

25. Jacobs, L.F. 2012. From chemotaxis to the cognitive map: the function of olfaction. *Proceedings of the National Academy of Sciences,* 109 (Suppl. 1):10693–10700.

26. Johnsen, P.B. and Teeter, J.H. 1985. Behavioral responses of bonnethead sharks (Sphyrna tiburo) to controlled olfactory stimulation. *Mar. Behav. Physiol.* 11: 283-291

27. Kass, R.E. Raftery, A.E. 1995. Bayes Factors. *Journal of the American Statistical Association,* 90 (430): 773-795.

28. Kajiura, S.M., 2001. Head morphology and electrosensory pore distribution of carcharhinid and sphyrnid sharks. *Environmental Biology of Fishes*, 61, 125–133.

29. Kempster, R.M., McCarthy, I.D., Collin, S.P. 2012. Phylogenetic and ecological factors influencing the number and distribution of electroreceptors in elasmobranchs. *Journal of Fish Biology*, 80, 2055–88.

30. Koester D.M., Spirito C.P. 2003. Punting: An unusual mode of locomotion in the little skate, *Leucoraja erinacea* (Chondrichthyes: Rajidae). *Copeia*, 2003:553–561.

31. Last, P. A., W. White, M.R. de Carvalho, B. Séret, M. Stehmann, and G.P. Naylor. (Eds.). 2016a. Rays of the World. CSIRO Publishing, Melbourne, Australia.

32. Last, P.R., Seret, B., Naylor, G.J.P. 2016b. *Rhinobatos borneensis* sp. nov. with a redefinition of the Rhinopristiformes. *Zootaxa*, 4117, 451-475.

33. Lisney, T.J., Collin, S.P. 2007. Relative eye size in elasmobranchs. *Brain, Behavior and Evolution,* 69, 266–79.

34. Macesic L.J., Kajiura S.M. 2010. Comparative punting kinematics and pelvic fin musculature of benthic batoids. *Journal of Morphology*. 271:1219–1228.

35. Mathewson, R.F. and Hodgson, E.S. 1972. Klinotaxis and rheotaxis in orientation of sharks toward chemical stimuli, *Comparative Biochemistry and Physiology Part A: Physiology*, 42, 1: 79-84.

36. Meng, Q. Yin, M. 1981. A study of the olfactory organ of the sharks. *Transactions of the Chinese Ichthyological Society*. 1981; 2:1–24.

37. Meredith, T.L., Kajiura, S.M. 2010. Olfactory morphology and physiology of elasmobranchs. *The Journal of Experimental Biology*, 213, 3449-3456.

38. Meredith, T.L., Caprio, J., Kajiura, S.M. 2012. Sensitivity and specificity of the olfactory epithelia of two elasmobranch species to bile salts. *The Journal of Experimental Biology*, 215, 2660-2667.

39. Michael, S.W. 1993. Reef sharks and rays of the world. A guide to their identification, behaviour, and ecology. vi, 107p. Monterey, California: Sea Challengers. *Journal of the Marine Biological Association of the United Kingdom*, 73(4), 987-987.

40. Northcutt, R.G. 1978. Brain organization in the cartilaginous fishes. In: Hodgson ES, Mathewson RF, editors. Sensory biology of sharks, skates, and rays. Washington, D.C.: Office of Naval Research, Department of the Navy; p. 117– 93.

41. R Core Team. A language and environment for statistical computing. Vienna: R Foundation for Statistical Computing; 2019. Available from: https://www.r-project.org/.

42. Rosenberger, L. J. 2001. Pectoral fin locomotion in batoid fishes: undulation versus oscillation. *Journal of Experimental Biology*. 204:379–394.

43. Rosenberger, L. J., Westneat, M. W. 1999. Functional morphology of undulatory pectoral fin locomotion in the stingray *Taeniura lymma* (Chondrichthyes: Dasyatidae). *Journal of Experimental Biology*. 202, 3523-3539.

44. Rutledge, K.M. Summers, A.P., Kolmann, M.A. 2019. Killing them softly: Ontogeny of jaw mechanics and stiffness in mollusk feeding freshwater stingrays. *Journal of Morphology*, 280: 796–808.

45. Schaefer, J. T. and Summers, A. P. 2005. Batoid wing skeletal structure: novel morphologies, mechanical implications, and phylogenetic patterns. *Journal of Morphology,* 264, 298-313

46. Schluessel, V., Bennett, M.B., Bleckmann, H., Blomberg, S., Collin, S.P., 2008. Morphometric and ultrastructural comparison of the olfactory system in elasmobranchs: the significance of structure–function relationships based on phylogeny and ecology. *Journal of Morphology*. 269, 1365–1386.

47. Schluessel, V., Bennett, M.B., Bleckman, H., Collin, S.P., 2010. The role of olfaction throughout juvenile development: functional adaptations in elasmobranchs. *Journal of Morphology*. 271, 451–461.

48. Settles, G.S. 2005. Sniffers: fluid-dynamic sampling for olfactory trace detection in nature and homeland security. *Journal of Fluids Engineering*, 127, 189-218.

49. Simonitis, L.E., Marshall, C.D. 2022. Microstructure of the Bonnethead Shark (*Sphyrna tiburo*) Olfactory Rosette, *Integrative Organismal Biology*, 4:1.

50. Stein, R. W., Mull, C. G., Kuhn, T. S., Aschliman, N. C., Davidson, L. N., Joy, J. B., … Mooers, A. O. 2018. Global priorities for conserving the evolutionary history of sharks, rays and chimaeras. Nature Ecology and Evolution, 2(2), 288–298.

51. Takami, S., Luer, C. A., Graziadei, P. P. C. (1994). Microscopic structure of the olfactory organ of the clearnose skate, *Raja eglanteria*. *Italian Journal of Anatomy and Embryology*. 190, 211–230.

52. Tester, A.L., 1963. Olfaction, gustation, and the common chemical sense in sharks. In: Gilbert, P.W. (Ed.), Sharks and Survival. D.C, Heath and Co, Lexington, pp. 255–282.

53. Theiss, S.M., Hart, N.S., Collin, S.P. 2009. Morphological indicators of olfactory capability in wobbegong sharks (Orectolobidae, Elasmobranchii). *Brain Behavior and Evolution*, 73, 91–101.

54. Theisen, B., Zeiske, E., Breucker, H. 1986. Functional morphology of the olfactory organs in the spiny dogfish (*Squalus acanthias*) and the small spotted catshark (*Schliorhinus canicula*). *Acta Zool. (Stockholm)*, 67:73-8

55. Timm, L.L., Fish, F.E. 2012. A comparative morphological study of the head shape and olfactory cavities of sharks inhabiting benthic and coastal/pelagic environments. *Journal of Experimental Marine Biology and Ecology*, 414(415), 75-84.

56. Uyeda, J.C., Caetano, D.S., Pennell, M.W. 2015. Comparative Analysis of Principal Components Can be Misleading. *Systematic Biology*. 64(4):677–689.

57. Vogel, S. 1977. Flows in organisms induced by movements of the external medium. In Scale effects in animal locomotion (ed. T. J. Pedley), pp. 285–297. London, UK: Academic Press.

58. Webb, P. W. (1998). Swimming. In The Physiology of Fishes, second edition (ed. D. H. Evans), pp. 3–24. New York: CRC Press.

59. Wilga, C. D. and Lauder, G. V. 2002. Function of the heterocercal tail in sharks: quantitative wake dynamics during steady horizontal swimming and vertical maneuvering. *Journal of Experimental Biology,* 205, 2365-2374.

60. Yopak, K.E., Lisney, T.J., Collin, S.P. 2015. Not all sharks are "swimming noses:" variation in olfactory bulb size in cartilaginous fishes. *Brain Structure Function*, 220, 1127-1143.

61. Yopak, K.E., McMeans, B.C., Mull, C.G., Feindel, K.W., Kovacs, K.M., Lydersen, C., et al. 2019. Comparative Brain Morphology of the Greenland and Pacific Sleeper Sharks and its Functional Implications. *Scientific Reports*, 9(1):10022.

62. Zeiske, E., Theisen, B., Gruber, S.H., 1987. Functional morphology of the olfactory organ of two carcharhinid shark species. *Canadian Journal of Zoology*. 65, 2406–2412.

Chapter 2

The fluid dynamics of chemical scent detection in

stingrays and their relatives (Elasmobranchii: Batoidea)

Kelsi M. Rutledge[1], Christin T. Murphy[3], Jeff D. Eldredge[2], Malcolm S. Gordon[1]

[1]Department of Ecology and Evolutionary Biology, Department of Mechanical and Aerospace Engineering[2], University of California Los Angeles, Los Angeles, California 90095. [3]US Navy, Naval Research Lab, Newport, RI 02841.

ABSTRACT

The olfactory organs of batoid fishes are remarkably accurate, sensitive, and efficient in underwater chemical detection. The batoid nose varies in position, shape and external protuberances. This diversity includes three primary morphotypes: open, protruding, and flush nares. These fishes rely on water flow to direct odors into their noses. With diffusion-impeding boundary layers and no special pump systems producing flows, how do these fishes efficiently capture chemical stimuli? This paper describes the fluid dynamic bases for odor capture in the three morphotypes, plus one subtype (comma nares), seen in batoids. We visualized water flows through the nostrils of 3D-printed models of the heads of each morphotype. We used dye visualization methods and quantified the time it took for dye injected one cm from the leading edge of all models to reach important components of the olfactory systems. We explored the effects on nasal irrigation of Reynolds number (Re = 100, 500), head pitch (0°, 8°), and mouth induced respiratory flows. We hypothesized that increasing Re, head angle, and mouth suction would result in faster nasal irrigation times. However, we found that the influence of these parameters differed across nasal morphotypes. Batoid nasal morphotypes were classified as dynamic or specific smellers, with specific smellers requiring certain parameters to irrigate their nares. The dynamic smellers captured and circulated odorants at both head orientations and Re

without the influence of the respiratory pump. These dynamic smellers may offer insights into chemical sensors aboard underwater autonomous vehicles limited by the power of the pump.

INTRODUCTION

Fish olfaction involves two major stages: the transport of dissolved odorants 1) from the environment to the nostrils and 2) to the olfactory receptors. The batoid fishes (rays, skates, sawfishes and guitarfishes) are particularly interesting in both regards. Specifically, the anatomical positions and morphologies of their nostrils are varied, and they lack a direct pump-like mechanism for irrigating their nostrils. Our paper explores the odorant delivery system of a diverse array of nostril morphologies seen in batoid fishes.

Batoid noses vary in their anatomy, with differences in nostril shapes, sizes, relative positions, and internal geometries (Bell, 1993; Last et al., 2016; Agbesi et al., 2016; Rutledge, 2022). The olfactory chambers occur as a pair of blind (no internal connections), non-muscular, capsules on the ventromedial surface of the fish. The nostrils are near, but disconnected from the mouth and gills, and physically separate olfaction from respiration. Batoids also lack olfactory accessory sacs, the pump-like organs located behind the olfactory chambers seen in many teleost fishes (Bell, 1993). Therefore, there is no known direct pump-like mechanism to irrigate their olfactory organs (Tester, 1963; Theisen et al., 1986; Zeiske et al., 1987; Abel et al., 2010; Compagno, 1999). Each nostril is composed of an anterior inlet nostril though which water enters (incurrent channel) and a posterior outlet nostril (excurrent channel) through which water leaves (Bell, 1993; Zeiske et al., 1987; Abel et al., 2010; Compagno, 1999). Housed between the incurrent and excurrent channels is the olfactory rosette, which is composed of a longitudinal array of numerous plates of tissue, called lamellae, that are coated in sensory and non-sensory epithelium and kinociliated cells (Ferrando et al. 2017; Simonitis and Marshall, 2022).

Kinociliated cells are small (10-20 μm) non-sensory cells with beating cilia (Døving et al., 1977; Schluessel et al., 2008). These cells have been suggested to assist in the circulation of water or mucus through the small channels of the olfactory lamellae but are unable to generate flow into the inlet nostrils alone (Settles, 2005; Cox, 2008; Cox, 2013). The incurrent nostrils range from vertical slits to horizontal ovals to tube-like funnels, and more. Situated around the inlet hole is at least one dividing nasal flap. In many species, this flap, called the nasal curtain, loosely covers the excurrent nostril, forming a distinct channel for water exiting the nose. External nasal diversity was classified into three major groups, or morphotypes, termed: open, flush, or protruding nares, with three flush nare subtypes (circle, comma, and intermediate) (Fig. 2; see Rutledge, 2022 for a review of the morphology). These morphotypes are observed across the batoid phylogeny and appear to be convergent on specific nostril shapes and features. Although this anatomical diversity was recently documented (Rutledge, 2022), the mechanisms for odor capture across these morphotypes are unknown.

Odorants must be actively drawn by bulk flow into the nasal chambers for efficient olfaction (Cox, 2008). With the absence of a pump system producing flows, batoids must rely on harnessing external flows to irrigate their nostrils. Possible external flows include: the relative forward motion of a swimming fish (the motion-pump), harnessing the indirect respiratory current (buccopharyngeal pump), and pressure (Vogel, 1977; Timm-Davis and Fish, 2015; Agbesi et al., 2016; Garwood et al., 2019, 2020).

The motion-pump is an irrigation mechanism used by fishes with their inlet nostrils positioned in the path of the freestream flow. This is an effective way to ventilate the nose of a fast-swimming hammerhead with forward-facing nostrils (Abel et al., 2010; Rygg et al., 2013). However, batoids swimming parallel to the freestream flow have their inlet nostrils at a right

angle to the incoming flow. This, coupled with the impeding boundary layer (the layer of almost stationary fluid that encapsulates a swimming fish) will limit the efficacy of the motion-pump (Fig. 1). Furthermore, these challenges are compounded in slow-swimming or sedentary batoids. However, changes in head orientation may mediate this sensing problem. In fact, the swimming mode of these animals closely correlates with nasal morphotype, suggesting that changes in body orientation are likely influential to odor capture (Rutledge, 2022). Stingrays will angle their bodies upwards to approximately 8° with increased swimming speeds (Blevins and Lauder, 2012). Guitarfishes will alternate between maintaining a horizontal position and positive body angle while swimming steadily (Rosenberger, 2000). Resting batoids have also been observed to prop themselves up on their pectoral fins with their head pitched upwards into the incoming flow (Supp. Fig. 1).

Another possible nasal irrigation mechanism relies on indirect respiratory suction generated by the buccopharyngeal pump. Batoids have several modes of respiration. Batoids respire through their 1) spiracle only, 2) mouth and spiracle together, and 3) mouth only (Summers and Ferry, 2001). Spiracle-only respiration is often observed in resting batoids, while the mouth and spiracle rhythmically pumping water together is often observed in swimming batoids. Many batoids have their excurrent nostrils positioned directly above their mouth, suggesting respiratory-induced mouth suction could influence olfactory flow (Bell, 1993). In fact, respiration minimally aids nasal irrigation in live guitarfishes (Agbesi et al., 2016). Dogfish (*Squalus acanthias*) also use this mechanism to help generate flow through their nostrils (Theisen et al., 1996).

The relative position and morphology of the incurrent and excurrent nostrils can also generate flow through the olfactory chamber. Nostrils positioned at a right angle to each other, or

at different heights, can generate a pressure-induced flow through pitot- and venturi-like mechanisms, respectively (Theisen, 1970; Vogel, 1978; Zeiske et al. 1994; Cox, 2008). Stationary fluid inside a tube can be drawn out if the inlet is oriented perpendicular to a large shearing force, called viscous entrainment. This could act in conjunction with the above mechanisms (Vogel, 1994). Other morphological features, like the position and number of nasal flaps, likely have a hydrodynamic function in odor capture (Theisen et al., 1986; Shankar and Deshpande, 2000). The flaps situated around the inlet of guitarfish nostrils produce vortex-like structures that likely aid in odor entrainment (Agbesi et al., 2016).

We experimentally investigated these possible mechanisms in four species of batoids, each representing one of the nasal morphotypes (open, flush, protruding) and one intermediate subtype (comma) using dye visualization methods on 3D printed models. We tested models at varying Reynolds number (Re = 100, 500), head pitch (0°, 8°), and mouth induced respiratory flows. We hypothesized that increasing Re, head angle, and mouth suction would result in faster nasal irrigation times. We aimed to understand how different morphotypes harness odorants at low Re and how body orientation and respiration may impact nasal irrigation. Do morphotypes differ in their odor-capturing mechanisms and efficiency (i.e., speed of odor entrainment)? Are certain morphologies better suited for odor entrainment at low Reynolds number? We expect our study will advance our knowledge of chemoreception in a unique and morphologically diverse group of fishes and may be applicable to the design of artificial aquatic sensors (Gardiner et al., 2012; Wang, 2017).

METHODS

Specimens

One representative species from each of the four nasal morphotypes was obtained from the Natural History Museum of Los Angeles (Fig. 2). Species were chosen based on museum availability, the preservation of the internal nasal chambers, and the resulting CT-scan quality. Specimens of larger body size were also preferred for higher CT-scanning resolution.

The open nare morphotype, exclusively seen in Rhinopristiformes, was represented by the bowmouth guitarfish, *Rhina ancylostoma*. The specimen used in this study (LACM 38117-38) has a disc width of 0.49 meters and a nostril width of 0.032 meters. The bowmouth guitarfish is a large (up to ~3 meters in total length) shark-like batoid with a broad, rounded snout that likely operates at higher Reynolds numbers than most batoids (Table 1).

The flush nare morphotype (subtype: circle), seen in myliobatids, dasyatids, narcinids, and gymnurids, was represented by the electric ray, *Narcine entemedor*. The specimen used in this study (LACM 696327) has a disc width of 0.19 meters and a nostril width of 0.003 meters. The electric ray is generally a small to medium sized (up to ~0.7 meters total length) batoid with a round, elongated head that likely operates at low Reynolds numbers relative to other batoids (Table 1).

The comma nare morphotype, a subtype of the flush morphotype, seen in rhinopterids, rhinobatids, and potamotrygonids is represented by the fiddler ray, *Trygonorhinna fasciata.* The specimen used in this study (LACM 42623-8) has a disc width of 0.19 meters and a nostril width of 0.006 meters. The fiddler ray is a medium sized (up to ~1.3 meters total length) batoid with a diamond shaped head and a short snout, operating at Reynolds numbers in between the other two

morphotypes (Table 1). This species was chosen because, like the bowmouth guitarfish, it is also a member of the Rhinopristiformes, but the only member of this group with this nose morphology, suggesting convergence on this flush (subtype: comma) morphotype. However, unlike many other members of the flush morphotype, the incurrent nostrils possess additional nasal flaps, suggesting intermediate features between the open and flush morphotypes.

The protruding nare morphotype, seen in torpedids, narkids, and rajids, is represented by the California skate, *Beringraja inornata.* The specimen used in this study (LACM 20) has a disc width of 0.23 meters and a nostril width of 0.005 meters. The skate is a small to medium (up to ~0.8 meters total length) batoid with a broad, pointed head that operates at Reynolds numbers similar to the comma nare morphotype (Table 1).

Computed Tomography Scanning

Specimens were CT-scanned at UCLA's Medical Plaza Imaging Center (Fig. 3). Due to their large size, specimens were scanned in the Siemens Somatom whole-body CT-scanner at a resolution of 0.5 mm. This resolution was sufficient for capturing the external and internal geometry of the nose and olfactory chamber but limited in resolving some of the internal olfactory lamellae. Before scanning, specimens were patted dry, and their nasal chambers were fully emptied of preservative.

Model Creation

An STL model of the head of each of the four morphotypes was digitally rendered from the CT-scans using the image processing software 3D Slicer. STL models were edited in the 3D modeling software Blender and Meshmixer. Specifically, the mouths of each model were

digitally opened (1-2 mm depth) along the entire mouth width of each model. The orobranchial chamber of each model was digitally closed except for a small region at the posterior end of the body cavity where tubing was later inserted. The bent rostrum (snout) of the protruding nare morphotype was also digitally straightened before printing. Support structures to mount models in the flume were built in AutoCAD and manually affixed to the first set of models and digitally affixed to the second set of models.

The heads (from tip of snout to the last gill arch) of the representative morphotypes were 3D-printed with a Formlabs Form3 printer in a clear resin at 100 μm (x,y,z) resolution. No support structures were printed in the nasal chambers to preserve the internal geometry. At faster velocity trials (Re=500) there was dye break-up, therefore a second set of identical, scaled-up models were 3D-printed to test at slower speeds to ensure smooth dye pathlines. The protruding nare morphotype was printed at 0.8 and 2.0 scale. The flush nare morphotype was printed at 1.0 and 4.0 scale. The intermediate nare morphotype was printed at 0.8 and 2.0 scale. Only one model was printed for the open nare morphotype, at 0.4 scale, as it was tested at corresponding slower velocities and did not have dye break-up. Dye visualization experiments revealed there was no interaction between the paired nostrils in all the models (flow is separate between nostrils) except for the flush morphotype. Therefore, only half the head was printed for the larger models, except for the flush morphotype where the whole head was printed.

To mimic the suction generated from the mouth during respiration, plastic tubing was inserted into the body cavity of each model and extended directly into the orobranchial chamber.

Parameters

3D-printed models were tested at varying low Reynolds number (Re= 100, 500), head

pitch (angle= 0° and 8°), and with respiration (mouth suction= on and off). Each configuration was repeated five times representing 160 trials for the four models. To minimize model disturbance, the Reynolds number and mouth suction trials were varied first before the pitch of the models were changed. The pitch angles chosen are biologically relevant as mentioned above (Blevins and Lauder, 2012; Rosenberger, 2000). To replicate the same approximate path line of dye between trials, dye was injected at the same spot for every trial. This spot was marked on the model approximately 1 cm from the leading edge of all models, directly upstream from the lateral edge of the incurrent nostril, and 5 mm away from the body of the model. If the dye probe was positioned closer to the body of the model, it would inject directly into the boundary layer as observed by the dye slowly diffusing along the body (Supp. Video. 1).

To determine if mouth suction during respiration had an influence on nasal irrigation, the tubing inserted into the back of the model was connected to a syringe pump that withdrew water from the orobranchial cavity at 0.001 L/s. The volume of water entering a batoid's mouth during respiration has not been measured directly. Here, the volume per ventilatory bout was roughly estimated. The volume of the distended orobranchial cavity was subtracted from the closed orobranchial cavity. The volume of the distended orobranchial cavity was approximated by multiplying 1x mouth width by 4x mouth width (estimated length to last gill slit) by 4 mm depth (Summers, pers. comm.). The closed cavity was estimated to be 1 mm depth. Models had mouth widths between 12-25 mm suggesting the volume of the orobranchial chamber is 0.002-0.01L distended and 0.0006-0.003L closed. A complete breath cycle in the hedgehog skate takes ~2 seconds (Summers and Ferry, 2001), suggesting a rate of 0.0007-0.004 L/s. This suggests that the suction rate (0.001 L/s) of the syringe pump was slow to moderate.

The Reynolds number (Re) at the nostril was determined by:

$$Re = \frac{UL}{v} \qquad (1)$$

where U is the swimming velocity, L is the diameter of the exposed inlet nostril, and v is the average kinematic viscosity of seawater (1.3×10^{-6} m^2/s). The velocity at the inlet nostril is not known, therefore the velocity here was approximated by the swimming velocity of the animal, calculated as disc lengths (DL) per second, similar to other fish nasal irrigation studies (Agbesi et al., 2016; Rygg et al., 2013; Garwood et al. 2019, 2020). The congeners of the batoids studied here are known to swim at slow to cruising speeds between 0.20 and 1 DL/s, with faster, burst speeds up to 2 DL/s. *Narcine brasiliensis* was recorded punting, a type of benthic locomotion, at 0.23 DL/s, while *Urobatis jamaicensis* was recorded at 0.20 DL/s, and *Raja eglanteria* was recorded at 0.41 DL/s (Macesic and Kajiura, 2010).The little skate, *Leucoraja erinacea*, was recorded to have an optimal cruising speed of 1 DL/s (Di Santo and Kenaley, 2016). It has also been noted that typical batoid swimming speeds observed in aquaria and around coral reefs are between 1-2 DL/s (Rosenberger and Westneat, 2000). The species tested here operate at a wide range of Reynolds numbers throughout their life history (Table 1). The smallest juveniles swimming at 0.25 DL/s will live at Reynolds numbers between 9 and 259 (Table 1). Large, sexually mature adults swimming at cruising swimming speeds of 1 DL/s will live at Reynolds numbers between 363 and 38023 (Table 1). This suggests that models tested at Re=100 and 500 correspond to a slow to cruising swimming speed for these species. The open nare morphotype, represented by the very large bowmouth guitarfish (*R. ancylostoma*) is the only morphotype that likely does not operate at Re=100, with its lower limit at Re=259.However, as previously mentioned, other species within this nasal morphotype (many other rhinobatids) operate within

the lower Reynolds number tested here.

Dye Visualization

Models were mounted on T-slot 80/20 aluminum in the middle of a closed-circuit, free-surface, continuous flow flume housed in the Bioinspired Research and Design Laboratory at the Naval Undersea Warfare Center in Newport, RI (pictures of the set-up are not allowed for public release). The working section was optical glass measuring 2.25 x 0.5 x 0.5 m. The models were sufficiently small compared to the cross-sectional area of the flume, ensuring negligible wall effects. Dye solutions were neutrally buoyant and injected into the flow using stainless steel tubing. The dye injector apparatus was connected to a syringe pump that injected dye into the water at a constant rate matching the freestream velocity. The flow rate (Q) of the syringe pump was determined by:

$$Q = VA \qquad (2)$$

where V is the velocity and A is the area of the dye port injector hole. Dye transit times were measured over a fixed distance. Trials were filmed in the dark for enhanced contrast and illuminated by Lyra studio lights (LBX5) and filmed with a Nikon D5600 DSLR at 1920 x 1080 pixels at 60fps. This frame rate was sufficient to capture this slow, laminar flow regime. The videos were uploaded in Adobe and analyzed per frame, recording 5 time metrics relevant to sensing, including: the time for dye to reach the inlet hole after being released from the dye port; the time for dye to reach the olfactory lamellae (that houses the sensory epithelium; as seen in physical models and informed by manual dissections); the time for dye to circulate through the

chamber (from first entrance into the incurrent nostril to first exit out the excurrent channel); the time for the majority of dye to flush from the chamber ($\geq$ 90%); and the time it takes for any lingering dye to fully flush from the chamber.

Statistics

As five replicate trials were taken per configuration, we tested the statistical significance of the different configurations. To determine if there was a statistically significance difference between pitch angle across the five time variables, four Welch two-sample t-tests (1 for each combination of parameters: Re held constant, respiration held constant, varying pitch only) were run (20 combinations). This was repeated for each of the four morphotypes (80 tests total). An additional four two-sample t-tests (Re held constant, pitch held constant, varying respiration only) were run to determine if there was a statistically significant difference between respiration (another 80 tests total). This configuration of tests ensured the same parameters were being compared within morphotypes. Analyses were conducted is R Studio (R Core Team, 2021).

Navier-Stokes Simulation

Navier-Stokes simulations were performed to determine if the internal recirculation observed in the protruding morphotype (and to a lesser degree the comma morphotype) could be replicated a) on a simplified pipe geometry without olfactory lamellae and b) at higher Reynolds number flows that could not be tested with dye visualization methods. Laminar pipe flow was simulated in a simplified geometry of the protruding nare morphotype using COMSOL Multiphysics. Measurements of the internal geometry were taken on the volume rendering of the segmented negative space of the nasal chamber from the CT-scan in 3D Slicer. A simplified

geometry was created in AutoCAD 3D, drawn as a series of circles with varying diameters. The geometry was meshed with coarse and fine computational meshes of 28,501 and 68,401 domain elements to ensure mesh independence. The qualitative features of the meshes were consistent, with no visual differences in overall flow patterns or velocity distributions.

Flow was modeled as stationary, incompressible, laminar pipe flow with a pressure difference applied over the inlet and outlet. The no slip condition was applied at the walls. COMSOL then solves the Navier-Stokes and continuity equations:

$$\rho \frac{Du}{Dt} = -\nabla P + \mu \nabla^2 u \qquad (3)$$

$$\nabla \cdot u = 0 \qquad (4)$$

where ρ is the density of seawater, μ the viscosity of seawater (T= 20 °C), u is the velocity, and P is the pressure. Possible relevant pressure differences at the inlet and outlet were calculated by:

$$P_1 - P_2 = \frac{1}{2} \rho V^2 \qquad (5)$$

Where P is the pressure, ρ is the density of seawater, and V is the velocity. Because the velocity is not known at the nasal chamber, the velocity was estimated as the swimming speed. Two simulations were run at pressure differentials of 9 Pa and 32 Pa applied to the inlet of the nasal chamber. These pressure differences represented two swimming speeds: 0.5 DL/s and 1 DL/s corresponding to a Reynolds number of 562 (similar to the physical experiments tested here at Re= 500) and 1012 (not tested with physical models).

RESULTS

Open Nare Morphotype

The open nare morphotype, seen in guitarfishes and sawfishes, is characterized by an open geometry, where the olfactory lamellae are directly exposed to the environment and line the entire length of the nasal chamber. The incurrent nostril is flanked with multiple flap-like structures. The open nare morphotype has large nostrils relative to head length that are positioned relatively far from the mouth and close to the lateral edge of the head.

Dye was observed entering the most lateral region of the inlet nostril, immediately flowing into the small olfactory lamellae channels, swirling up to the more anterior region of the olfactory chamber, then forming a small eddy underneath the anterior nasal flap, and exiting the olfactory chamber at about 2/3 its total length (Fig. 4). Some dye was also observed exiting from the small hole formed by the posterior nasal flap meeting the central nasal flap.

Of the four morphotypes, the open nare exhibited the most rapid arrival of dye to the inlet (M= 0.73 s, SD= 0.24), and olfactory lamellae(M= 0.24 s, SD= 0.22). Dye circulated through the chamber most quickly at Re= 500, pitch=0, and respiration= on (M= 1.3 s, SD= 0.21). Dye also flushed through the chamber the fastest at Re= 500, pitch=0, and respiration= on (M= 1.97 s, SD=0.07) (Fig. 5).

Head pitch did not visually or statistically influence any of the five time variables ($p \geq$ 0.05; see Supplementary Table 1 for list of all p-values). There were a few instances where p=0.05-0.06, in these cases close to significance, a pitch of 0° was slightly advantageous over 8°, with faster circulation and flushing times.

Respiration also did not appear to play any significant role in the path of dye and no

visible dye entered the mouth during suction trials. However, there was a statistically significant difference in the time it took for dye to circulate through the chamber (t= -2.49, p-value= 0.04), mostly flush (t= -2.56, p= 0.03), and fully flush (t= -4.57, p-value= 0.01) from the chamber with respiration at Re=100 and a pitch of 8°, with respiration quickening these speeds. At Re= 500 there was no significant difference in these time metrics with respiration.

Reynolds number was by far the most important parameter for this morphotype, with much faster odor capture and circulation speeds at Re=500 for all time variables (Fig. 5). At Re=100 dye moved very slowly upon entering the nasal chamber, with dye lingering in the small sensory channels of the lamellae for up to ~7 minutes.

Protruding Nare Morphotype

The protruding nare morphotype, seen in skates and electric rays, is characterized by a funnel- or tube-like extension that distally protrudes from the inlet nostril. In this morphotype, the nostrils are positioned close to the mouth and medially.

Dye was observed to enter the lateral edge of the inlet hole, several millimeters away from the funnel-like inlet flap and flow unidirectionally to the medial edge of the olfactory chamber where it came into contact with the wall of the olfactory chamber and reversed direction, flowing upwards to the olfactory lamellae and then back down towards the lateral edge of the chamber, filling the chamber up laterally (Fig. 4). As the chamber filled with dye, the dye entering the inlet oscillated, moving laterally to the edge of the inlet chamber, and causing some of the dye to separate. The dye that broke off from the edge of the inlet then flowed underneath the funnel-like flap and was momentarily stuck in this region directly behind the funnel before it formed a series of eddies resembling shedding vortices. Dye leaving the olfactory chamber

exited with some dye entering the mouth during respiration.

Similar to the open nare morphotype, this morphotype had very quick odor capture. Dye reached the inlet most quickly with Re= 500, pitch=0°, and respiration=on (M=1.04 s, SD= 0.12). Dye circulated through the chamber most rapidly with Re= 100, pitch=8°, and respiration=on (M= 5.9 s, SD= 0.78). Dye was flushed from the chamber the fastest with Re= 500, pitch= 0°, and respiration= off (M=10.73 s, SD=6.7) (Fig. 5).

There were several statistically significant differences between head pitch in all five time variables (Supp. Table 1). However, there was not as clear of a trend in optimal head pitch angle, with differences across the five time variables. Generally, an 8° pitch aided in chamber circulation, while a 0° pitch resulted in faster chamber flushing. When respiration was off, a 0° pitch resulted in faster chamber circulation, but when respiration was on, an 8° pitch was faster. The time to reach the inlet was significantly faster (t= -8.54, p-value=0.000001) at an 8° pitch (vs. 0°) at the lower Re (Re=100, respiration=on). However, at the higher Re (Re= 500, respiration= off) the time to reach the inlet was significantly faster (t= 3.25, p-value= 0.02) with a 0° pitch. At the lower Re (Re=100, respiration=on) the time to reach the olfactory lamellae was also significantly faster (t= -3.56, p-value=0.02) at an 8° pitch. But, with respiration off, the time to reach the olfactory lamellae was significantly faster (t= 2.77, p-value= 0.04) at a 0° pitch. At the higher Re (Re= 500, respiration=off) the time to reach the olfactory lamellae was significantly faster (t=-2.57, p-value=0.03) at an 8° pitch. The time to circulate through the chamber was also significantly faster (t=-6.09, p-value=0.003) at an 8° pitch with Re=100, and respiration=on. At the higher Re (Re= 500, respiration=off), the time to circulate through the chamber was significantly faster (t= -2.40, p-value=0.03) at an 8° pitch. The time to mostly flush from the chamber was significantly faster (t=-8.16, p-value= 0.00004) at an 8° pitch at Re=100,

respiration=on. At the higher Re (Re=500, respiration=off) the time to mostly flush from the chamber was significantly faster (t=2.57, p-value= 0.02) at a 0° pitch. The time to fully flush from the chamber was significantly faster (t=7.77, p-value=0.0001) at a 0° pitch at Re=100, respiration=off.

Some of the dye leaving the excurrent nostril was observed entering the mouth during respiration. When respiration was off, more dye entered the mouth at pitch=0° when compared to pitch=8°. Respiration was found to aid in odor capture, circulation, and flushing at low Reynolds number only, with no statistically significant differences in time variables at Re=500 (Supplementary Table 1). Respiration lessened the time it took for dye to reach the olfactory lamellae (t= -3.81, p-value= 0.01) and fully flush from the chamber (t= -6.06, p-value=0.0003) at Re=100 and pitch=8°.

There was no clear trend in nasal irrigation with Reynolds number for this morphotype. At Re= 500 dye reached the inlet faster (1-2 seconds vs. 4-5 seconds at Re=100), but once inside the nasal chamber there was no significant difference in nasal irrigation and flushing times. The time for dye to reach the olfactory lamellae was slightly faster at the higher Reynolds number when pitch=8°, but not when pitch=0°.

The Navier-Stokes simulations for this morphotype resulted in similar flow patterns through the simplified pipe geometry (Fig. 6). Specifically, the simulation displayed the same pattern of fluid recirculation near the olfactory lamellae at both pressure differentials. However, this recirculation region was slightly less defined at the higher-pressure differential. Velocities in the chamber ranged from 0.02-0.18 m/s for a 0.5 DL/s swimming speed and 0.05-0.39 for 1 DL/s.

Flush Nare Morphotype

The flush nare morphotype, seen in many stingrays, electric rays, and myliobatid rays, is characterized by an incurrent nostril that is flush on the head. Dye was observed entering the most posterior region of the inlet and swirling up and around the olfactory lamellae, then closely following the back wall of the olfactory chamber, remaining quite streamlined throughout (Fig. 4). After following the back edge of the chamber, it moved out of the excurrent channel, across the tissue underneath the nasal curtain (anterior to the animal's mouth) and in some cases, exited out of the opposite excurrent nostril (Fig. 4). With respiration=on, dye exited out of its corresponding excurrent channel. Dye then exits with about 50% of the dye entering the mouth during respiration.

The flush nare morphotype was the slowest in terms of many of the time variables. At a pitch of 0°, no dye would enter the nose of the animal, passing directly in front of the inlet but not entering it. The position of the dye probe was moved from its replicate spot to determine if movements in the x or y plane along a different path line could generate flow into the nostril at a pitch of 0°, however after many attempts, it could not. Dye would only enter the incurrent nostril at a 0° pitch if the dye probe was moved in the z direction, closer to the body of the model, injecting dye directly into the boundary layer. This morphotype was also the slowest for dye to circulate through the chambers, taking 11-20 seconds on average.

Dye reached the inlet fastest at Re=500, respiration= off, pitch=8° (M=1.27, SD= 0.40). Dye reached the olfactory lamellae fastest at Re=500, respiration= off, pitch=8° (M=2.63, SD= 0.28). Dye circulated through the chamber (M=11.52, SD= 0.76), mostly flushed from the chamber (M= 8.29, SD= 2.66), and fully flushed from the chamber (M=21.31, SD=3.68) fastest at Re=500, respiration= on, pitch=8° (Fig. 5).

Head pitch was very influential for odor capture, but because no dye entered the nose at pitch=0°, tests of statistical significance at the different pitch angles were not performed for those trials.

Respiration was also very influential in this morphotype, with respiration quickening the speed at which odor was captured, circulated, and flushed from the chamber at both Reynolds numbers. Dye reached the inlet (t=3.01, p-value= 0.02), the olfactory lamellae(t=-4.11, p-value=0.01), and circulated through the chamber (t=-5.00, p-value=0.007) significantly faster with respiration on at Re=100, pitch=8°. Dye mostly flushed from the chamber significantly faster with respiration on at Re=500, pitch°=8 (t=-3.01, p-value= 0.02).

Reynolds number influenced the time for dye to reach the inlet, circulate through the chamber, and flush from the chamber. The time for dye to reach the inlet was faster at the higher Reynolds number. It took on average 1-5 seconds at Re=500 and 3-6 seconds at Re=100. The time for dye to reach the olfactory lamellae was much faster at Re=500, taking on average 2-3 seconds compared to 4-10 seconds at Re=100. The time for dye to mostly flush from the chamber was much faster at Re=500, taking on average 10-15 seconds compared to 20-60 seconds at Re=100.

Comma Nare Morphotype

The comma nare morphotype, seen in some stingrays, freshwater rays, and one guitarfish, is characterized by an inlet opening that resembles a comma or curved kidney bean. Specifically, the inlet nostril opening has a distinct, identifiable constriction in the medial region of the incurrent nostril. In this morphotype, the nostrils are positioned close to the mouth and moderately close to the lateral edge of the head (closer than the circular flush morphotype but

farther than the open nare morphotype). Additionally, this species possesses intermediate traits between the open morphotype and circular flush morphotype, as it has a nasal curtain and sits almost flush on the head but has a small nasal flap that flanks the incurrent nostril.

Dye was observed entering the mediolateral edge of the inlet hole, using the first internal inlet flap as almost a stair-step into the main chamber (Fig. 4). Dye then flows medially into the nasal chamber, remaining several millimeters from the posterior wall of the chamber. Dye immediately entered the olfactory lamellae where its flow became chaotic and oscillated between the anterior and posterior walls of the olfactory chamber. It some cases it also appears to swirl around the entire outer edge of the olfactory chamber. Dye circulated through the entire chamber and exited the olfactory chamber at several regions, exiting from underneath the nasal curtain and into and past the mouth.

This morphotype had quick nasal irrigation at both high and low Reynolds number and was the quickest of all morphotypes to capture odor at low Reynolds number. Dye reached the inlet fastest at Re=100, respiration=off, pitch=0° (M=1.40, SD=0.32). However, dye reached the inlet almost as fast at Re=500, respiration=off, pitch=8° (M=1.60, SD= 0.44). Dye reached the olfactory lamellae fastest at Re=500, respiration= on, pitch=8° (M=0.535, SD= 0.45). Dye circulated through the chamber fastest at Re=100, respiration=on, pitch=8° (M=3.14, SD= 0.42) and Re=500, respiration=off, pitch=8° (M=3.92, SD=0.71). Dye flushed from the chamber fastest at Re=100, respiration=on, pitch=8° (M=4.45, SD=1.39) and Re=500, respiration=on, pitch=8° (M=5.38, SD=0.57) (Fig. 5).

Head pitch resulted in statistically significant differences for several combinations of the time variables (see Supp. Table 1 for all 16 significant p-values). A head pitch of 8° resulted in significantly faster times than a head pitch of 0° for odor capture at low Reynolds number only,

74

irrespective of respiration (respiration = on: t=-4.05, p-value= 0.006; respiration = off: t= 5.33, p-value=0.0004). A head pitch of 8° resulted in dye reaching the olfactory lamellae and circulating through the chamber more quickly at both Reynolds numbers (Supp. Table 1). It took on average 0.5-1 second for dye to reach the olfactory lamellae at 8° pitch and 3-6 seconds at 0° pitch. An 8° head pitch resulted in significantly faster chamber flushing only at low Reynolds number when respiration was on (mostly flush, t=-10.23, p-value=0.0001; fully flush, t= -13.02, p-value= 0.00001).

Respiration also resulted in several statistically significant differences between the time variables, but trends were not as clear (Supp. Table 1). Respiration generally aided in odor circulation, especially at low Reynolds number. It took on average 2-6 seconds for odor to circulate through the chamber with respiration on, and 5-12 seconds with respiration off. However, respiration did not appear to be as influential in odor capture and flushing and the time for dye to reach the olfactory lamellae, at either Reynolds number. Specifically, there were a few instances where it resulted in slower times for these variables. The time for dye to reach the inlet was significantly faster with respiration= off at Re=100, pitch=0° (t= 4.36, p-value=0.006). The time for dye to mostly (t= 8.72, p-value=0.0002) and fully flush (t=9.47, p-value=0.00001) from the chamber was also significantly faster with respiration off at Re=100, pitch=0°. Some dye was observed entering the mouth during respiration.

There was no clear trend in nasal irrigation with Reynolds number for this morphotype. Similar to the protruding morphotype, at Re= 500 dye reached the inlet faster, but once inside the nasal chamber there was no significant difference in nasal irrigation and flushing times. At higher Reynolds number an 8° pitch this morphotype was slightly faster in terms of odor capture, time to reach the olfactory lamellae, circulation, and flushing. However, at a 0° pitch Reynolds

number did not seem to influence these time variables, with similarly quick performance.

DISCUSSION

The ventromedial placement of the nostrils of batoid fishes present several challenges for odor capture and circulation, especially at low Reynolds number flows. To receive an olfactory stimulus, odor must transverse the boundary layer as it flows away from the streamwise flow into the nostril, circulates through the sensory chamber, and flushes from the excurrent nostril in good time. With the absence of a direct pump-like mechanism to irrigate their nostrils, batoids must rely on their nasal morphology or behavioral modifications to harness externally generated flows (Tester, 1963; Agbesi et al., 2016). In this study, we tested how changes in behavior, like head pitch, respiratory mode (mouth suction), and swimming speed (Reynolds number) impact nasal irrigation in the differing nasal geometries seen in batoid fishes. We hypothesized that increasing head angle, mouth suction, and Reynolds number would result in faster nasal irrigation times. However, we found that these parameters influenced nasal irrigation differently across nasal morphotypes. Of the 4 nasal morphotypes tested, 2 (comma, protruding) did not have a clear Reynolds number dependence. This is surprising because a five-fold increase in Reynolds number (swimming velocity) did not result in significantly faster nasal irrigation times. Interestingly, these morphotypes display internal recirculation near the olfactory lamellae. The flow patterns of these morphotypes are more "complex" than the other 2 morphotypes that have generally unidirectional flow through the chamber. These flow patterns with fluid slowing down and changing direction near the olfactory lamellae could be one reason why they these morphotypes are not as influenced by increased Reynolds number.

Head pitch is also only influential for 2 (flush, comma) of the 4 morphotypes. In these

morphotypes, head pitch aids in initial odor capture at both Reynolds numbers. This positive body angle may help to position the nostrils more in line with the freestream flow direction. Conversely, the morphotypes that performed equally fast at both head angles (open, protruding) have flap-like protrusions that extend from their head, encircling the inlet nostrils. These flaps create a more forward-facing inlet that efficiently capture odorants when oriented horizontally and with their heads pitched up. These flaps may create a region of high pressure at the inlet and a region of low pressure inside and posterior to the nasal chamber, generating flow through the chamber and swirling down the body as a series of eddies. The funnel-like flap seen in the protruding nare is also sufficiently long to extend out of the boundary layer, mitigating this challenge of odor uptake (see boundary layer thickness in Cox, 2008). The flush, circular shaped nare, lacking any flap-like inlet features, is unable to capture odorants when oriented parallel to the incoming flow, and must rely on behavioral modifications of its head position to capture odorants.

The influence of respiratory flow (mouth suction) on nasal irrigation is most significant for the morphotypes with a Reynolds number dependence (flush, open). Specifically, respiratory flow is only significant for the open morphotype at low Reynolds number, but significant for the flush morphotype at both Reynolds numbers. Respiration aided in chamber circulation and flushing and directed exiting olfactory flow into the mouth. The flush nare is the only morphotype where dye exiting the olfactory chamber of one nostril entered into the opposite excurrent channel of the other nostril. However, with respiratory suction, dye does not enter the opposite channel and instead exits the chamber and enters the mouth. This strange flow pattern is likely due to the incomplete separation of this species' nasal chambers. The evolution of the very protrusible jaws in this species appears to have influenced the geometry of the posterior nasal

chamber, which is observed in the museum specimen. Therefore, respiration is likely especially crucial for this morphotype. The open nare morphotype also benefits from respiratory flow at low Reynolds number. Without respiratory assistance, it took ~7 minutes for dye to fully flush from the chamber at Re=100, which is on the time scale of diffusion (Cox, 2008). To efficiently irrigate the nostrils of this morphotype, there are likely other factors aiding olfaction at low Reynolds numbers (i.e., swimming mode, kinociliated cells).

Swimming mode was previously found to closely correlate with batoid nasal morphology and likely plays a role in nasal irrigation (Rutledge, 2022). Specifically, the open nare morphotype is exclusively observed in body-caudal-fin swimmers (guitarfishes and sawfishes), which swim with a yawing like motion as their robust tail propels them forward (Breder, 1926; Webb, 1998). The results of this study found that the open nare morphotype performed poorly at low Reynolds number, with difficultly flushing lingering dye stuck in the lamellar channels. While the adult species tested here (Bowmouth guitarfish) operates at Re>100, other species with the open nare morphotype operate at this low Reynolds number. It could be that the yawing motion of their swimming mode may help circulate and flush their exposed, horizontally oriented nasal chambers at a faster rate than observed in these stationary experiments. Additionally, oscillatory swimmers, like eagle rays and bats rays, generate thrust by pitching their body as they "flap" their pectoral fins (Heine, 1992). Oscillatory swimmers possess the flush nare morphotype, which requires a positive body angle to capture odorants. These pitching movements may help to further generate flow through the nostrils of this morphotype. The protruding nare, seen in skates and electric rays, is often observed in undulatory swimmers that also display a type of benthic locomotion called punting (Koester and Spirito, 2003; Macesic and Kajiura, 2010). Undulatory swimmers are more dynamic in their body movements, with quick

movements and turns, and the protruding nare allowed for quick odor capture at both head orientations. The funnel-like flap of the protruding nare may also be advantageous in slow velocity flows that likely occur during punting. Future studies should explore how these different swimming modes may complement nasal irrigation.

Specific batoid nasal morphotypes are better candidates for bioinspired design than others. Viewed through the lens of a chemical detection system only, the open and circular flush nare morphotypes performed the worst in terms of dynamic odor capture and circulation. The open nare was unable to flush odorants from the nasal chamber in a timely manner at low Reynolds numbers. However, the open nare had the fastest times for dye to reach the sensor and circulate through the chamber at higher Reynolds numbers. Therefore, the open nare could be an efficient model system for higher velocity flow conditions. The flush nare, with its simple circular inlet, resembles the intake valve of commercial aquatic sensor hardware (ex. Seabed AUV). This morphotype required a certain head pitch and the indirect respiratory pump to effectively harness odorants. This system therefore requires the power of an indirect pump and a specific angle of attack. Therefore, the open and flush nares are classified here as "specific smellers," which necessitate specific conditions for effective chemoreception (Figure 7). The geometries of the protruding and intermediate nare allow for a more dynamic odor capturing system and were classified as "dynamic smellers" (Figure 7). The protruding nare allowed for quick odor capture and circulation at both head pitch angles and was minimally influenced by the respiratory pump. The comma nare morphotype, with intermediate features, allowed for fast odor capture and circulation at both Reynolds numbers and was also minimally influenced by the respiratory pump. Therefore, these geometries could be potentially good candidates for underwater vehicles with onboard chemical detection systems. Specifically, these odor-

harnessing morphologies do not depend on a pump to bring water to their sensory structures (olfactory lamellae) and are effective smellers at low Reynolds number and with changing orientation into a plume.

The dynamic smellers displayed an interesting internal pattern of flow, that recirculated fluid back to the olfactory lamellae (where the sensory epithelium is housed). This internal geometry could be beneficial for increasing the likelihood that an odorant comes in contract with the olfactory lamellae. This region of slow recirculation may also help to protect the delicate sensory lamellae at high speeds (Rygg et al., 2013). This internal pattern of flow was replicated computationally with a dynamically similar, but simplified pipe geometry representing the protruding nare morphotype. The computational analysis found that this pattern of recirculation persists with a simplified geometry, suggesting that this flow pattern can be replicated relatively easily. This recirculating geometry could be used in AUV flow cell compartments to increase the likelihood an odorant binds with the sensor. Additionally, the computational analysis found that this region of recirculation persists at higher Reynolds numbers (Re>1000) which may be more relevant to underwater vehicles. Respiration and an 8° head pitch was not assessed computationally, as this would be more complicated to model, but both parameters were not necessary to generate this recirculation region as seen here and in the physical models.

There were several limitations of this study that could be explored in future work. First, the flow rates of mouth respiration were fairly slow. Because mouth suction did influence nasal irrigation for some morphotypes, it would be interesting to explore if faster respiratory rates or different respiratory modes impact olfactory flow. Batoids will also respire by rhythmically pumping water into their mouth and spiracle. This pulsatile flow may influence irrigation times and diffusion at the epithelial surface. The net flux of chemical odorants to the epithelium will

depend on the concentration gradient (LaBarbera and Vogel, 1982). A constant flow over the epithelium will help maintain this gradient, a pulsative flow may allow for a momentary lapse in exchange, which could influence sensory processing times. Second, some of the small, internal olfactory lamellae were not resolved in these models. This limitation likely affected some of the models' microscale flow patterns, however the general flow pattern throughout the nasal chamber is preserved. Olfactory lamellae may locally slow down the flow and result in slower chamber circulation and flushing times. CT scanning large specimens limited the scan resolution, but future studies could dissect out the olfactory rosette containing the lamellae. This smaller region could then be micro-CT scanned at a higher resolution; however, the internal flow patterns may have to be explored separately from the head of the animal which would also be a limitation for understanding the internal flow patterns. Third, the effects of the kinociliated cells noted on the olfactory lamellae could also not be accounted for. But, as dye would get stuck in the lamellar channels, kinociliated cells could play an important role in the circulation of water through these small structures. However, at faster speeds, circulation through these channels could be generated by external flow, as observed in the sea catfish (*Ariopsis felis*) (Cox, 2021). Fourth, the models printed here are rigid, while the external flap-like features seen in many batoids have some degree of flexibility. However, live animal observations in aquaria show that movements of these flap-like features are minimal during swimming (Agbesi et al. 2016). Nevertheless, the nasal curtain that extends directly above the mouth can move quite substantially during mouth respiration or feeding (pers. obs.). Finally, additional unknown mechanical agitation could also play a role in nasal irrigation and were not explored here. There is some evidence that the movement of the mouth or spiracles may influence olfactory flow, which would be an interesting avenue for future research (Summers and Ferry, 2001; Agbesi et

al. 2016).

In summary, batoids likely rely on the relative forward motion of water (motion-"pump"), respiratory suction, and pressure to irrigate their nostrils. These mechanisms appear to work in concert with the morphology, behavior, and ecology of the animal. Specifically, flap-like morphological nasal adaptations or increasing head angle help to position the nostrils in the path of the freestream flow. Some morphotypes display quicker odor entrainment and circulation times at higher Reynolds numbers, while other morphotypes with internal recirculatory flow are not significantly influenced by Reynolds number. Respiratory suction is crucial for nasal irrigation in some morphotypes at low Reynolds number and not significant for others. Swimming mode may help to further flush the nares at low Reynolds number. The ability to generate flow through the nasal chamber with changes in behavior (head orientation, respiratory mode, swimming speed) suggests batoids could play an active role in their own chemoreception. This challenges the longstanding theory that most fishes passively sense their chemical environment and are not active "sniffers." This study provides new insights into fish chemoreception, highlighting the complex and multifactorial nature of successful odor uptake and circulation.

ACKNOWLEDGEMENTS
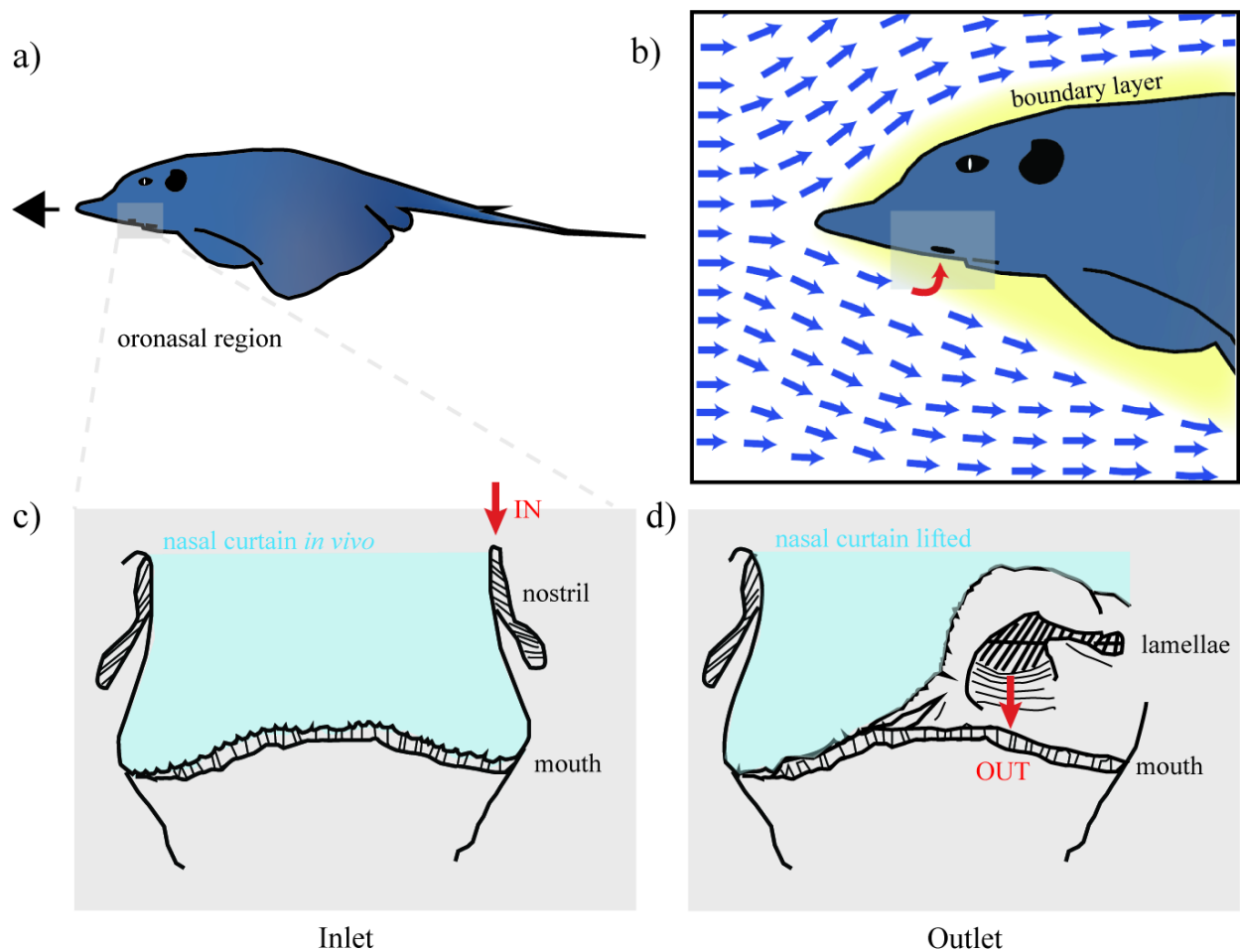
Figure 1. A schematic of odor capture and olfactory flow in batoids. a) A stingray swimming horizontally through the water column with the mouth and nose on its ventral surface b) The path of water flow around the head of the stingray (blue arrows) and the path that water must take to enter the nostril (red arrow) through the boundary layer (yellow). c) A ventral view of the oronasal region, showing the paired nostrils, the nasal curtain in blue, and the flow of water into the inlet nostril. d) A ventral view of the oronasal region with the nasal curtain lifted to show water exiting from underneath the nasal curtain near the mouth.
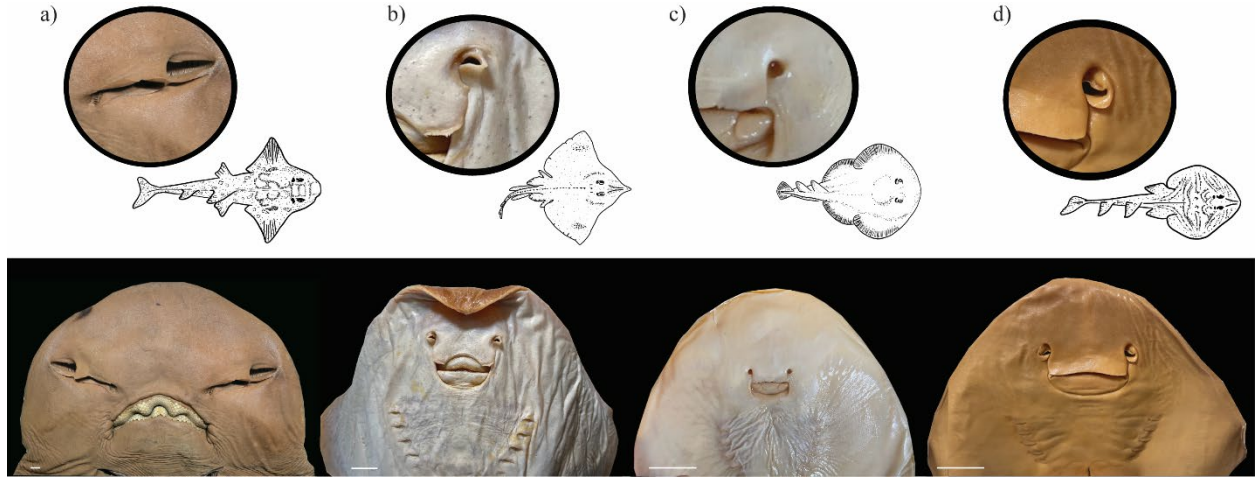
Figure 2. a) Open nare morphotype represented by *Rhina ancylostoma* b) Protruding nare morphotype represented by *Beringraja rhina* c) Flush nare morphotype represented by *Narcine entemedor* d) Comma nare morphotype represented by *Trygonorrhina fasciata*. Scale bar 25 mm.
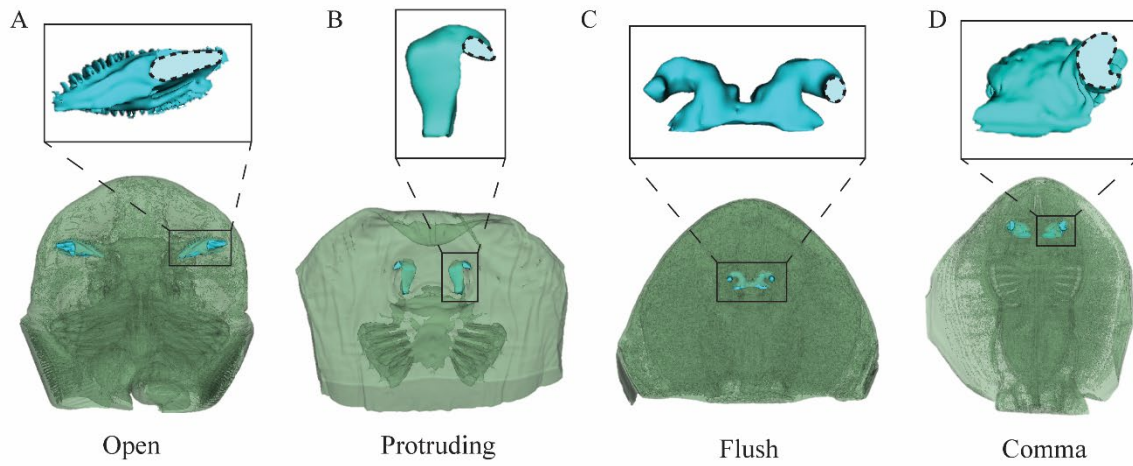
Figure 3. CT-scans of the heads of the 4 nasal morphotypes in green (from left to right: *Rhina ancylostoma, Beringraja rhina, Narcine entemedor, Trygonorrhina fasciata)* . The segmented negative space of the nasal chamber is in blue, and the approximate shape of the inlet hole is designated by the lighter blue color and dashed, black line.
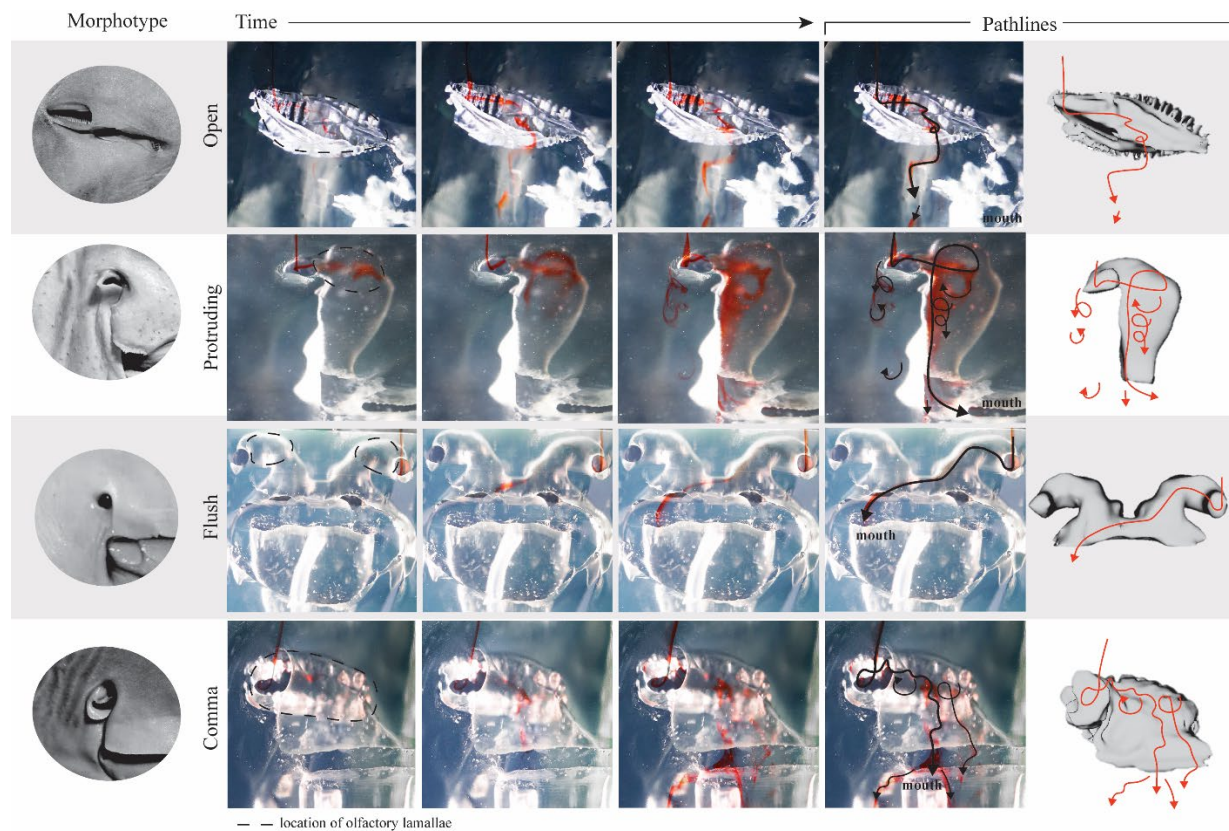
Figure 4. Dye visualization showing flow into and through the nasal chambers of 3D-printed models of 4 nasal morphotypes with increasing time since dye injection. The last two panels show the pathlines overlayed on the dye visualization and the negative space of the nasal chamber. Images were contrast enhanced for a brighter red hue to make the dye more visible.
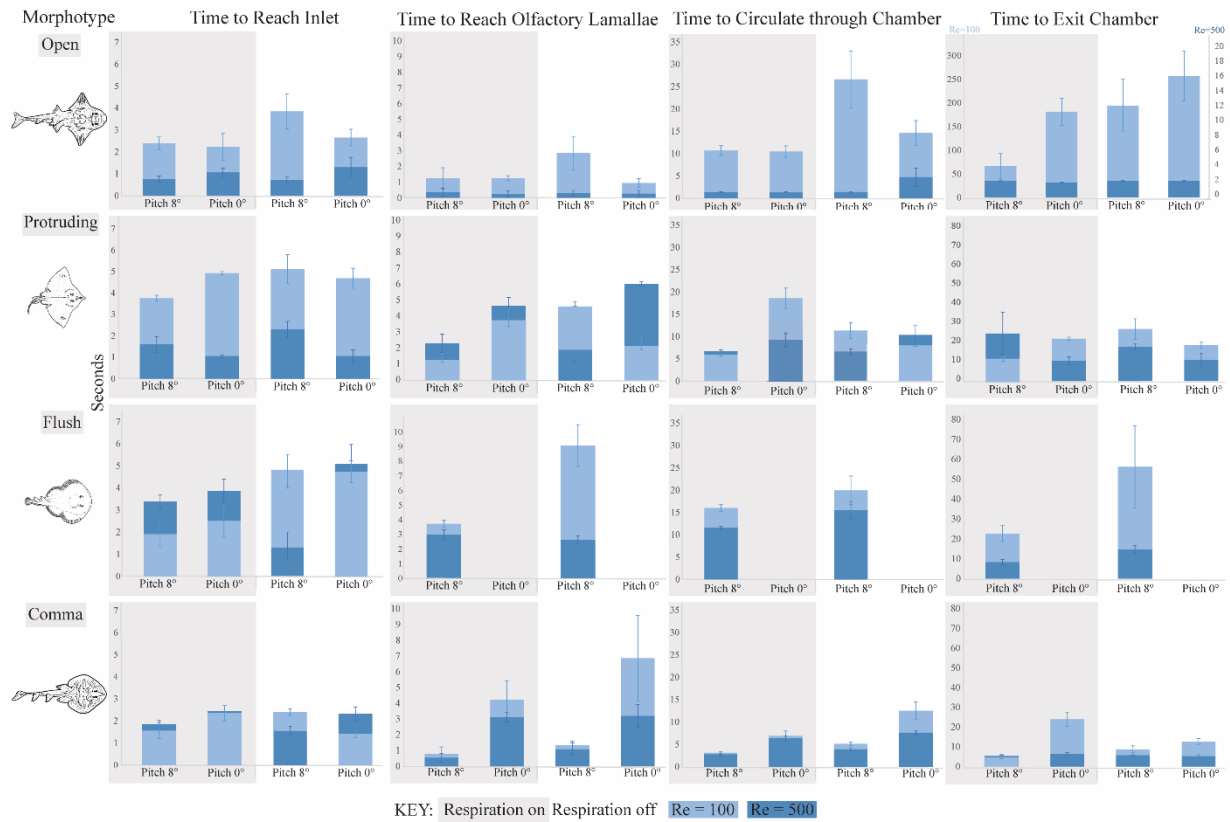
Figure 5. Means and standard deviations of relevant sensing time variables measured across the 4 nasal morphotypes. The open and flush morphotype were the most influenced by Reynolds number. The comma morphotype was the least influenced by Reynolds number. The flush morphotype was the most influenced by changes in pitch and could not generate flow through the nasal chamber at a head pitch of 0°. The open and flush morphotypes were most influenced by respiration at low Reynolds number.
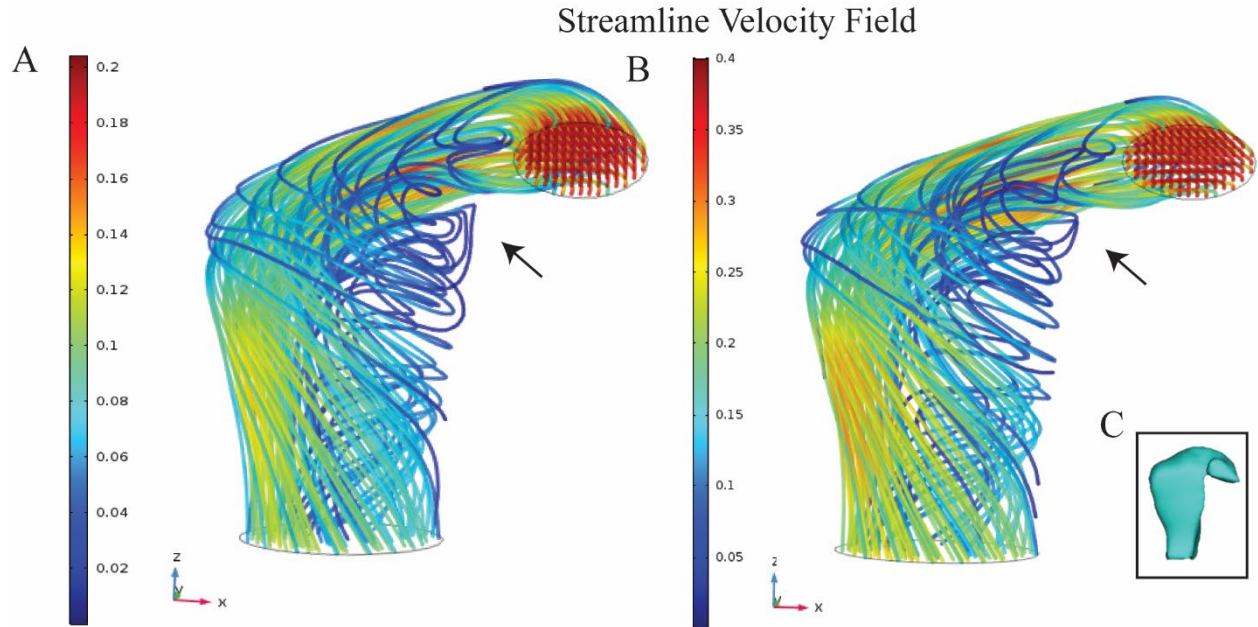
Figure 6. Laminar pipe flow simulated in a simplified geometry representing the nasal chamber a 0° head pitch without respiratory flow of the protruding nare morphotype at a) 0.5 DL/s (Re= 562) and b) 1 DL/s swimming speed (Re= 1012). The actual geometry of the nasal chamber is shown in c). The arrows point to the flow recirculation region that are also observed in dye visualization experiments at Re=100 and 500.
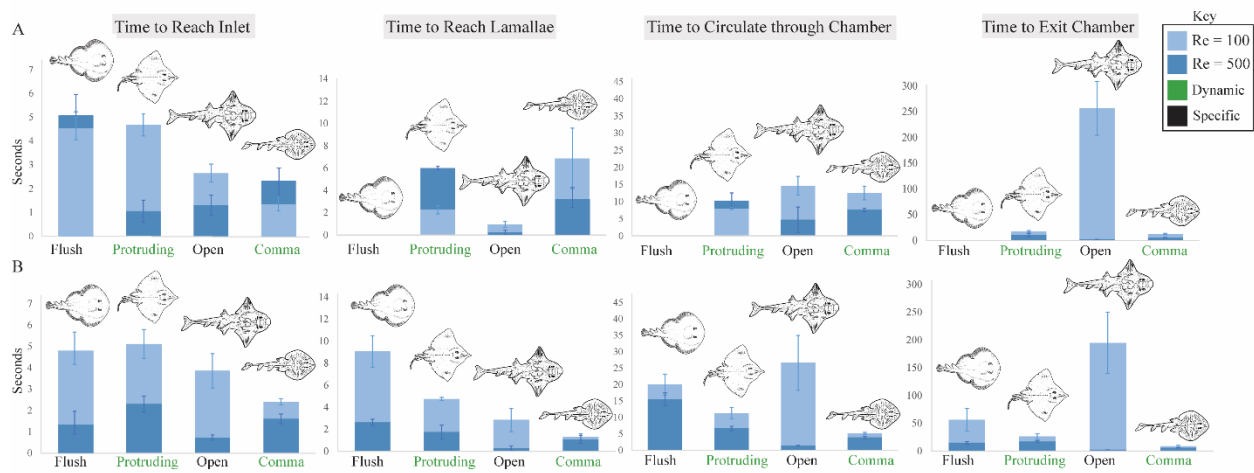
Figure 7. Means and standard deviations of relevant sensing time variables showing comparisons across the nasal geometries at both Reynolds number without respiration at a) pitch 0° and b) pitch 8°. Nasal morphotype is color-coded by the type of "smeller": dynamic or specific. The open and flush nares are classified here as "specific smellers," which necessitate specific behavioral conditions (Reynolds number/swimming speed, head pitch, respiratory flow) for effective chemoreception. The protruding and intermediate nare are classified as "dynamic smellers," which perform similarly at a variety of behavioral conditions. The protruding nare allowed for quick odor capture and circulation at both head pitch angles and was minimally influenced by the respiratory pump. The comma nare morphotype, with intermediate features, allowed for fast odor capture and circulation at both Reynolds numbers and was also minimally influenced by the respiratory pump. The flush morphotype was not able to capture dye at a pitch of 0° and performed slower in odor capturing metrics at a pitch of 8°. The open morphotype had some of the quickest capture and circulation times at Re= 500 but was by far the slowest morphotype at Re=100, taking minutes for dye to diffuse from the chamber.

Table 1. Representative species for each of the 4 morphotypes highlighting the range in Reynolds number throughout ontogeny. Body size ranges from the size at birth to the average size of a sexually mature adult (size metrics all obtained from Last et al. 2016). The range of nostril widths was approximated using the proportion of the nostril width with body size from the measurements taken on the specimens used in this study. Reynolds number was calculated using the inlet nostril width, swimming velocity (ranging from 0.25-1 DL/s), and the average kinematic viscosity of seawater.

Species	Morphotype	Body Size (m)	Characteristic Length (m)	Reynolds Number (Re)
		Disc Length Range	Inlet Nostril Width Range	Minimum-Maximum
Narcine entemedor	Flush	0.055-0.18	0.001-0.003	9-363
Beringraja rhina	Protruding	0.06-0.37	0.001-0.007	10-1992
Rhina ancylostoma	Open	0.15-0.87	0.009-0.057	259-38023
Trygonorrhina fasciata	Comma	0.12-0.55	0.004-0.017	92-7192

CHAPTER 2-SUPPLEMENTARY MATERIALS

Supplementary Materials

Figure 1. Bat ray, bluespotted ray, and Atlantic guitarfish using their pectoral fins to orient upwards on the substrate. Picture credit left to right: Monterey Bay Aquarium, Alan Sutton, Oceana.org.

Videos:

Video 1. If the dye probe was positioned too close to the body of the model, it would shoot directly into the boundary layer, as shown here by the dye diffusing slowly down the model.

Video 2. Dye visualization of the open nare morphotype at Re=500, pitch=8, respiration=on.

Video 3. Dye visualization of the protruding nare morphotype at Re=500, pitch=8, respiration=on.

Video 4. Dye visualization of the flush nare morphotype at Re=500, pitch=8, respiration=on.

Video 5. Dye visualization of the intermediate nare morphotype at Re=500, pitch=8, respiration=on.

Table 1. Results of the welch two-sample t-tests for all 5 time variables across the 4 morphotypes.

Model	Parameter Tested	Time to:	Re	Respiration	mean1	mean2	t	df	p-value
Open	pitch 8 vs. 0	reach inlet	100	on	2.39	2.24	0.19	2.64	0.86
			100	off	3.86	2.65	1.27	7.38	0.24
			500	on	0.76	1.07	-1.46	7.57	0.18
			500	off	0.73	1.31	-1.45	4.67	0.21
		reach lamallae	100	on	1.25	1.27	-0.05	3.33	0.96
			100	off	2.85	0.94	2.43	6.26	0.05
			500	on	0.36	0.24	0.75	7.88	0.47
			500	off	0.29	0.27	0.12	6.63	0.91
		ciculate through chamber	100	on	10.68	10.46	0.12	4.01	0.90
			100	off	26.62	14.64	1.79	7.48	0.11
			500	on	1.35	1.30	0.34	7.99	0.74
			500	off	1.38	4.71	-0.99	4.00	0.38
		mostly flush from chamber	100	on	65.98	181.14	-2.70	4.34	0.05
			100	off	194.55	256.73	-1.03	10.87	0.32
			500	on	2.15	1.97	2.50	6.18	0.05
			500	off	2.18	43.43	-0.99	4.00	0.37
		fully flush from chamber	100	on	122.72	331.81	-2.65	4.93	0.05
			100	off	315.72	424.50	-2.34	7.78	0.05
			500	on	2.15	1.97	2.50	6.18	0.05
			500	off	2.18	43.43	-0.99	4.00	0.37

			Re	Pitch	mean1	mean2	t	df	p-value
	respiration on vs. off	reach inlet	100	8	2.38	3.85	-1.55	7.14	0.16
			100	0	2.23	2.65	-0.53	2.76	0.64
			500	8	0.76	0.73	0.18	7.80	0.86
			500	0	1.07	1.30	-0.57	5.46	0.59
		reach lamallae	100	8	1.25	2.85	-1.89	7.90	0.09
			100	0	1.27	0.94	2.28	6.94	0.06
			500	8	0.35	0.27	0.48	7.69	0.64
			500	0	0.24	0.27	-0.16	7.28	0.87
		ciculate through chamber	100	8	10.68	26.62	-2.49	6.36	0.04
			100	0	10.46	14.64	-1.66	6.99	0.16
			500	8	1.35	1.38	-0.17	7.64	0.86
			500	0	1.30	4.70	-1.01	4.00	0.37
		mostly flush from chamber	100	8	65.98	194.55	-2.56	8.94	0.03
			100	0	181.14	256.73	-1.40	6.76	0.20
			500	8	2.15	2.18	-0.26	6.87	0.80
			500	0	1.97	43.43	-1.00	4.00	0.37
		fully flush from chamber	100	8	122.72	424.50	-4.57	3.43	0.01
			100	0	331.81	724.50	-1.88	2.56	0.17
			500	8	2.15	2.18	-0.26	6.87	0.80
			500	0	1.97	77.44	-1.00	4.00	0.37

Model	Parameter Tested	Time to:	Re	Respiration	mean1	mean2	t	df	p-value
Protruding	pitch 8 vs. 0	reach inlet	100	on	3.75	4.91	-8.54	6.32	0.000010
			100	off	5.10	4.68	0.36	6.33	0.73
			500	on	1.59	1.048	1.64	4.21	0.17
			500	off	2.29	1.05	3.25	6.41	0.02
		reach lamallae	100	on	1.372	3.874	-3.56	4.28	0.02
			100	off	4.748333	2.27	2.77	5.38	0.035
			500	on	2.278	4.616	-1.45	4.21	0.21
			500	off	1.748	5.999	-2.57	9.51	0.03
		ciculate through chamber	100	on	5.914	18.578	-6.09	4.23	0.003
			100	off	11.29667	8.01	2.26	5.29	0.07
			500	on	6.702	9.224	-1.88	4.35	0.12
			500	off	6.658	10.329	-2.40	11.55	0.03
		mostly flush from chamber	100	on	11.95	21.292	-8.16	7.84	0.00004
			100	off	26.16	18.066	1.81	6.02	0.118
			500	on	23.902	10.148	1.41	4.30	0.225
			500	off	17.346	10.73	2.57	12.99	0.02
		fully flush from chamber	100	on	39.32	30.91	2.43	4.77	0.06
			100	off	80.18333	27.026	7.77	7.93	0.0001
			500	on	62.02	41.17	0.48	7.82	0.64
			500	off	33.59	37.5	-0.24	12.20	0.81

			Re	Pitch	mean1	mean2	t	df	p-value
	respiration on vs. off	reach inlet	100	8	3.75	5.1	-1.20	5.11	0.27
			100	0	4.91	4.68	0.55	4.20	0.6
			500	8	1.59	2.298	-1.51	7.99	0.16
			500	0	1.04	1.05	-0.01	10.47	0.98
		reach lamallae	100	8	1.372	4.748333	-3.81	5.22	0.01
			100	0	3.87	2.27	2.25	4.49	0.08
			500	8	2.278	5.999	-2.25	9.44	0.05
			500	0	4.61	5.99	-0.61	11.31	0.55
		ciculate through chamber	100	8	5.91	11.29	-3.64	5.58	0.01
			100	0	8.01	18.5	5.12	4.11	0.006
			500	8	6.702	6.658	0.06	5.72	0.94
			500	0	9.22	10.32	-0.57	11.69	0.57
		mostly flush from chamber	100	8	11.95	26.16	-3.29	5.41	0.02
			100	0	21.29	18.06	2.06	6.19	0.08
			500	8	23.902	17.346	0.67	4.18	0.53
			500	0	10.148	10.733	-0.21	12.13	0.84
		fully flush from chamber	100	8	39.322	80.18333	-6.06	7.69	0.0003
			100	0	30.91	27.026	1.06	4.68	0.34
			500	8	62.024	33.592	0.85	4.36	0.43
			500	0	41.17	37.503	0.12	6.19	0.91

Model	Parameter Tested	Time to:	Re	Pitch	mean1	mean2	t	df	p-value
Flush	respiration on vs. off	reach inlet	500	8	1.27	1.91	3.01	6.46	0.02
			100	8	3.39	4.76	-1.89	5.29	0.11
		reach lamallae	100	8	3.72	9.07	-4.11	4.33	0.01
			500	8	2.97	4.31	-1.62	5.32	0.16
		ciculate through chamber	100	8	5.61	19.97	-5.00	4.06	0.007
			500	8	11.52	15.48	-2.21	4.30	0.08
		mostly flush from chamber	100	8	22.72	56.18	-1.25	4.17	0.27
			500	8	8.29	14.63	-3.01	7.08	0.02
		fully flush from chamber	100	8	22.72	68.6	-1.57	4.14	0.18
			500	8	21.31	27.04	-1.49	5.71	0.19

Model	Parameter Tested	Time to:	Re	Respiration	mean1	mean2	t	df	p-value
Comma	pitch 8 vs. 0	reach inlet	100	on	1.55	5.36	-4.02	6.2	0.006
			100	off	2.4	1.4	5.33	8.86	0.0004
			500	on	1.84	2.44	-2.1	6.46	0.07
			500	off	1.6	2.32	-2.11	7.29	0.07
		reach lamallae	100	on	0.79	4.22	-3.72	5.45	0.01
			100	off	1.33	6.58	-3.63	5.06	0.01
			500	on	0.53	3.12	-4.18	4.79	0.009
			500	off	1.08	3.18	-5.75	6.09	0.0011
		ciculate through chamber	100	on	3.18	6.91	-4.09	5.43	0.007
			100	off	5.14	12.53	-4.41	5.33	0.005
			500	on	2.77	6.35	-5.82	5.95	0.001
			500	off	3.92	7.63	-6.92	7.36	0.0001
		mostly flush from chamber	100	on	4.45	64.48	-10.23	5.11	0.0001
			100	off	8.71	12.63	-2.00	7.81	0.08
			500	on	5.38	6.51	-1.73	5.2	0.14
			500	off	5.75	5.3	0.68	4.68	0.52
		fully flush from chamber	100	on	8.45	95.28	-13.02	6.07	0.00001
			100	off	27.02	24.92	0.266	6.45	0.79
			500	on	5.38	6.51	-1.7	5.2	0.14
			500	off	5.75	5.3	0.68	4.68	0.52

			Re	Pitch	mean1	mean2	t	df	p-value
	respiration on vs. off	reach inlet	100	8	1.55	2.4	-2.47	5.38	0.05
			100	0	5.36	1.4	-4.39	5.21	0.006
			500	8	1.84	1.606	0.98	7.47	0.35
			500	0	2.44	2.32	0.32	7.9	0.75
		reach lamallae	100	8	0.79	1.32	-2.34	6.66	0.05
			100	0	4.22	6.85	-1.48	8.14	0.17
			500	8	0.53	3.18	-7.1	6.5	0.0002
			500	0	3.12	3.18	-0.09	6.2	0.93
		ciculate through chamber	100	8	3.13	5.14	-5.64	6.75	0.0008
			100	0	6.92	12.52	-2.99	7.75	0.02
			500	8	2.77	3.92	-2.72	8.43	0.03
			500	0	6.35	7.63	-1.83	7.57	0.11
		mostly flush from chamber	100	8	4.45	8.71	-2.52	5.24	0.05
			100	0	64.48	12.63	8.72	5.4	0.0002
			500	8	5.38	5.75	-1.23	8.84	0.25
			500	0	6.51	5.3	1.38	7.99	0.2
		fully flush from chamber	100	8	8.45	27.02	-2.59	4.74	0.05
			100	0	95.28	24.92	9.47	8.3	0.00001
			500	8	5.38	5.75	-1.23	8.84	0.25
			500	0	6.51	5.3	1.38	7.99	0.2

REFERENCES

1. Abel, R.L., Maclaine, J.S., Cotton,R., Xuan, V. B., Nickels, T.B., Clark, T.H.,Wang, Z., Cox, J.P.L. 2010. Functional morphology of the nasal region of a hammerhead shark. *Comparative Biochemistry and Physiology - Part* A, 155, 464-475.

2. Agbesi, M.P.K., Naylor,S., Perkins, S., Borsuk, H.S., Sykes, D., Maclaine, J.S. Wang, Z., Cox, J.P.L. 2016. Complex flow in the nasal region of guitarfishes. *Comparative Biochemistry and Physiology - Part A*, 193, 52-63.

3. Bell, M.A., 1993. Convergent evolution of nasal structure in sedentary elasmobranchs. *Copeia* 1993, 144–158.

4. Blevins, E. L. and Lauder, G.V. 2012. Rajiform locomotion: three-dimensional kinematics of the pectoral fin surface during swimming in the freshwater stingray *Potamotrygon orbignyi. Journal of Experimental Biology*. 215, 3231-3241.

5. Breder, C. M. 1926. The locomotion of fishes. *Zoologica*, 50, 159–297.

6. Compagno, L.J.V., 1999. Systematics and body form. In: Hamlet, W.C. (Ed.), Sharks, Skates, and Rays: The Biology of Elasmobranch Fishes. Johns Hopkins University Press, Baltimore, 1–42.

7. Cox, J.P.L. 2008. Hydrodynamic aspects of fish olfaction. *Journal of the Royal Society Interface*, 5, 575-593.

8. Cox, J.P.L., 2013. Ciliary function in the olfactory organs of sharks and rays. *Fish F*ish. 14, 364–390.

9. Cox, M.A.L., Garwood, J.B., Hunt, J.N., Dalby, L.J., Graham, S.M., Maclaine, J.S., Wang, Z., Cox, J.P.L. 2021. Olfactory flow in the sea catfish, Ariopsis felis (L.): Origin, regulation, and resampling. *Comparative Biochemistry and Physiology Part A: Molecular & Integrative Physiology*. 256: 110933.

10. Di Santo, V., Blevins, E.L., Lauder, G.V. 2017. Batoid locomotion: effects of speed on pectoral fin deformation in the little skate, *Leucoraja erinacea. Journal of Experimental Biology*. 220 (4): 705–712.

11. Di Santo, V. and Kenaley, C. P. 2016. Skating by: low energetic costs of swimming in a batoid fish. *Journal of Experimental Biology*. 219, 1804-1807.

12. Døving, K.B., Dubios-Dauphin, M., Holley, A., Jourdan, F. 1977. Functional Anatomy of the Olfactory Organ of Fish and the Ciliary Mechanism of Water Transport. *Acta Zoologica Stockholm*, 58, 245-255.

13. Gardiner, J.M., Hueter, R.M., Maruska, K.P., Sisneros, J.A., Casper, B.M., Mann, D.A., Demski, L.S. 2012. Ch. 12: Sensory physiology and behavior of elasmobranchs. In Biology of Sharks and their Relatives, 2nd Ed., edited by E.C. Carrier, J.A. Musick, M.R. Heithaus (CRC Press: Boca Raton, FL).

14. Garwood, R. J. Behnsen, J. Haysom, H.K., Hunt, J.N., Dalby, L.J. Quilter, S.K., Maclaine, J.S., Cox, J.P. 2019. **Olfactory flow in the sturgeon is externally driven.** *Comp. Biochem. Physiol. A*, 235 (2019), pp. 211-225

15. Garwood, R.J., Behnsen, J., Ramsey, A.T., Haysom, H.K., Dalby, L.J., Quilter, S.K., Maclaine, J.S., Wang, Z., Cox, J.P.L., 2020. The functional anatomy of the pike, *Esox lucius* (L.). *Comp. Biochem. Physiol. A* 244, 110688.

16. Heine, C. E. 1992. Mechanics of flapping fin locomotion in the cownose ray, *Rhinoptera bonasus* (Elasmobranchii: Myliobatidae). PhD thesis, Duke University, Durham, NC, USA.

17. Johnsen, P. B. and Teeter, J. H. 1985. Behavioral responses of bonnethead sharks (*Sphyrna tiburo*) to controlled olfactory stimulation. *Mar. Behav. Physiol* 11 (4), 283–291.

18. Koester D.M., Spirito C. P. 2003. Punting: An unusual mode of locomotion in the little skate, *Leucoraja erinacea* (Chondrichthyes: Rajidae). *Copeia*, 2003:553–561.

19. Last, P. A., W. White, M.R. de Carvalho, B. Séret, M. Stehmann, and G.P. Naylor. (Eds.). 2016. Rays of the World. CSIRO Publishing, Melbourne, Australia.

20. Macesic L.J., Kajiura S.M. 2010. Comparative punting kinematics and pelvic fin musculature of benthic batoids. *Journal of Morphology*. 271:1219–1228.

21. Meredith, T.L., Kajiura, S.M. 2010. Olfactory morphology and physiology of elasmobranchs. *The Journal of Experimental Biology*, 213, 3449-3456.

22. Parker, G. H. 1914. The directive influence of the sense of smell in the dogfish. *Bull. U. S. Bur. Fish.* 33 (798), 61–68.

23. Parker, G. H. and Sheldon, R. E. 1913. The sense of smell in fishes. *Bull.U. S. Bur. Fish.* 32, 33–46.

24. R Core Team. A language and environment for statistical computing. Vienna: R Foundation for Statistical Computing; 2021. Available from: https://www.r-project.org/.

25. Rosenberger, L. & Westneat, M. 2000. Functional morphology of undulatory pectoral fin locomotion in the Stingray *Taeniura lymma* (Chondrichthyes: Dasyatidae). *Journal of Experimental Biology*. 202 (24): 3523-39.

26. Rosenberger, L. J. 2001. Pectoral fin locomotion in batoid fishes: undulation versus oscillation. *Journal of Experimental Biology*. 204 (2): 379–394.

27. Rutledge, 2022. Sniffing out Stingray Noses: The Functional Morphology of Batoid Olfaction. *Integrative and Organismal Biology*, obac043.

28. Rygg, A.D., Cox, J.P., Abel, R., Webb, A.G., Smith, N.B., Craven, B.A. 2013. A computational study of the hydrodynamics in the nasal region of a hammerhead shark (*Sphyrna tudes*): Implications for Olfaction. *PLoS ONE*, 8(3): e59783

29. Schluessel, V., Bennett, M.B., Bleckmann, H., Blomberg, S., Collin, S.P., 2008. Morphometric and ultrastructural comparison of the olfactory system in elasmobranchs: the significance of structure–function relationships based on phylogeny and ecology. *Journal of Morphology*. 269, 1365–1386.

30. Settles, G.S. 2005. Sniffers: fluid-dynamic sampling for olfactory trace detection in nature and homeland security. *Journal of Fluids Engineering*, 127, 189-218.

31. Simonitis L E, Marshall C D. 2022. Microstructure of the Bonnethead Shark (*Sphyrna tiburo*) Olfactory Rosette. *Integrative Organismal Biology*, 4:1.

32. A.P. Summers, Ferry-Graham, L.A. 2001. Ventilatory modes and mechanics of the hedgehog skate (*Leucoraja erinacea*): testing the continuous flow model. *Journal of Experimental Biology*. 204 (9): 1577–1587.

33. Tester, A.L., 1963. Olfaction, gustation, and the common chemical sense in sharks. In: Gilbert, P.W. (Ed.), Sharks and Survival. D.C, Heath and Co, Lexington, pp. 255–282.

34. Theisen, B. 1970. The morphology and vascularization of the olfactory organ in *Calamoichthys calabaricus* (Pisces, Polypteridae). *Vidensk. Meddr. dansk naturh. Foren.* 133, 31–50.

35. Theisen, B., Zeiske, E., Breucker, H. 1986. Functional morphology of the olfactory organs in the spiny dogfish (*Squalus acanthias*) and the small spotted catshark (*Schliorhinus canicula*). *Acta Zool. (Stockholm)*, 67:73-8

36. Timm, L.L., Fish, F.E. 2012. A comparative morphological study of the head shape and olfactory cavities of sharks inhabiting benthic and coastal/pelagic environments. *Journal of Experimental Marine Biology and Ecology*, 414(415), 75-84.

37. Vogel, S. 1977. Flows in organisms induced by movements of the external medium. In Scale effects in animal locomotion (ed. T. J. Pedley), pp. 285–297. London, UK: Academic Press.

38. Vogel, S. 1978. Organisms that capture currents. *Sci. Am.* 239, (Aug.), 108–117.

39. Vogel, S. 1994. Life in moving fluids, 2nd edn. Princeton, NJ: Princeton University Press.

40. Wang, N. 2017. Biological Olfaction Inspired Chemical Sensors. In: Biomimetic Microsensors Inspired by Marine Life, edited by Kottapalli, A.G.P., Asadnia, M., Miao, J., Triantafyllou, M.S. (Springer International Publishing AG: Cham, Switzerland).

41. Webb, P. W. 1998. Swimming. In The Physiology of Fishes, second edition (ed. D. H. Evans), pp. 3–24. New York: CRC Press.

42. Zeiske, E., Theisen, B., Gruber, S.H., 1987. Functional morphology of the olfactory organ of two carcharhinid shark species. *Canadian Journal of Zoology*. 65, 2406–2412.

Chapter 3

Complex flow in stingray (Elasmobranchii: Batoidea)

nostril geometry may passively enhance odor capture

Kelsi M. Rutledge[1], Malcolm S. Gordon[1], John O. Dabiri[2,3]

[1]Department of Ecology and Evolutionary Biology, University of California Los Angeles, Los Angeles, California 90095. [2]Graduate Aerospace Laboratories (GALCIT), California Institute of Technology, Pasadena, CA, USA. [3]Department of Mechanical and Civil Engineering, California Institute of Technology, Pasadena, CA, USA.

ABSTRACT

Stingrays and their relatives (batoids) rely on their sense of smell as one of their primary senses for survival. Olfaction is crucial for prey recognition, navigation/tracking, and reproductive signaling. The first step in olfaction is harnessing water and odorants from the external environment into the nostrils (nares). However, stingray nares are blind chambers that lack any internal pump-like mechanism to aid in nasal irrigation. The nares are also positioned on the medioventral surface of their head and are situated at a right angle to the freestream flow direction. A pump-less nasal irrigation system and medioventrally positioned nares are two apparent hydrodynamic challenges involved in batoid odor capture. Batoid fishes appear to have evolved a diverse and unusual nasal morphology to aid in odor uptake. In this paper, we focus on three nasal morphotypes seen in batoid fishes with unique flap-like protrusions situated around each nare: open, comma, and protruding morphotypes. We aimed to understand how morphologically diverse external nare anatomy can influence flow patterns and odor capture potential. We hypothesized that morphotypes with a longer sagittal nostril protrusion will have a greater nostril reach and odor capture potential. Models of the nasal morphotypes were 3D printed and mounted in a water tunnel with the incoming flow visualized with particle image

velocimetry methods (PIV). Models were tested at varied Reynolds numbers (Re = 500, 1000, 2000, 3000, 6000), angles of attack (0°, 8°), and with and without respiratory induced mouth suction. To obtain velocity data, a continuous wave laser beam was spread into a thin sheet by a cylindrical lens. The resulting laser sheet was oriented to illuminate streamwise cross-sections of the flow near the nostrils. Image sequences were cross-correlated to determine local flow velocity. This was the first time PIV was used to visualize olfactory flow around the nare of a fish and we found several surprising results. Olfactory flow was much more complex and expansive than previously thought. Specifically, we document the first recorded occurrence of multidirectional olfactory flow into the incurrent nostril of a fish. In all morphotypes, the flap-like structures appear to play an important role in protruding out of the boundary layer and locally disturbing the flow to create recirculation regions around the nares. In two of the three morphotypes, these recirculation regions funnel water into the incurrent nostril from multiple directions, greatly expanding the reach and odor capture potential of the nares. The comma morphotype had the largest nostril reach and odor capture potential, capturing water over three times the width of its incurrent nostril. The open morphotype also had unexpected flow patterns, with a large portion of water entering what was thought to be the excurrent nostril. Head pitch, respiration, and Reynolds number were found to impact odor capture differently across morphotypes. Our hypothesis that increasing nostril protrusion depth would increase nostril reach was not supported and the nasal morphotypes with relatively shorter nostril protrusions had the largest nostril reach. These results are likely a reflection of different odor capture strategies and tradeoffs between nasal geometry and ecology.

INTRODUCTION

Chemoreception is an important sensory modality for survival and reproduction in stingrays and their relatives (i.e., batoid fishes). Specifically, olfaction, or smell, is one of their longest-range sensory systems (Collin, Kempster, and Yopak, 2015). Olfactory cues are often the first alert to the presence of a stimulus and are critical for long distance tracking, finding prey, and recognizing conspecific cues such as distress and reproductive signaling (Gardiner and Atema, 2012; Gardiner et al., 2012; Hart and Collin, 2015). However, little is known about how these fishes harness olfactory cues. This paper aims to better understand this important system of detection by examining the fluid dynamics of odor capture in this unique group of fishes.

Batoid fishes are interesting model organisms for the study of fluid dynamics of olfaction for several reasons. First, batoids have a diverse nasal anatomy that is often independent of shared ancestry, suggesting evolutionary convergence on optimal designs (Rutledge, 2022). Second, their nostrils, called nares, are non-muscular, blind chambers that lack any internal pump-like mechanism to aid in nasal irrigation (Tester, 1963; Theisen et al., 1986; Zeiske et al., 1987; Compagno, 1999; Abel et al., 2010). The nares are physically separate from the mouth and gills and lack pumping nasal accessory sacs, as seen in other fishes (Bell, 1993; Schluessel et al. 2008). Third, batoids are dorsoventrally flattened fishes, with their nares positioned on the medioventral surface (i.e., middle and underside) of their head. Therefore, when swimming against a current, their inlet nostrils are situated at a right angle to the freestream flow direction. This, coupled with the impeding boundary layer (the layer of almost stationary fluid that encapsulates a swimming fish) likely limits the efficacy of odor uptake. To overcome these apparent hydrodynamic challenges, batoid fishes appear to have evolved a diverse and unusual nasal morphology to harness odorants.

100

The batoid nare has three major morphological components: an anterior inlet nostril (incurrent channel) though which water enters, the olfactory chamber where water circulates and a posterior outlet nostril (excurrent channel) where water leaves (Bell, 1993; Zeiske et al., 1987; Compagno, 1999; Abel et al., 2010). The olfactory chamber houses the olfactory lamellae, which are small sheets of tissue coated with sensory and non-sensory epithelium and kinociliated cells. Kinociliated cells are small (10-20 μm) non-sensory cells with beating cilia (Døving et al., 1977; Ferrando et al. 2017; Simonitis and Marshall, 2022). These cells have been suggested to assist in the circulation of water or mucus through the small channels of the olfactory lamellae but are unable to generate flow into the nares by themselves (Settles, 2005; Cox, 2008; Cox, 2013). Incurrent nostrils range from vertical slits to horizontal ovals to tube-like funnels, and more (Rutledge, 2022). Situated around the incurrent nostril is one or more nasal flaps. The excurrent nostril is less obvious and often not visible as a distinct hole for exiting water as in many other fishes. In all but one group of batoid fishes (i.e., Rhinopristiformes) the excurrent channel is formed by a flap of tissue that extends across the border of the incurrent nostrils and down to the mouth. This non-muscular flap of tissue, called the nasal curtain, conceals the excurrent channel and extends the outlet to be situated above the mouth. The shape and length of the nasal curtain varies across groups and some lack it entirely (Last et al. 2016). The Rhinopristiformes (guitarfishes, wedgefishes, and sawfishes) have a rudimentary nasal curtain known as the anterior nasal flap (a homologous structure) (Last, Seret, and Naylor, 2016). Unlike the nasal curtain, the anterior nasal flap does not cover the excurrent nostril or extend below the nare. In this group, the olfactory chamber is not enclosed and the lamellae are freely exposed to the environment. Batoids with this nasal morphology are classified as having open nares (Rutledge, 2022). Batoids with a nasal curtain are classified as having either protruding or flush nares, with

several subtypes (i.e., comma, circle, intermediate) depending on the morphology of the incurrent nostril. Specifically, the comma morphotype is classified under the flush morphotype, but represents an intermediate morphology between the open and protruding nares (see Rutledge, 2022 for further review of morphology).

These distinct nasal morphotypes may rely on different mechanisms to irrigate their nares. Without a pump system producing flows, batoids must rely on harnessing external flows to irrigate their nostrils. Possible external flows include: the relative forward motion of a swimming fish (the motion "pump"), harnessing the indirect respiratory current (flow generated during mouth suction), and pressure (Vogel, 1977; Abel et al., 2010; Rygg et al., 2013; Timm-Davis and Fish, 2015; Agbesi et al., 2016; Garwood et al., 2019, 2020). Previous research provided important insights on the influence of behavioral and ecological factors on internal nasal irrigation across morphotypes at low Reynolds numbers (Re =100, 500) and indicated that batoids likely rely on these mechanisms to differing degrees (Rutledge et al. 2023, in revision JEB). Reliance on these mechanisms is mediated by the fish's morphology, behavior, and ecology. Specifically, swimming mode (body-caudal-fin vs. undulatory vs. oscillatory vs. intermediate) is the best ecological predictor of nasal morphotype (Rutledge, 2022). Swimming speed (Reynolds number), head pitch, and respiration are also important parameters for some morphotypes and less influential for others. A positive body angle increases water circulation times in some but not all morphotypes. Similarly, respiration aids in nasal circulation and flushing speeds in some morphotypes and is most influential in low Reynolds number flows (Rutledge et al. 2023, in revision JEB).

Here we use particle image velocimetry (PIV, a fluid visualization method using high-powered lasers and neutrally buoyant optical tracer particles) to visualize the external flow

patterns around the nares of three distinct morphotypes (open, protruding, comma). We tested morphotypes at relevant Reynolds numbers (Re = 500, 1000, 2000 and 3000, 6000 for one morphotype) and behavioral parameters (head pitch, respiratory flow). We aim to understand how the morphologically diverse flap-like features seen in these nasal morphotypes influence external flow and odor capture. We hypothesize that each morphotype results in different patterns of external olfactory flow and that morphotypes with a longer sagittal nostril protrusion (protruding> open> comma) will have a greater nostril reach and odor capture potential.

METHODS

Museum Specimens

Three species were chosen to represent the three nasal morphotypes (open, flush: subtype comma, protruding) with flap-like nasal morphology seen in batoid fishes as outlined in Rutledge (2022). Fluid-preserved specimens were chosen from the ichthyology collections of the Los Angeles County Museum of Natural History based on museum availability with a preference for larger body size (to enhance CT scan quality) and with well-preserved internal and external nasal anatomy. The open nare morphotype was represented by the bowmouth guitarfish, *Rhina ancylostoma*. The chosen specimen (LACM 38117-38) has a disc width of 0.49 meters and a nostril width of 0.032 m. This species was chosen because it is the largest species within the open nare morphotype and swims at higher Reynolds numbers compared with its congeners (Table 1). The comma morphotype was represented by the fiddler ray, *Trygonorhinna fasciata.* The chosen specimen (LACM 42623-8) has a disc width of 0.19 m and a nostril width of 0.006 m. This species was chosen because, like the bowmouth guitarfish, it is also a member of the Rhinopristiformes, but is the only member of this group with the comma morphotype, suggesting convergent evolution on a morphology shared with other, more distantly related batoids. Finally,

the protruding morphotype was represented by the California Skate, *Beringraja inornata.* The chosen specimen (LACM 20) has a disc width of 0.23 m and a nostril width of 0.005 m. Because all skates have the protruding nare morphotype, any species could have been chosen, but preference was given to this larger specimen with a fully in-tact nasal chamber.

Computed Tomography Scanning

Museum specimens were CT-scanned at UCLA's Medical Plaza Imaging Center in the Siemens Somatom whole-body CT-scanner at a resolution of 0.5 mm. This resolution was sufficient for capturing the external and internal geometry of the nose and olfactory chamber but limited in resolving some of the small, internal olfactory lamellae. However, as this study focused on odor capture, it is unlikely to influence the external flows around the nose. Prior to scanning, specimens were patted dry and their nasal chambers were fully emptied of preservative.

Model Creation

An STL (Stereo Lithography) model of the head of each morphotype was digitally rendered from the CT-scans using the image processing software 3D Slicer. STL models were edited in the 3D modeling software Blender and Meshmixer. Specifically, the mouths of each model were digitally opened (1-2 mm depth) along the entire mouth width of each model. The orobranchial chamber of each model was digitally closed except for a small region at the posterior end of the body cavity where tubing was later inserted. The bent rostrum (snout) of the protruding nare morphotype was also digitally straightened before printing. Support structures to mount models in the flume were drawn in AutoCAD and digitally affixed to the models.

The heads (from tip of snout to the last gill arch) of the representative morphotypes were 3D-printed with a Formlabs Form3 printer in a clear resin at 100 μm (x,y,z) resolution. No

support structures were printed in the nasal chambers to preserve the internal geometry. The protruding and intermediate nare morphotypes were printed at 2.0 scale. The open nare morphotype was printed at 0.4 scale because of its very large size. Previous dye visualization experiments revealed there was no interaction between the paired nostrils in these models, therefore, only half the head was printed for the morphotypes printed at 2.0 scale. To mimic the suction generated from the mouth during respiration, plastic tubing was inserted into the body cavity of each model and extended directly into the orobranchial chamber.

Reynolds Number

3D-printed models were tested at Reynolds numbers of 500, 1000, 2000, and one morphotype was also tested at 3000 and 6000. The open nare morphotype was tested at these additional higher Reynolds numbers because it operates at higher maximum Reynolds numbers compared with the other species. Additionally, this morphotype was not tested at a Reynolds number of 500 due to limitations in water tunnel minimum flow speeds. The Reynolds number (Re) at the nostril was determined by:

$$Re = \frac{UL}{v} \qquad (1)$$

where U is the swimming velocity, L is the diameter of the exposed inlet nostril, and v is the average kinematic viscosity of seawater ($1.3 \times 10^{-6}\, m^2/s$). The velocity at the inlet nostril was not known, and therefore velocity was approximated by the swimming velocity of the animal, calculated as disc lengths (DL) per second, similar to other fish nasal irrigation studies (Agbesi et al., 2016; Rygg et al., 2013; Garwood et al. 2019, 2020). The congeners of the batoids studied here are known to swim at slow to cruising speeds between 0.20 and 1 DL/s, with faster, burst speeds up to 2 DL/s (Macesic and Kajiura, 2010; Di Santo and Kenaley, 2016). It has also been noted that typical batoid swimming speeds observed in aquaria and around coral reefs are

between 1-2 DL/s (Rosenberger and Westneat, 2000). The species tested here operate at a wide range of Reynolds numbers throughout their life histories (Table 1). The smallest juveniles swimming at 0.25 DL/s live at Reynolds numbers between 10 and 259 (Table 1). The largest recorded body size of these species swimming at cruising swimming speeds of 1 DL/s live at Reynolds numbers between 1992 and 38023 (Table 1). The Reynolds numbers for the exact specimens used in this study have lower maximum swimming speeds due to their relatively smaller body size than the maximum for the species (Table 2). The protruding nare morphotype at the body size of the CT-scanned specimen operates at Reynolds numbers between 234-1869 (Table 2). The open nare morphotype at the body size of the CT-scanned specimen operates at Reynolds numbers between 3044-24356 (Table 2). The comma nare morphotype at the body size of the CT-scanned specimen operates at Reynolds numbers between 220-1762 (Table 2). Therefore, for the protruding and comma nare morphotypes, a Re of 500 is a slow swimming speed (~0.5 DL/s), a Re of 1000 is a cruising swimming speed (~1 DL/s), and a Re of 2000 is a fast-swimming speed (~2 DL/s). For the open nare morphotype at this body size, a Re of 1000 and 2000 is lower than their minimum swimming speed, a Re of 3000 is around their minimum swimming speed, and a Re of 6000 is somewhere between the minimum and cruising speed of this species at this body size (~0.5 DL/s). However, as noted in the range of Reynolds numbers for this species, smaller individuals of this species will operate at Reynolds numbers of 1000 and 2000.

Boundary Layer Thickness

The thickness of the boundary layer (δ) at the anterior incurrent nostril of the different morphotypes was estimated using the equation:

$$\delta = 5\sqrt{\frac{xv}{U}} \qquad (2)$$

where x is the distance from the tip of the batoid's snout to the anterior incurrent nostril, $\square$ is the average kinematic viscosity of seawater at 10° C, and U is the corresponding swimming speed. The swimming speeds used are the minimum, cruising, and fast swimming speeds for the representative species of each morphotype (Table 2). All body size measurements are direct measurements from the individual museum specimen that was CT scanned. It should also be noted that in this equation, x is usually the distance from the leading edge of a flat plate oriented parallel to the flow. Therefore, this will be an approximate estimate of boundary layer thickness in these fishes.

Respiration

Batoids have several modes of respiration. Batoids respire through their 1) spiracle only, 2) mouth and spiracle together, and 3) mouth only (Summers and Ferry, 2001). Spiracle-only respiration is often observed in resting batoids, while the other modes are observed in swimming batoids. Models were tested with a continuous mouth only respiration (mouth suction) on or off. Mouth suction was replicated by inserting tubing into the back of the model which was connected to a syringe pump that withdrew water from the orobranchial cavity at 0.001 L/s. The volume of water entering a batoid's mouth during respiration has not been measured directly. Here, the volume per ventilatory bout was roughly estimated. The volume of the distended orobranchial cavity was subtracted from the closed orobranchial cavity. The volume of the distended orobranchial cavity was approximated by multiplying 1x mouth width by 4x mouth length (estimated length to last gill slit) by 4 mm depth (A. Summers, pers. comm.). The closed cavity was estimated to be 1 mm in depth. Models had mouth widths between 12-25 mm suggesting the volume of the orobranchial chamber is 0.002-0.01L distended and 0.0006-0.003L closed. A complete breath cycle in the hedgehog skate takes ~2 seconds (Summers and Ferry,

2001), suggesting a rate of 0.0007-0.004 L/s. This suggests that the suction rate (0.001 L/s) of the syringe pump was slow to moderate.

Head Pitch

Models were also tested at a head pitch of 0° and 8°, except for the open nare morphotype. This morphotype, due to its differing geometry, could not be successfully aligned in the plane of the laser at a head pitch of 8° while still observing flow into the nostril; therefore all trials were completed at a head pitch of 0°. The pitch angles chosen are biologically relevant (Blevins and Lauder, 2012; Rosenberger, 2000; Rutledge et al. 2023 under review).

Particle Image Velocimetry

Flow patterns around the nostrils were quantified using particle image velocimetry (PIV). A flume (optical glass working section measuring 1.6m x 1.0m x 1.0m housed in the Dabiri Laboratory at Caltech was seeded with neutrally buoyant particles of 12-15 μm (Potters Industries; Conduct-o-fil silver coated spheres). The particles were illuminated by a continuous wave laser beam (Laserglow; 5-W, 532nm) that was spread into a thin sheet by a plano-concave cylindrical lens (Thorlabs; f= -100.0 mm) and reflected upwards into the flume by a 45° mirror. The 3D printed models were mounted on 80/20 so that the frontal plane of the head was facing the camera and the laser illuminated streamwise cross-sections of the flow at the inlet nostrils (Figure 1). We recorded the movement of the particles with a highspeed camera (Edgertonic; SC1) for 8 seconds 300-621 frames per second, with a resolution of 1280 × 1024 pixels, and exposures of 1/300-1/621 s, depending on the model and flow speeds. Image sequences were cross-correlated to determine local flow velocity and time averaged streamlines were generated using PIVlab (Thielicke, 2014; Thielicke and Stamhuis, 2014; Thielicke and Sonntag, 2021) in MATLAB.

2-D Nostril Flux

To determine the flow rate across the incurrent nostril geometries so that we could estimate odor capture potential (see: Odor Capture Potential) a two-dimensional nostril flux was calculated using the velocity fields generated by the PIV analysis. We first approximated the inlet as an ellipse where we defined the major axis of the nostril ellipse as the longest diameter of the incurrent nostril (D_L) and the minor axis was the shortest diameter of the incurrent nostril (D_s) (Supplementary Figure 1). We then defined a new ellipse with axes D_L and $2 \times D_s$ to standardize the ellipses across geometries. The ellipses were plotted at the center of the incurrent nostril where axes cross. We then interpolated the measured velocity field at an increasing number of points around the ellipse with the goal of identifying the number of points needed to converge (n = 5, 10, 20, 30, 40, 50, 100, 200, 300, 400). Convergence was defined as within +/- 5% of the asymptotic value, which was 30 points. Normal vectors were computed at each of the 30 points around the ellipse. A 2-D closed loop flux integral was calculated using the equation:

$$\oint F \cdot \hat{n} \, ds \quad (3)$$

where F represents the velocity field (u, v) and $\hat{n}$ represents the unit normal vectors (n_x, n_y) and ds represents the tiny change in arc length along the curve of the ellipse. All calculations were performed in MATLAB.

Odor Capture Potential

Odor capture could not be measured directly but was approximated in two different ways: 1) nostril reach: the transverse reach of the incurrent nostril relative to the incurrent nostril width and 2) odor capture potential: the ratio of the incurrent nostril flux ($Flux_{In}$) to the potential available flux directly upstream from the nostril ($Flux_{Up}$).

To determine the nostril reach, we measured the width of the transverse extent of the time

averaged streamlines that directly enter the incurrent nostril as shown by their vector direction and destination of the terminal point (Figure 2, panel 3, No. 1). If the terminal point was inside the incurrent nostril, it was assumed to be entering the incurrent nostril. Because our results then found flow entering the incurrent nostril both from upstream and downstream (opposite the freestream direction) of the incurrent nostril, we defined two metrics for nostril reach: anterior (Figure 2, panel 3, No. 2) and posterior (Figure 2, panel 3, No. 3) nostril reach. Nostril reach was defined as a percentage of the incurrent nostril width.

To determine the upstream available flux, a line integral was computed using a uniform flow field with the same direction and magnitude as the freestream flow (U_∞) for each case. The length of the line was the same length as the major axis of the ellipse, D_L (Supplementary Figure 1). Because the velocity field was uniform the flux calculation was simply $U_\infty \times D_L$. The line D_L was transverse to the flow direction and therefore represented the maximum possible flux through the major axis (D_L) of each ellipse. Odor capture potential was defined as $Flux_{In}/Flux_{Up}$. A negative flux indicates that most of the flow is entering the ellipse while a positive flux indicates that most of the flux is leaving the ellipse. An odor capture potential of 0 indicates that all the flow entering the ellipse is also exiting the ellipse in that two-dimensional plane. An odor capture potential of -1 indicates that none of the flow entering the ellipse is exiting the ellipse in that two-dimensional plane. An odor capture potential of some negative fraction indicates that a fraction of the flow is not exiting the ellipse and because this is a 2D analysis, it must be going into the third dimension. Because the ellipses surround the incurrent nostril, this "missing" portion of the 2D flow represents the maximum amount of flow that could be entering into the incurrent nostril. This "missing" flow is either entering the incurrent nostril (i.e., going into the page) or leaving the ellipse in the opposite direction (i.e., going out of the page).

RESULTS

Comma morphotype

The comma morphotype had the largest nostril reach and odor capture potential ($Flux_{In}/Flux_{Up}$) across all morphotypes (Figure 3, Table 4). Water entered the incurrent nostril at an anterior nostril reach that ranged from 65-306% of the incurrent nostril width (Figure 2, No. 1). The anterior nostril reach for this morphotype was similar from Re= 500 to Re= 1000, ranging from 65- 94% of the incurrent nostril width. From Re=1000 to Re=2000, the anterior nostril reach more than quadrupled (74% vs. 306%). From Re=500-1000, the water that enters the incurrent nostril is directly upstream of the nostril. However, at Re=2000 water entered the incurrent nostril from multiple directions. Water entered the incurrent nostril from 1) directly upstream, 2) the medial side of the incurrent nostril, along the nasal curtain 3) downstream of the incurrent nostril, and 4) to a small degree the lateral edge of the incurrent nostril. This resulted in a posterior nostril reach ranging from 277-353% of the incurrent nostril width.

Odor capture potential ($Flux_{In}/Flux_{Up}$) ranged from -0.67 to -0.78, remaining fairly consistent with a slight increase with Re. The largest anterior nostril reach (306%) and odor capture potential (-0.78) occurred at Re=2000 at a 0° head pitch with respiration off.

Respiration did not substantially affect anterior nostril reach, odor capture potential ($Flux_{In}/Flux_{Up}$), or have any noticeable effect on flow patterns. Respiration had a 1-7% difference in anterior nostril reach and <3% difference in odor capture potential across all parameters for this morphotype.

Head pitch had some influence on nostril reach, odor capture potential, and flow patterns. Generally, this morphotype had a larger nostril reach at a 0° head pitch, with an average anterior nostril reach of 158% at pitch 0° and 135% at pitch 8°. The average odor capture potential

($Flux_{In}/Flux_{Up}$) at a 0° head pitch was -0.75 and -0.71 at pitch 8°. Flow patterns also changed with head pitch, with head pitch changing the direction that water enters the incurrent nostril. Specifically, at a 0° head pitch water entered the incurrent nostril and turned towards the lateral edge of the nostril. At an 8° head pitch, water entered the incurrent nostril without turning, flowing straight into the inlet with a slight bend towards the medial edge of the nostril. At an 8° head pitch the posterior recirculation region was also smaller, resulting in a smaller posterior inlet reach. The average posterior reach at a 0° pitch was 352% and 277% at pitch 8°.

Open morphotype

The open morphotype was intermediate to the other two morphotypes in terms of its nostril reach (Figure 3, Table 5). Water entered both the incurrent and "excurrent" nostril with an anterior nostril reach that ranges from 64-167% of the incurrent nostril width (Figure 2, No. 1). The anterior nostril reach increased consistently with increasing Re, with an average anterior nostril reach of 70% the incurrent nostril width at Re= 1000, 101% at Re =2000, 105% at Re=3000, and 162% at Re = 6000. At Re=1000-3000, the water that enters the incurrent and excurrent nostril was upstream of the nostrils. At these Re, the water entering the incurrent and excurrent nostrils was directly adjacent to the anterior nostril flap. Water does not appear to enter the entire width of incurrent nostril until Re=6000. At Re=6000, upstream water entered the entire length of the incurrent nostril and approximately half of the designated "excurrent" nostril. At Re=6000 water also entered both the incurrent and "excurrent" nostril from downstream. This resulted in a posterior nostril reach ranging from 165-169% of the incurrent nostril width.

Odor capture potential ($Flux_{In}/Flux_{Up}$) was the lowest of all three morphotypes and remained consistent with a slight decrease with increasing Re, with a flux ratio between -0.25 and -0.33. However, it should be noted that in the open morphotype, flux was measured over the

112

entire nare (incurrent and excurrent channels) due to its open morphology with no clear inlet and outlet. The largest anterior potential odor capture was at Re=1000 (-0.33) while the smallest anterior odor capture potential occured at Re =6000 (-0.25).

In contrast with the comma morphotype, respiration did appear to affect nostril reach, potential odor capture, and visually influence flow patterns. With respiration there was a 1-37% difference in anterior nostril reach. This was also the only morphotype where respiration may significantly affect potential odor capture as the standard deviations did not overlap. Across all parameters, the average anterior nostril reach was 117% with respiration and 102% without respiration. The average odor capture potential was 30% with respiration and 25% without respiration. The posterior recirculation region also visually appeared to be affected by respiration, with flow directed more into the mouth with respiration. However, the posterior nostril reach had only a 4% increase with respiration.

The laser could not be oriented into the plane where water could be seen entering the nostril at a head pitch of 8°. Therefore, this morphotype was not tested at an 8° head pitch.

Protruding morphotype

The protruding morphotype had the smallest nostril reach and second smallest odor capture potential ($Flux_{In}/Flux_{Up}$), with similar values and flow patterns across Re (Figure 4, Table 6). Water entered the incurrent nostril at an anterior nostril reach that ranged from 53-64% of the incurrent nostril width (Figure 2, No. 1). The anterior nostril reach for this morphotype was similar across Re= 1000-2000 and water entered the incurrent nostril directly upstream of the nostril. It was not clear if water was entering the incurrent nostril at Re = 500 and no nostril reach was recorded at this Re. While this morphotype has a posterior region of recirculation behind the incurrent nostril protrusion, there was no evidence of water entering the incurrent

nostril from downstream. Streamlines approach the edge of the incurrent nostril but the recirculating fluid did not appear to enter the incurrent nostril and therefore this morphotype did not have a posterior nostril reach.

Odor capture potential ($Flux_{In}/Flux_{Up}$) in the protruding morphotype ranged from -0.35 to -0.50 and was the second lowest of all morphotypes. Odor capture potential remained consistent across Re with a slight rise with increasing Re. The largest anterior nostril reach (64%) occurred at Re=2000, with a 8° head pitch, and respiration off. The largest odor capture potential occured at Re= 2000, with a 0° head pitch, and respiration off.

Respiration did not appear to affect nostril reach, potential odor capture, or visually influence flow patterns. Across all parameters, the average anterior nostril reach with respiration was 58% and 60% without respiration.

Head pitch had some influence on nostril reach, odor capture potential, and flow patterns. The average odor capture potential ($Flux_{In}/Flux_{Up}$) was -0.40 with a 0° head pitch and -0.34 at an 8° pitch. This was also the only morphotype where head pitch might significantly affect potential odor capture as the standard deviations did not overlap. However, there was only a 2% difference in average anterior nostril reach with head pitch (58% vs. 60%). The posterior recirculation width appeared to also have been affected by head pitch, with an 8° pitch generally resulting in more posterior recirculation, and tighter spiral-like eddies behind the protrusion.

DISCUSSION

Batoid fishes face several hydrodynamic challenges when attempting successful odor capture. These challenges include: 1) the medioventral position of their incurrent nostrils (at a right angle to incoming flow), 2) no internal pump system producing flows (disconnection of nostrils from mouth and no pumping accessory sacs), and 3) the odor-impeding boundary layer

114

that surrounds a swimming fish. Because of these challenges, batoid fishes must harness external flows (motion-pump, buccopharyngeal-pump, pressure; see introduction for definitions) to irrigate their nares. Behavioral modifications (body orientation, swimming speed, respiratory mode) and anatomical adaptations will further aid in harnessing external flows. Our study of flow hydrodynamics found that the unique multi-flap nasal morphology seen in the open, protruding, and comma nasal morphotypes appears to be an adaptation to aid in water capture. However, our hypothesis that a longer sagittal nostril protrusion will divert more flow into the incurrent nostril, increasing nostril reach and odor capture potential was not supported. Instead, we found that nostril reach is inversely proportional to nostril protrusion length in the three morphotypes.

The comma morphotype, with the smallest nasal protrusion depth (43% of its incurrent nostril width) has the largest nostril reach. The nostril reach of the comma morphotype is over three times the length of its own incurrent nostril width, circulating fluid into the nostril from multiple directions. Surprisingly, the incurrent nostril of this morphotype only slightly protrudes beyond the boundary layer (see boundary layer ratios, Table 3) and may be enclosed in the boundary layer at slow swimming speeds (Re= 500). However, this morphotype still displays streamlines terminating in the incurrent nostril at Re= 500, suggesting that even without the assistance of respiratory flow, the geometry of the comma morphotype has a pressure differential that drives fluid flow into the nostril.

The nasal curtain also plays an important role in increasing the nostril reach of the comma morphotype. This was unexpected, as the protruding region of the nasal curtain is positioned behind the incurrent nostril. Throughout all swimming speeds (Re), the nasal curtain appears to locally disturb the flow, with water from the medial region of the head of the animal

diverted towards the incurrent nostril. The water downstream of the nasal curtain flows backwards over the nasal curtain in the opposite direction of the freestream flow. These two opposing flows meet and form a central channel of water along the nasal curtain that directs fluid ~90° towards the incurrent nostril. However, at Re= 500 and 1000 it is unclear if the water that is disturbed by the nasal curtain enters the incurrent nostril, as the streamlines terminate with a spiral-like motion just before the entrance of the incurrent nostril. It is possible that the spiral-like flow may enter the incurrent nostril in a different plane than we were able to visualize. But, at Re= 2000, the central channel of water along the nasal curtain does appear to enter the incurrent nostril. At this higher Re, the anterior nasal flap also appears to locally disturb the flow enough to create a recirculation region that directs water from behind the nostril back into the incurrent nostril. The multidirectional flow around the incurrent nostril likely increases the likelihood that an odorant is captured by increasing the expanse of sampled water.

The open morphotype, with an intermediate nostril protrusion length, has the second largest nostril reach. The nostril reach of the open morphotype is up to 1.6 times the length of its own incurrent nostril width. However, our results demonstrate that the anatomical terms for the "incurrent" and "excurrent" nostril of this morphotype oversimplify the flow patterns through its nares. It appears that only about half of the "excurrent" nostril actually has excurrent flow. Because of this, we suggest referring to the two nostrils of a single naris by their anatomical positions rather than their flow patterns. The incurrent nostril can be referred to as the lateral nostril and the excurrent nostril can be referred to as the medial nostril. The lateral nostril has incurrent flow and the medial nostril has both incurrent and excurrent flow.

The open morphotype was the only morphotype where flow through the entire naris was visualized, due to its unique open geometry and lack of a nasal curtain that would normally

obscure the excurrent flow. We found that at Re= 1000, 2000, and 3000 most of the flow

entering the naris is in the medial region, on either side of the anterior nasal flap. The anterior

nasal flap protrudes out of the boundary layer at even the lowest Re for this species and this

protruding flap appears to direct a minor amount of the incoming flow along this protrusion and

into a small portion of the medial and lateral nostril. At Re= 6000, water enters the entire length

of the lateral nostril and half of the medial nostril. Large posterior recirculation regions also

persist behind the nostrils and similar to the comma morphotype, these regions circulate the

downstream fluid back into the nostrils. Because the open morphotype has the least pipe-like

internal geometry, more complex flow patterns may be needed to generate flow into its open

nasal chamber.

The protruding morphotype, with the longest nostril protrusion (133%), has the smallest

nostril reach with no posterior nostril reach, capturing fluid ~3/5 the width of its incurrent nostril.

Unlike the other morphotypes, the protruding morphotype only captures fluid directly in the path

of the incurrent nostril. It appears that the protruding flap that encircles the incurrent nostril of

the protruding morphotype creates a physical impediment to the incoming flow, channeling flow

up and into the incurrent nostril. While the protruding nasal morphotype also has a nasal curtain

like the comma morphotype, the morphology of their nasal curtains is very different. The comma

morphotype has a square nasal curtain that freely extends from the head, while the protruding

morphotype has a skirt-shaped nasal curtain that is flush with the body. Without a slightly

protruding nasal curtain, this morphotype has a much smaller nostril reach. However, the

protruding nostril geometry is sufficiently long to extend out of the boundary layer even at its

slowest swimming speed. Specifically, this morphotype is observed in skates and electric rays

that display a very slow form of aquatic locomotion called "punting" in which they use their

pelvic fins to create a walking type of gait across the seafloor (see "true punters;" Macesic and Kajiura, 2010). A very long nostril protrusion may be advantageous during this slow locomotion, ensuring possible odorant uptake despite a relatively thick boundary layer. But, compared with the other morphotypes that exhibit multidirectional incurrent flow, this morphotype may have a reduced likelihood of encountering odorants from multiple directions.

The results of the flux analysis indicate that odor capture potential ($Flux_{In}/Flux_{Up}$) remains relatively constant across Re for all three morphotypes. While the absolute flux increased with increasing Re, the odor capture potential relative to the upstream available flux ($Flux_{In}/Flux_{Up}$) remained relatively constant, suggesting that regardless of the differing flow patterns, a similar amount of fluid travels across and potentially enters the nostrils. The comma morphotype, with the largest inlet reach, also has the largest odor capture potential ($Flux_{In}/Flux_{Up}$ = -0.79). A negative flux indicates flow direction (i.e., traveling into the region around the incurrent nostril rather than out) and 0.79 indicates that almost 80% of the available upstream flux is not exiting the area around the nostril. Therefore, the incurrent nostril may be capturing up to 80% of the available upstream flow. However, the streamlines show that a large portion of the water entering the incurrent nostril is not only from the upstream direction. The protruding morphotype has a much smaller nostril flux, with an odor capture potential about half of the comma morphotype ($Flux_{In}/Flux_{Up}$ = -0.37). Their reduced odor capture potential could be because this morphotype harnesses flow in only one direction. Notably, odor capture potential in the protruding morphotype was influenced by head pitch, with a 0° head pitch resulting in higher odor capture potential than an 8° head pitch. This could reflect the fact that the long nasal protrusion of this morphotype is perpendicular to the freestream flow at a 0° head pitch, which could result in more water capture.

The open morphotype has the smallest odor capture potential ($Flux_{In}/Flux_{Up}$), however the flux analysis measured something different for this morphotype. Whereas the fluxes of the other morphotypes were calculated across an ellipse that encircles their incurrent nostril, the flux of the open morphotype was calculated across an ellipse that encircles its entire naris. $Flux_{In}$ represents the flux around the naris with both incurrent and excurrent flow. Therefore, we expect the flux values to be significantly lower in the open than in the other two morphotypes, as the incurrent nostril flow should be similar to the excurrent flow. For the open morphotype, lower flux values may indicate that more fluid is being sampled by the nostril. For example, this morphotype has odor capture potential ($Flux_{In}/Flux_{Up}$) values of approximately -0.20, suggesting only 20% of the upstream available flow is not leaving the ellipse (and 80% of the incoming flow is exiting). This morphotype was also the only morphotype significantly affected by indirect respiratory flow. However, this might be because the open morphotype was the only one where both incurrent and excurrent flow was quantified. But, research looking at dye visualization through the internal olfactory chamber of this morphotype found that respiration was important for flushing the olfactory chamber (Rutledge et al. 2023, in revision JEB). Additionally, harnessing the indirect respiratory flow may be more crucial for a nostril geometry that is not pipe-like, with no distinct inlet and outlet, and therefore may have a smaller pressure differential.

These three differing nostril morphologies may highlight tradeoffs in morphology and successful odor capture with differing environments and behaviors. At very low Re, the protruding nasal morphotype likely benefits from a very long nostril protrusion that always extends out of the boundary layer. Because their nares are also positioned the farthest from the leading edge of the head of the animal, a longer nasal protrusion may also be required to mitigate a relatively thicker boundary layer than nares positioned more anteriorly. However, this long

119

protrusion prevents multidirectional flow and comes at the cost of a reduced nostril reach and odor capture potential. Odor capture potential was also affected by changing head pitch in the protruding nasal morphotype, resulting in a less dynamic odor capture ability. However, this morphotype was the least dependent on a changing Re, with consistent (albeit lower) potential odor capture abilities. Conversely, the open and comma morphotypes have nostril flaps that are long enough to locally disturb the flow, but short enough to allow for flow to enter from multiple directions around the incurrent nostril. However, the large posterior recirculating regions of these two morphotypes may add some drag during swimming. The comma morphotype is the most dynamic nostril geometry and captures a consistently large amount of water at low and high Re, independent of head pitch and respiration.

The comma nasal morphotype could be a possible candidate geometry for bioinspired chemical sensors. Specifically, this morphotype does not depend on an internal pump to bring water to their olfactory lamellae and is effective at irrigating its nares across a range of Reynolds numbers and with changing orientation into a plume. The internal geometry of this morphotype recirculates fluid around the sensory structures (Rutledge et al. 2023, in revision JEB) and the external geometry passively captures water over 3 times the width of its own nostril. Therefore, this geometry could be a potentially efficient geometry for chemical detection systems onboard underwater vehicles that are often limited by the power demand of the pump. By just changing the geometry of the inlet, there may be potential to passively increase the amount of water sampled.

There were several limitations to this study. The models tested here were printed with a rigid resin that does not match the material properties of the live animals. Specifically, there is some degree of flexibility in both the anterior nasal flaps and the nasal curtain. Live animal

aquaria observations show that there is minimal movement of the anterior nasal flaps while swimming. However, the author has observed that there can be significant movement of the nasal curtain in vivo. Specifically, the nasal curtain has been observed to move in sync with the respiration of the animal. It is unclear in which morphotypes this occurs and how often, but the author has observed this nasal curtain movement in dasyatid rays (Supplementary Video 1). Because the protrusion depth of the nasal curtain played an important role in nostril reach in one morphotype, future live animal experiments would be beneficial to determine how nasal curtain movement may influence odor capture. Finally, the main limitation of this study was that the analysis was two-dimensional. Because the results of this study highlight surprisingly complex flow patterns, a 3-D PIV analysis would be beneficial to resolve the complete picture of flow around the nares.

In summary, our study is the first to use particle image velocimetry to visualize flow into and around the nares of a fish. We tested three distinct flap-like nasal morphotypes seen in batoid fishes and found several surprising results, including that olfactory flow around the nares is much more complex and expansive than previously thought. We document the first recorded occurrence of multidirectional olfactory flow into the incurrent nostril of a fish. The complex flow patterns seen in two of the morphotypes appear to greatly expand the reach and odor capture potential ($Flux_{In}/Flux_{Up}$) of the nares, increasing the expanse of water sampled. Head pitch, respiration, and Reynolds number were found to impact odor capture differently across morphotypes. These results are likely a reflection of different odor capture strategies and tradeoffs with nasal geometry and ecology.
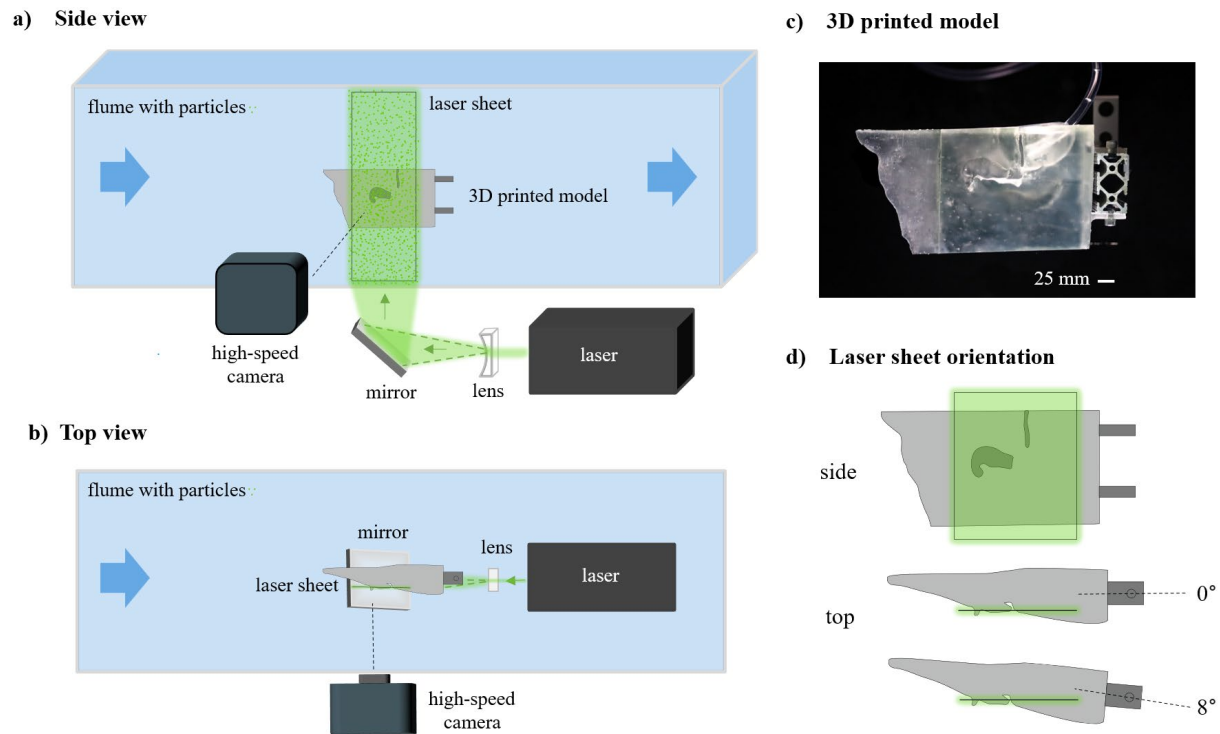
ACKNOWLEDGEMENTS

Figure 1. Particle image velocimetry methods showing a schematic of the experimental set-up with a flume seeded with neutrally buoyant, optical particles and a high-powered laser, cylindrical lens, and angled mirror that create a laser sheet over the frontal plane of the 3D-printed model from a) side view b) top-down view c) photograph of the model mounted on 80/20 in the flume with a black background for photography contrast d) closer view of laser sheet orientation from side and top, with the top view highlighting the two head pitch angles tested.
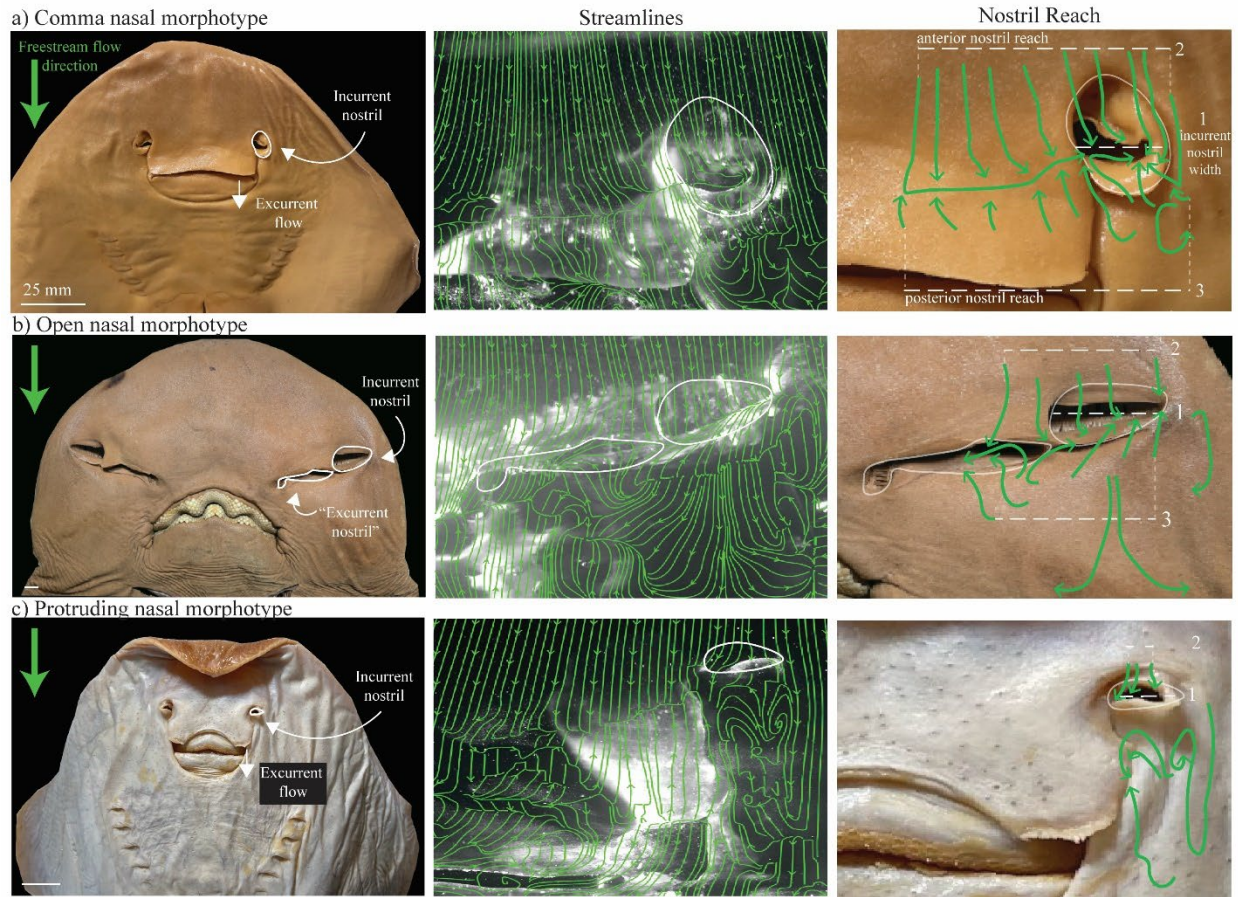
Figure 2. The three morphotypes of batoid fishes with flap-like inlet nostrils and their associated nostril flow patterns. The left panel shows the three nasal morphotypes: a) comma (represented by *Trygonorhinna fasciata*), b) open (represented by *Rhina ancylostoma*), and c) protruding (represented by *Beringraja rhina*). The middle panel shows the time averaged streamlines around and into the inlet nostril at a cruising swimming speed (~1 DL/s) with select streamlines outlined in green. The right panel shows the same outlined streamlines on the associated museum specimens and diagrams the anterior (2) and posterior (3) odor capture widths, which were measured out of the respective inlet incurrent nostril diameter (Ds) (1) of the animal.

Figure 3. Time averaged streamlines for the comma nare morphotype across Re (500,1000, 200), head pitch (0, 8), and respiration (on, off).

Figure 4. Time averaged streamlines for the open nare morphotype across Re (1000, 2000, 3000), head pitch (0, 8), and respiration (on, off).
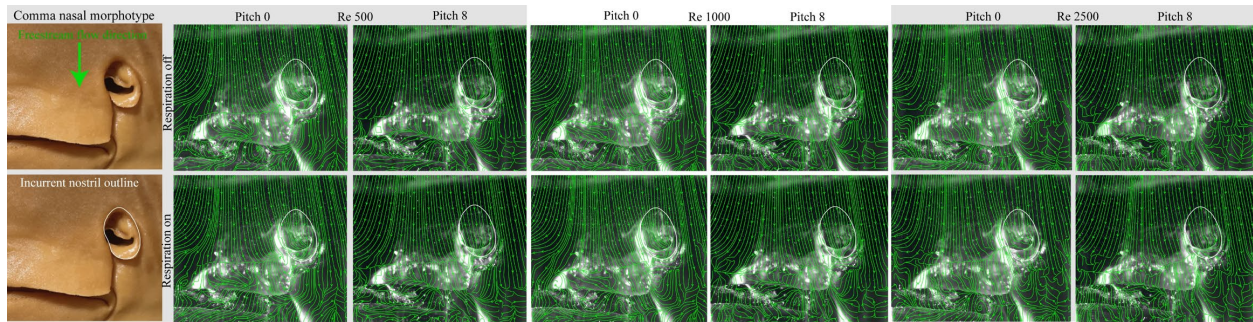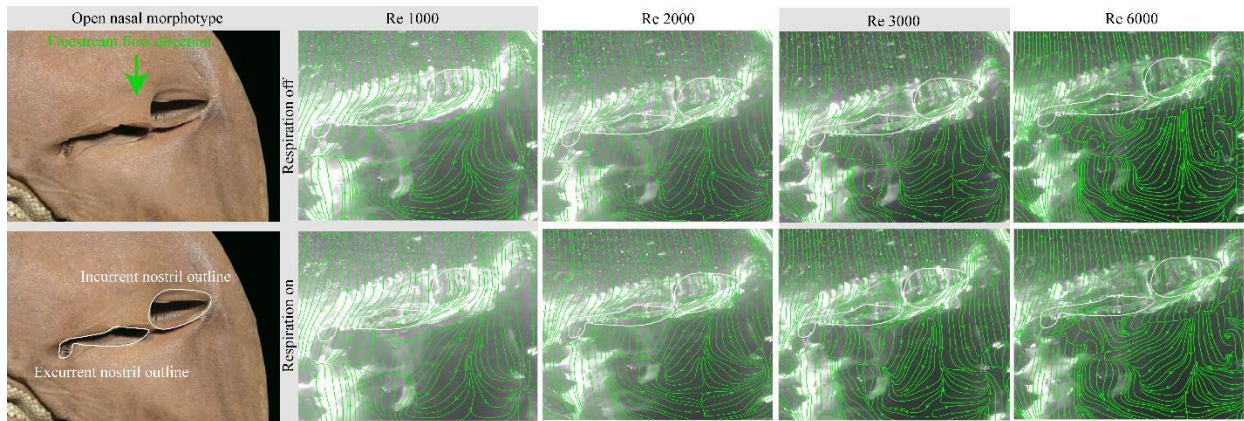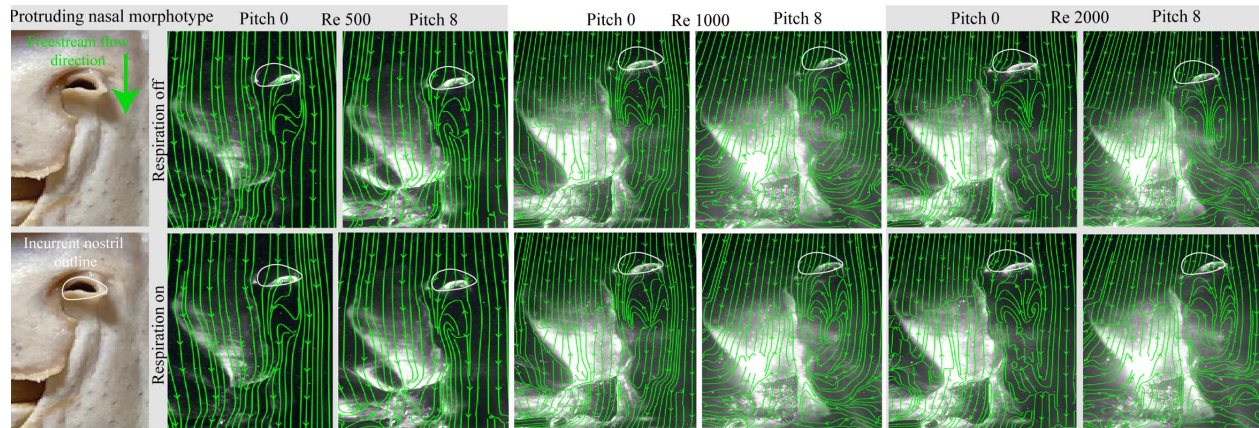
Figure 5. Time averaged streamlines for the protruding nare morphotype across Re (500,1000, 2000), head pitch(0, 8), and respiration (on, off).
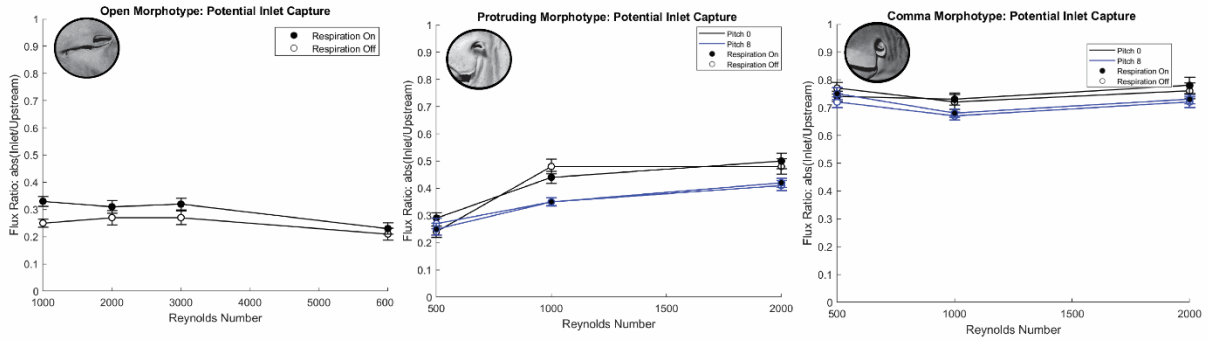
Figure 6. Odor capture potential (Flux$_{In}$/Flux$_{Up}$) across morphotypes. Standard deviation bars are calculated based on instantaneous flux.

Table 1. Representative species for the 3 morphotypes tested here, highlighting the range in Reynolds number throughout ontogeny. Body size ranges from the size at birth to the maximum size of a sexually mature adult (size metrics all obtained from Last et al. 2016). The range of incurrent nostril diameter (Ds) was approximated using the proportion of the incurrent nostril diameter (Ds) at body size from the measurements taken on the specimens used in this study. Reynolds number was calculated using the inlet incurrent nostril diameter (Ds), swimming velocity (ranging from 0.25-1 DL/s), and the average kinematic viscosity of seawater.

Species	Morphotype	Body Size (m)	Characteristic Length (m)	Reynolds Number (Re)
		Disc Length (DL) Range	Inlet Nostril Width Range	Swimming Speed 0.25-1 DL/s
Beringraja rhina	Protruding	0.06-0.37	0.001-0.007	10-1992
Rhina ancylostoma	Open	0.15-0.87	0.009-0.057	259-38023
Trygonorrhina fasciata	Comma	0.12-0.55	0.004-0.017	92-7192

Table 2. The museum accession numbers, body sizes, incurrent nostril width, swimming speeds, and range of Reynolds numbers for the museum specimens used to create the 3D printed models.

Mueseum Number	Species	Morphotype	Body Size (m)	Characteristic Length (m)	Swimming Speed (DL/s)			Velocity U (m/s)			Reynolds Number (Re)		
			Disc Length	Inlet Nostril Width	Min.	Cruising	Max.	Min.	Cruising	Max.	Min.	Cruising	Max.
LACM 20	*Beringraja rhina*	Protruding	0.23	0.005	0.25	1	2	0.06	0.23	0.46	234	935	1869
LACM 38117-38	*Rhina ancylostoma*	Open	0.49	0.032	0.25	1	2	0.12	0.49	0.99	3044	12178	24356
LACM 42623-8	*Trygonorrhina fasciata*	Comma	0.19	0.006	0.25	1	2	0.05	0.19	0.38	220	881	1762

Table 3. The boundary layer thickness for each morphotype across swimming speeds.

Morphotype	Species	Tip of Snout to Incurrent Nostril	Nostril protrusion depth	Nostril depth as % of incurrent nostril width	Boundary Layer Thickness (mm)			Protrusion Depth/Boundary Thickness		
					0.25 DL/s	1 DL/s	2 DL/s	0.25 DL/s	1 DL/s	2 DL/s
Protruding	*Beringraja rhina*	65.2	6.0	133%	5.9	3.0	2.1	1.0	2.0	2.8
Open	*Rhina ancylostoma*	153.4	16.6	52%	6.4	3.1	2.2	2.6	5.3	7.5
Comma	*Trygonorrhina fasciata*	60.1	3.7	43%	6.2	3.2	2.3	0.6	1.2	1.6

Table 4. Odor capture widths at various Reynolds numbers (Re), head pitch, and with respiration on and off for the comma nasal morphotype.

Morphotype	Re	Pitch	Respiration	Anterior Nostril Reach*	Posterior Nostril Reach*
Comma	500	0	off	89%	0%
	500	0	on	94%	0%
	500	8	off	83%	0%
	500	8	on	86%	0%
	1000	0	off	74%	0%
	1000	0	on	81%	0%
	1000	8	off	65%	0%
	1000	8	on	66%	0%
	2000	0	off	306%	353%
	2000	0	on	304%	350%
	2000	8	off	257%	276%
	2000	8	on	253%	277%

*(% of incurrent nostril width)

Table 5. Odor capture widths at various Reynolds numbers (Re), head pitch, and with respiration on and off for the open nasal morphotype.

| Morphotype	Re	Pitch	Respiration	Anterior Nostril Reach*	Posterior Nostril Reach*
Open	1000	0	off	64%	0%
	1000	0	on	75%	0%
	2000	0	off	100%	0%
	2000	0	on	101%	0%
	3000	0	off	86%	0%
	3000	0	on	123%	0%
	6000	0	off	156%	165%
	6000	0	on	167%	169%

*(% of incurrent nostril width)

Table 6. Odor capture widths at various Reynolds numbers (Re), head pitch, and with respiration on and off for the protruding nasal morphotype.

Morphotype	Re	Pitch	Respiration	Anterior Nostril Reach*	Posterior Nostril Reach*
Protruding	500	0	off	-	0%
	500	0	on	-	0%
	500	8	off	-	0%
	500	8	on	-	0%
	1000	0	off	53%	0%
	1000	0	on	57%	0%
	1000	8	off	62%	0%
	1000	8	on	53%	0%
	2000	0	off	62%	0%
	2000	0	on	61%	0%
	2000	8	off	64%	0%
	2000	8	on	60%	0%

*(% of incurrent nostril width)

CHAPTER 3- SUPPLEMENTARY MATERIAL
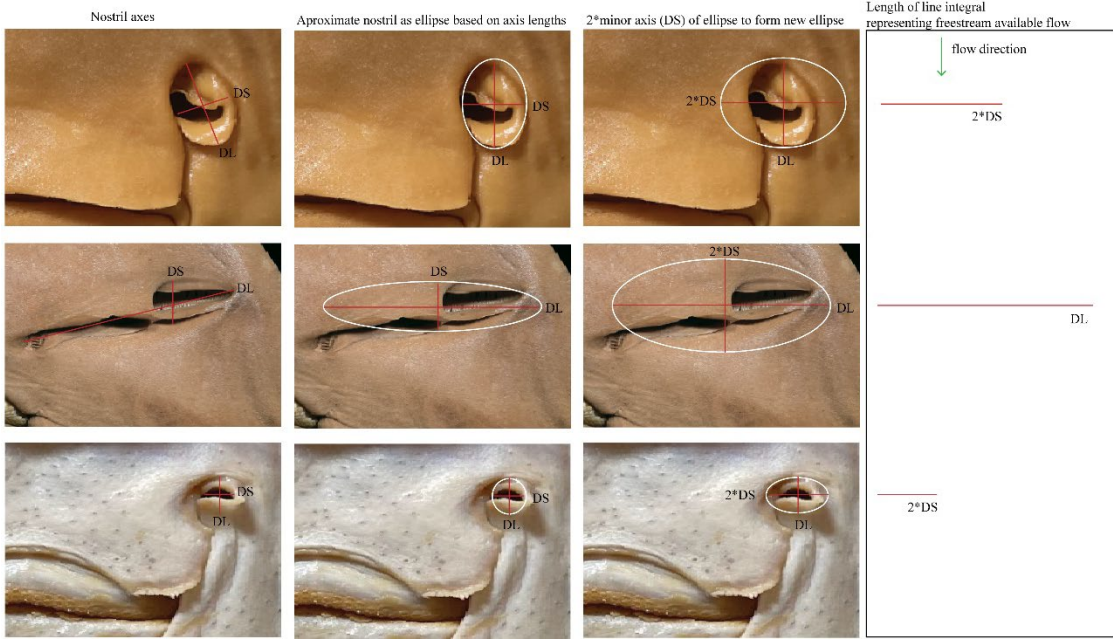
Supplementary Figure 1. The ellipses and nostril axes used to calculate the 2D closed loop flux integral.

REFERENCES

1. Abel, R.L., Maclaine, J.S., Cotton,R., Xuan, V. B., Nickels, T.B., Clark, T.H.,Wang, Z., Cox, J.P.L. 2010. Functional morphology of the nasal region of a hammerhead shark. Comparative Biochemistry and Physiology - Part A, 155, 464-475.

2. Agbesi, M.P.K., Naylor,S., Perkins, S., Borsuk, H.S., Sykes, D., Maclaine, J.S. Wang, Z., Cox, J.P.L. 2016. Complex flow in the nasal region of guitarfishes. *Comparative Biochemistry and Physiology - Part A*, 193, 52-63.

3. Bell, M.A., 1993. Convergent evolution of nasal structure in sedentary elasmobranchs. Copeia 1993, 144–158.

4. Collin, S. P., Kempster, R. M., & Yopak, K. E. (2015). How elasmobranchs sense their environment. In Fish Physiology (Vol. 34, pp. 19-99). Academic Press.
Compagno, L.J.V., 1999. Systematics and body form. In: Hamlet, W.C. (Ed.), Sharks, Skates, and Rays: The Biology of Elasmobranch Fishes. Johns Hopkins University Press, Baltimore, 1–42.

5.Cox, J.P.L. 2008. Hydrodynamic aspects of fish olfaction. *Journal of the Royal Society Interface*, 5, 575-593.

6.Cox, J.P.L., 2013. Ciliary function in the olfactory organs of sharks and rays. *Fish Fish.* 14, 364–390.

7.Døving, K.B., Dubios-Dauphin, M., Holley, A., Jourdan, F. 1977. Functional Anatomy of the Olfactory Organ of Fish and the Ciliary Mechanism of Water Transport. Acta Zoologica Stockholm, 58, 245-255.

8. Hart, N.S., & Collin, S.P. 2015. Sharks senses and shark repellents. *Integrative zoology*, 10(1), 38-64 .

9. Ferrando, S., Gallus, L., Ghigliotti, L., Amaroli, A., Abbas, G., Vacchi, M. 2017. Clarification of the Terminology of the Olfactory Lamellae in Chondrichthyes. *The Anatomical Record*, 300, 2039-2045.

10. Garwood, R. J. Behnsen, J. Haysom, H.K., Hunt, J.N., Dalby, L.J. Quilter, S.K., Maclaine, J.S., Cox, J.P. 2019. Olfactory flow in the sturgeon is externally driven. Comp. Biochem. Physiol. A, 235 (2019), pp. 211-225

11. Garwood, R.J., Behnsen, J., Ramsey, A.T., Haysom, H.K., Dalby, L.J., Quilter, S.K., Maclaine, J.S., Wang, Z., Cox, J.P.L., 2020. The functional anatomy of the pike, Esox lucius (L.). Comp. Biochem. Physiol. A 244, 110688.

12. Gardiner, J. M., & Atema, J. 2010. The function of bilateral odor arrival time differences in olfactory orientation of sharks. *Current Biology*, 20(13), 1187-1191.

13. Gardiner, J.M.,Hueter, R.M., Maruska, K.P., Sisneros, J.A., Casper, B.M., Mann, D.A., Demski, L.S. 2012. Ch. 12 Sensory physiology and behavior of elasmobranchs. In Biology of Sharks and their Relatives, 2nd Ed., edited by E.C. Carrier, J.A. Musick, M.R. Heithaus (CRC Press: Boca Raton, FL)

14. Last, P. A., W. White, M.R. de Carvalho, B. Séret, M. Stehmann, and G.P. Naylor. (Eds.). 2016. Rays of the World. CSIRO Publishing, Melbourne, Australia.

15. Last P R, Seret B, Naylor G J P. 2016b. Rhinobatos borneensis sp. nov. with a redefinition of the Rhinopristiformes. Zootaxa 4117:451–75.

16. Rutledge, 2022. Sniffing out Stingray Noses: The Functional Morphology of Batoid Olfaction. *Integrative and Organismal Biology*, obac043.
Rygg, A.D., Cox, J.P., Abel, R., Webb, A.G., Smith, N.B., Craven, B.A. 2013. A computational study of the hydrodynamics in the nasal region of a hammerhead shark (*Sphyrna tudes*): Implications for Olfaction. *PLoS ONE*, 8(3): e59783

17. Settles, G.S. 2005. Sniffers: fluid-dynamic sampling for olfactory trace detection in nature and homeland security. *Journal of Fluids Engineering*, 127, 189-218.

18. Schluessel, V., Bennett, M.B., Bleckmann, H., Blomberg, S., Collin, S.P., 2008. Morphometric and ultrastructural comparison of the olfactory system in elasmobranchs: the significance of structure–function relationships based on phylogeny and ecology. *J. Morphol.* 269, 1365–1386.

19. Simonitis L E, Marshall C D. 2022. Microstructure of the Bonnethead Shark (Sphyrna tiburo) Olfactory Rosette. Integrative Organismal Biology, 4:1.

20. Tester, A.L., 1963. Olfaction, gustation, and the common chemical sense in sharks. In: Gilbert, P.W. (Ed.), Sharks and Survival. D.C, Heath and Co, Lexington, pp. 255–282.

21. Theisen, B. 1970. The morphology and vascularization of the olfactory organ in Calamoichthys calabaricus (Pisces, Polypteridae). Vidensk. Meddr. dansk naturh. Foren. 133, 31–50.

22. Thielicke, W. and Stamhuis, E.J. (2014): PIVlab – Towards User-friendly, Affordable and Accurate Digital Particle Image Velocimetry in MATLAB. Journal of Open Research Software 2(1):e30.

23. Thielicke, W., Sonntag, R. (2021) Particle Image Velocimetry for MATLAB: Accuracy and enhanced algorithms in PIVlab. Journal of Open Research Software, 9: 12.

24. Thielicke, W. (2014): The Flapping Flight of Birds - Analysis and Application. Phd thesis, Rijksuniversiteit Groningen.

25. Timm, L.L., Fish, F.E. 2012. A comparative morphological study of the head shape and

olfactory cavities of sharks inhabiting benthic and coastal/pelagic environments. *Journal of Experimental Marine Biology and Ecology*, 414(415), 75-84.

26. Vogel, S. 1977. Flows in organisms induced by movements of the external medium. In Scale effects in animal locomotion (ed. T. J. Pedley), pp. 285–297. London, UK: Academic Press.

27. Zeiske, E., Theisen, B., Gruber, S.H., 1987. Functional morphology of the olfactory organ of two carcharhinid shark species. *Canadian Journal of Zoology*. 65, 2406–2412.